



Technical University of Crete
School of Electrical & Computer Engineering

**Integrated Hyper Spectral Microscopy System:
Application Accuracy Improvement in Leukemia Diagnosis**

Diploma Thesis
by Emmanouil Vardoulakis

Committee:

Professor Constantinos Balas (*Supervisor*)
Assistant Professor Vasilios Samoladas
Dr Nathanail Kortsalioudakis

Chania, February 2017

Abstract

Microscopy is an invaluable tool employed by researchers and medical professionals of numerous fields for extracting crucial information about a sample. In the present thesis, microscopy is combined with spectral imaging in order to provide a novel, powerful instrument aiming to improve the diagnostic accuracy of the cancerous disease known as leukemia or blood cancer. An accurate diagnosis is of utmost importance as it determines the cancer type, stage and, ultimately, treatment, all of which directly affect the patient's life expectancy and quality. Current diagnostic methods are qualitative and subjective, hence prone to human error. The presented system provides accurate, objective and quantitative measurements that can be evaluated by the medical professional during the diagnostic procedure.

The system consists of three major components: The data analysis algorithms, the user interface and the hardware. Analysis algorithms are responsible for the resulting measurements and are implemented and optimized in C++. The user interface incorporates those algorithms and provides a practical and friendly way to obtain, analyze, view and locate the areas of interest. Lastly, the hardware is a custom microscope developed in the TUC Electronics Lab, including but not limited to a custom light source of various wavelengths relevant to the sample analysis and a positioning subsystem.

Acknowledgements

I would like to thank my family for their abundant love and the valuable lessons that has taught me throughout time. Especially my mother for being there when necessary, whether it was preventing me from making life destructive choices or next to me in the hospital. I hope this thesis makes my parents proud of their son while my beloved brother and sister proud of their older brother.

The next person I want to thank is my girlfriend, Despina, for believing in me when the prospect of graduation was hazy, supporting and standing by me throughout my recovery, this journey and putting up with my indecisiveness, lack of time and crazy work schedules. You will be in heart forever.

Two persons who had significant impact in my life are my good friends Manos and Diana. I would like to thank Manos for being there for me and supporting everyday my recovery from my illness, listening to my nonsense and sharing my burden. Your friendship is gold, my friend. And Diana, for teaching me that a good friend is regardless of sex, ethnicity or time, and for being the first to support my long recovery both mentally and physically of my disease.

Of course, I would like to thank and pay my respects to Mr. Costas Balas, who trusted me with significant projects although I was an old student and had still many subjects to pass. He gave me the chance to be part of this great laboratory, get involved with innovative ideas, technologies and get invaluable hands-on experience of the industry and development processes. What's more, he employed me in his newly formed company, something I would have not even dream several years ago, thus giving my career a kickstart.

Last but not least, I would like to thank the lab members Thanasis Tsapras, Christos Rossos, Marios Kastrinakis, Petros Zografos, Nathan Kortsalioudakis and especially Thanasis Papathanasiou, with whom I work more closely, for the great mood in the lab and the epic conversations, laughs and experiences during this time!

Table of Contents

Preface	11
Chapter 1: Optical Microscopy	13
1.1 Microscopy Introduction	13
1.2 A Brief History of Optical Microscopy	15
1.3 Anatomy of a Modern Microscope	17
1.4 Principles of Functionality	20
1.4.1 Lens	20
1.4.2 Optical Path & Magnification	23
1.4.3 Numerical Aperture	25
1.5 Positioning	28
Chapter 2: Introduction to Leukemia	29
2.1 Cell	29
2.2 Blood	31
2.3 Leukocytes	33
2.4 Leukemia	37
2.5 Diagnosis & Goals	39
2.6 Staining	40
2.6.1 Eosin Y	40
2.6.2 Methylene Blue	42
2.6.3 Azure B	44
Chapter 3: Proposed Hardware	46
3.1 Introduction	46
3.2 Microscope Overview	48
3.3 Positioning Subsystem	50
3.3.1 Magnification	50
3.3.2 Spatial Coordinates	52

Chapter 4: System Algorithms	58
4.1 Introduction.....	58
4.2 Data Analysis	59
4.2.1 Description	60
4.2.2 Algorithm Steps.....	57
4.2.3 C++ Implementation & Optimization	63
4.3 Background Light Extraction.....	66
4.3.1 Description	66
4.3.2 Spectral Image at 530 nm	67
4.3.3 Infrared Using Interpolation/Cubic Spline	68
4.3.4 Gaussian Curve Fitting	71
4.3.5 Extensive Testing.....	73
4.3.6 C++ Implementation	76
4.3.7 Final Algorithm	76
4.3.8 Algorithm Steps.....	77
4.3.9 Example of Analysis.....	77
4.4 WBCs Isolation Mask	79
4.2.1 Description	79
4.2.2 Algorithm Steps.....	79
4.2.3 C++ Implementation & Optimization	82
Chapter 5: User Interface	83
5.1 Qt.....	83
5.2 Initial Screen	84
5.3 View Mode	85
5.4 Acquisition Mode	91
5.5 Positioning & Navigation	96
Conclusion & Future Work	99
References	100
Annex A: Data Analysis Pseudo-Code	101
Annex B: WBC Isolation Pseudo-Code	104

Table of Figures

Figure 1.1: A common magnifying glass.....	13
Figure 1.2: Standard compound microscope	13
Figure 1.3: Microscope slide.....	14
Figure 1.4: The first microscope by Leeuwenhoek.....	15
Figure 1.5: Chromatic aberration visualized using ray optics	15
Figure 1.6: An optical microscope of 19 th century	16
Figure 1.7: Parts of a modern compound microscope.....	17
Figure 1.8: Geometric shape of convex & concave lenses	20
Figure 1.9: Beam path of a convex lens.....	20
Figure 1.10: A real image produced by a convex lens.....	21
Figure 1.11: Virtual image produced by a convex lens.....	22
Figure 1.12: Spherical aberration of a convex lens	23
Figure 1.13: Chromatic aberration of a convex lens	23
Figure 1.14: Optical path in the microscope	24
Figure 1.15: Numerical aperture	25
Figure 1.16: Different convex lenses and their corresponding N.A.	25
Figure 1.17: Airy pattern	26
Figure 1.18: Distinguishable and indistinguishable Airy Disks	26
Figure 1.19: Convex lenses and their corresponding Airy Disks	27
Figure 2.1: Inner parts of the cell	29
Figure 2.2: Artistic depiction of blood.....	31
Figure 2.3: Classification of blood cells	33
Figure 2.4: 3D perception of N.K. cell.....	34
Figure 2.5: Stained N.K. cells	34
Figure 2.6: 3D perception of T cell	34
Figure 2.7: 3D perception of B cell	34
Figure 2.8: Stained lymphocyte.....	34
Figure 2.9: 3D perception of Basophile.....	35
Figure 2.10: Stained Basophile	35
Figure 2.11: 3D perception of Neutrophil	35
Figure 2.12: Stained Neutrophil	35
Figure 2.13: 3D perception of Eosinophil	36

Figure 2.14: Stained Eosinophil	36
Figure 2.15: 3D perception of Monocyte	36
Figure 2.16: Stained Monocyte	36
Figure 2.17: Various blood cells stained with the May-Grünwald Giemsa stain.....	40
Figure 2.18: Chemical structure of Eosin Y.....	40
Figure 2.19: Eosin Y Diagram 1	41
Figure 2.20: Eosin Y Diagram 2	41
Figure 2.21: Eosin Y Diagram 3	41
Figure 2.22: Eosin Y Diagram 4	41
Figure 2.23 Eosin Y Diagram 5	42
Figure 2.24: Eosin Y Diagram 6	42
Figure 2.25: Eosin Y Diagram 7	42
Figure 2.26: Chemical structure of Methylene Blue	42
Figure 2.27: Methylene Blue Diagram 1.....	43
Figure 2.28: Methylene Blue Diagram 2.....	43
Figure 2.29: Methylene Blue Diagram 3.....	43
Figure 2.30: Methylene Blue Diagram 4.....	43
Figure 2.31: Methylene Blue Diagram 5.....	43
Figure 2.32: Methylene Blue Diagram 6.....	43
Figure 2.33: Methylene Blue Diagram 7	44
Figure 2.34: Chemical structure of Azure B.....	44
Figure 2.35: Azure B Diagram 1	44
Figure 2.36: Azure B Diagram 2	44
Figure 2.37: Azure B Diagram 3	45
Figure 2.38: Azure B Diagram 4	45
Figure 2.39: Azure B Diagram 5	45
Figure 2.40: Azure B Diagram 6	45
Figure 2.41: Azure B Diagram 7	45
Figure 3.1: 19 th Century Microscope	46
Figure 3.2: Modern microscope	46
Figure 3.3: The custom microscope	48
Figure 3.4: Magnification values on the parfocal lens	50
Figure 3.5: ADC value for known magnification	51
Figure 3.6: Polynomial fitting for magnification calibration.....	51
Figure 3.7: Smoothing spline for magnification calibration	52
Figure 3.8: A graphics tablet.....	52

Figure 3.9: Part of the grid of SL5 Cell Finder	53
Figure 3.10: Displacement sensitivity measurements (close to surface)	54
Figure 3.11: Displacement sensitivity measurements (far from the surface)	55
Figure 3.12: Displacement sensitivity measurements (medium distance from the surface) ..	55
Figure 3.13: Repetitiveness measurements (nearby)	56
Figure 3.14: Repetitiveness measurements (medium)	56
Figure 3.15: Repetitiveness measurements (long).....	57
Figure 4.1: Image at 465 nm.....	61
Figure 4.2: Image at 505nm.....	61
Figure 4.3: Image at 530 nm.....	61
Figure 4.4: Image at 600 nm.....	61
Figure 4.5: Image at 640 nm.....	61
Figure 4.6: Image at 685 nm.....	61
Figure 4.7: Eosin Y Pseudo-color Color Map	62
Figure 4.8: Eosin Y Pseudo-color Mono Map	62
Figure 4.9: Azure B Pseudo-color Color Map	62
Figure 4.10: Azure B Pseudo-color Mono Map	62
Figure 4.11: Methylene Blue Pseudo-color Color Map	62
Figure 4.12: Methylene Blue Pseudo-color Mono Map	62
Figure 4.13: Proportions Map of the three substances	63
Figure 4.14: Data analysis algorithm implementations execution speed comparison	64
Figure 4.15: Data analysis algorithm implementations RAM usage comparison.....	64
Figure 4.16: Infrared image of blood sample	68
Figure 4.17: Spatial profile across an infrared image.....	68
Figure 4.18: Peaks colored black on the infrared image	69
Figure 4.19: Application of Linear Spline.....	69
Figure 4.20: Application of 80x80 mean filter	70
Figure 4.21: Application of vertical spline for smoothing	70
Figure 4.22: Spatial profile accross the infrared	71
Figure 4.23: Spatial profile across the resulted image, same line	71
Figure 4.24: Final image using Gaussian fitting both vertically and horizontally.....	72
Figure 4.25: Spatial profile across the extracted background image	72
Figure 4.26: Uneven distribution of cells accompanied with dirt on one side.....	73
Figure 4.27: Very low magnification.....	73
Figure 4.28: The above background should be darker on the sides	74
Figure 4.29: The resulting background is now darker on the side	74

Figure 4.30: Image divided using Gaussian - Gaussian background.....	75
Figure 4.31: Image divided using Gaussian - Polynomial background	75
Figure 4.32: Extracted background without step	76
Figure 4.33: Extracted background using a step of 50	77
Figure 4.34: Example case (normal light)	78
Figure 4.35: Example case (low light).....	78
Figure 4.36: Proportion maps without background extraction for normal light	78
Figure 4.37: Proportion maps without background extraction for low light	78
Figure 4.38: Proportion maps with background extraction for normal light	78
Figure 4.39: Proportion maps with background extraction for low light	78
Figure 4.40: Color Image	81
Figure 4.41: Phase 1	81
Figure 4.42: Phase 2	81
Figure 4.43: Phase 3	81
Figure 4.44: Phase 4	81
Figure 4.45: Phase 5 (Final)	81
Figure 4.46: Final Mask Applied on the Original Image.....	81
Figure 5.1: Initial Screen	84
Figure 5.2: View Mode	85
Figure 5.3: Loaded case on the View Mode	86
Figure 5.4: Analysis performed.....	86
Figure 5.5: Switch button changes to monochrome maps	87
Figure 5.6: Multiple cursors pointing to the same spot	87
Figure 5.7: Zooming will cause zoom in all viewers	88
Figure 5.8: Azure B thumbnail highlighted and displayed in the second main viewer	88
Figure 5.9: Proportions map double clicked.....	89
Figure 5.10: Expanded plot widget.....	89
Figure 5.11: Acquisition Mode	91
Figure 5.12: Camera configuration.....	92
Figure 5.13: Selecting camera channel for live preview.....	93
Figure 5.14: Selecting a different wavelength for the illuminance	93
Figure 5.15: Illuminance switched to 520 nm	94
Figure 5.16: Freeze button pressed.....	94
Figure 5.17: Analysis is performed & currently the image acquired at 520 nm is displayed...	95
Figure 5.18: Low magnification while previewing using Acquisition Mode	96
Figure 5.19: New map is taken and displayed.....	96

Figure 5.20: Higher magnification cause a rectangle inside the map to become smaller97

Figure 5.21: Even higher magnification.....97

Preface

The human senses are wonderful and sophisticated instruments that help us interact and collect information about our environment as well as each other. It is well known though that these complex biological processes give us only a very limited and sometimes inaccurate perception of the physical world around us.

Vision, probably the most important of our senses, lets us see only a tiny fraction of what actually exists. Through thousands of years of evolution, our eyes and brains can perceive things on a certain scale. In detail, a human, under normal light conditions, can distinguish objects that have a minimum resolution around 0.116 mm at a viewing distance of 0.4 m while the visible spectrum band is only 350 nm wide (400 nm to 750 nm), also with a varying sensitivity depending on the wavelength as well as intensity. Consequently, the amount of information that can be extracted both structurally and qualitatively for a certain object using a naked eye is very narrow.

Nevertheless, the curiosity and inventiveness of the human nature, has led in numerous ways to circumvent our natural barriers and expand our perception capabilities. More specifically, microscopes have expanded our eyesight into the microworld giving us the opportunity to view and study objects that are far beyond the resolution of the eye. That alone changed dramatically the picture we have about the cosmos, the structure of nature and, more importantly, life itself. It revolutionized the field of biology as well as numerous other fields and opened the road to a different world: the microscopic, the kingdom of atoms, molecules, cells and microorganisms.

Meanwhile, advances in computer and semiconductor technology gave rise to a special type of photography, called spectral imaging. Images of an object are captured in different wavelengths creating a dataset known as the spectral cube. The X-axis and Y-axis of an image belonging to the cube refer to spatial coordination whereas the Z-axis to the wavelength. Visualization at a particular wavelength and the knowledge of the full spectrum for a certain object vastly enhances our perception. This knowledge reveals crucial information, previously unknown and undetected by the limited human eye, about the structure, composition and even origin or future of that object. As the technology continues to evolve rapidly, spectral imaging constantly gains more and more popularity among the scientific community.

In the present thesis, microscopy and spectral imaging are combined to provide a novel, powerful instrument aiming to improve the diagnostic accuracy of the lethal disease called leukemia.

Specifically, the goals set to achieve are to provide:

- Quantitative, objective measurements of high diagnostic value for further assisting the medical professional to evaluate an incidence. Up until now, the diagnosis is based purely on qualitative criteria as well as empirical data and is prone to human error.

- A stable, fast, accurate and consistent analysis of sample areas increasing both the throughput and accuracy of diagnosis. The reliable, repetitive measurements assist the medical professional to clarify even the most controversial cases.
- A practical, easy to use positioning and navigational system, making it easier and quicker for the user to explore the sample and locate the areas of interest than the conventional methods.
- A stable, simple, straightforward yet powerful user interface encapsulating all the above in a well defined manner. Software systems are notorious for causing much hassle, ruining the user experience and degrading the overall usefulness, something that is unacceptable in this case.
- Maintain a relatively low cost of the overall system design, whereas it is possible.

Having said the above, this thesis presents the aforementioned system, which is the result of the collaborative work of many talented and capable people. The author of this thesis contributed in various ways, and, although it contains a general presentation of the system, more weight and depth is given to the contributed parts. For further clarifications and detailed explanations on topics not covered in depth, the reader is referenced to the corresponding thesis.

The text consists of 6 chapters. Chapter 1 supplies the reader with the adequate information regarding microscopy. In a similar manner, Chapter 2 briefly introduces hematology and informs the reader about leukemia disease and the current diagnostic methods. In Chapter 3, the hardware setup is presented, with more weight given on the positioning subsystem. Moving on, Chapter 4 discusses the main algorithms that the analysis of data are based on, and, afterwards, in Chapter 5 the user interface is provided. Lastly, a conclusion follows, accompanied by the potential future work.

Chapter 1:

Optical Microscopy

1.1 Microscopy Introduction

The optical microscope, which is the first microscope invented, uses visible light and lenses in order to provide a magnified image of a small object. With the advances of science and technology, though, especially spectroscopy, wavelengths unseen by the human eye, such as ultra violet and infrared, are also incorporated nowadays in combination with cameras. This extends by far the capabilities as well as the applications of the optical microscope, thus creating entirely new fields of microscopy.

The simplest form of a microscope is essentially a single (convex) lens, and is known as the *magnifying glass*. It provides a relatively low magnification of an object, usually between 2x and 5x times its diameter, with the last as an upper threshold before the image starts to



Figure 1.1: A common magnifying glass

become blurry. The highest magnification is achieved by putting the magnifying glass very close to the eye and then move in order to achieve the best focus over the object, although most of the times the lens is placed close to the object instead. Despite the fact that the magnifying glass does not provide any valuable information regarding the micro world, it has various applications in everyday life in various situations, e.g. vision correction or soldering electronics components.

Undoubtedly, the most common microscope among researchers and scientists is the *compound* microscope. It provides a much higher magnification power compared to the magnifying glass, usually between 40x and 2,000x times and it is ideal for viewing objects that are not visible to the naked human eye, such as cells. Compound microscopes make use of two (or more) convex lenses at the same time to magnify the object, although there are more lenses available for the user to choose in order to adjust the magnification. Each one of the two lenses that are used has a different purpose: the lens close to the sample object is named the *objective* lens and its task is to collect light from the object. Then, the second lens (or



Figure 1.2: Standard Compound Microscope

sometimes group of lenses), called the *eyepiece*, magnifies the image produced by the objective lens thus giving the user an enlarged image of the object.

The object of interest examined under the microscope is called *specimen*. Specimens have to be very thin in order to let light pass through them without significant distortions, so the



Figure 1.3:
Microscope slide

final magnified image is clear. Most of the times, it is mounted on a thin flat piece of glass, the *microscope slide*, which is typically 75 mm by 26 mm and 1 mm thick. That act as both a holder and protective shield for the specimen since it is usually used with a *cover slip* (or *cover glass*), which is a thinner sheet of glass that is placed over the specimen thus securing it. The slide is then placed under the microscope for examination, using side clips to lock its position.

In the next chapters, a more thorough inspection of the compound microscope will be provided by analyzing its parts, followed by the theoretical principles of operation. Lastly, the current available positioning systems for microscopes will be explored, evaluating their operation and cost. However, before all of that, a quick overview on the evolution of the microscopy throughout the ages awaits.

1.2 A Brief History of Optical Microscopy

References for early forms of microscopy can be traced as back as 2000 BC in China as well as ancient Greece, while the oldest surviving lenses were made by Assyrians up to 612 BC. [1][6] However, it was not until the very late Middle Ages, around 1590, that the first actual microscope appeared in a form of what resembles a today's compound microscope. [1] While numerous great scientists contributed to the development of the microscope, this chapter will briefly cover the most important events throughout its evolution.

Although it is not yet entirely clear who invented the modern microscope, it is usually attributed to two Dutch spectacle-makers, Hans Jansen and his son Zacharias Jansen. [1] [2][6] This duo were the first to experiment with lenses, which until then were solely used as parts of glasses for vision correction. [1][2] They arranged several lenses one behind another in a tube thus being the first to discover that the object near the tube can be optically enlarged. [2] The Jansens made such microscopes for the Dutch royalty, and is said to have a magnification power of 9x and provide a somewhat blurry image. [3][6] Unfortunately, those instruments did not make it to this day and our knowledge is based only on references. [2]

Sometime later, in the 17th century, another Dutch called Anton van Leeuwenhoek, who was a draper and scientist, really pioneered the field of microscopy and became the first man to



Figure 1.4: The first microscope by Leeuwenhoek

create and use a real microscope by today's standards. [4][5] The main reason of his success is that he successfully developed ways to make superior lenses than his contemporaries. [4][5] He grinded and polished a small glass ball into a lens, achieving a magnification of around 270x [5] which was the highest magnification at the time. Other microscopes of that era could achieve significantly lower magnifications. Using that lens, he created the first small and portable microscope, [5] depicted at left. The specimen is put on the tiny holder next to the lens, and using the metal screw below the user is able to adjust focus. Although it used a single convex lens only, opposed to the compound microscope and what the Jansens had done earlier, it was the first true microscope in the sense that it provided a clear image and powerful magnification, enabling Leeuwenhoek to observe things never seen by any human before that time ever. [4][5] Specifically, he was the first to see and

describe bacteria, yeast plants, the teeming life in a drop of water, and the circulation of blood corpuscles in capillaries. [4][5] He is now commonly known as the Father of Microbiology. [4][5]

Despite the fact that the microscopes of that era had known flaws and defects, it was not until much later, almost 200 years, in the 19th century that the next major breakthroughs in the field happened. [6] Firstly, chromatic aberration, the phenomenon of which there is a failure of a lens to focus all colors to the same convergence point, was greatly reduced. [6] This happened by making lenses combining two different types of glasses thus greatly alleviating the effect. A

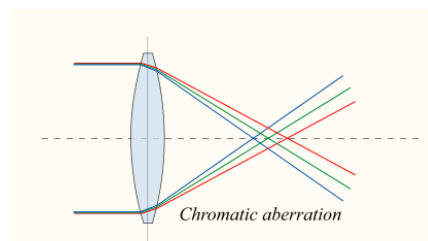


Figure 1.5: Chromatic aberration visualized using ray optics

complementary problem to the last one that was also resolved in that era was the Spherical aberration: the unequal bending of light that hits different parts of a lens, a problem solved by Joseph Jackson Lister in 1830. [6] Lister discovered that by putting lenses at precise distances from each other, the aberration from all but the first lens could be eliminated. Low power low curvature lenses could be made with minimal aberration and by using a lens of this type for the first in a series, the problem could be virtually eliminated.

Nevertheless, physicist Ernst Abbe in collaboration with Carl Zeiss made the most important contribution of that era in 1870's, resulting in vastly improving the quality of the microscopes optically as well as the manufacturing process. [6] He managed to determine



Figure 1.6: An optical microscope of 19th century

the physical laws that govern the collection of light by an objective lens and maximized this collection by using water and oil immersion lenses. Additionally, he formulated a mathematical theory, the Abbe sine condition, which is a condition that a lens must fulfill in order to produce sharp images. [6] At the same time, it is correlating resolution to the wavelength of light in which makes calculations of maximum resolution in microscopes possible. He concluded that the theoretical minimum size able to be viewed by an optical microscope is 200nm [6], since optical microscopes are only able focus on objects that are at least the size of a wavelength of light. The above contributions along with other technical innovations brought into existence the compound or optical microscope, as we know it today, and established it among

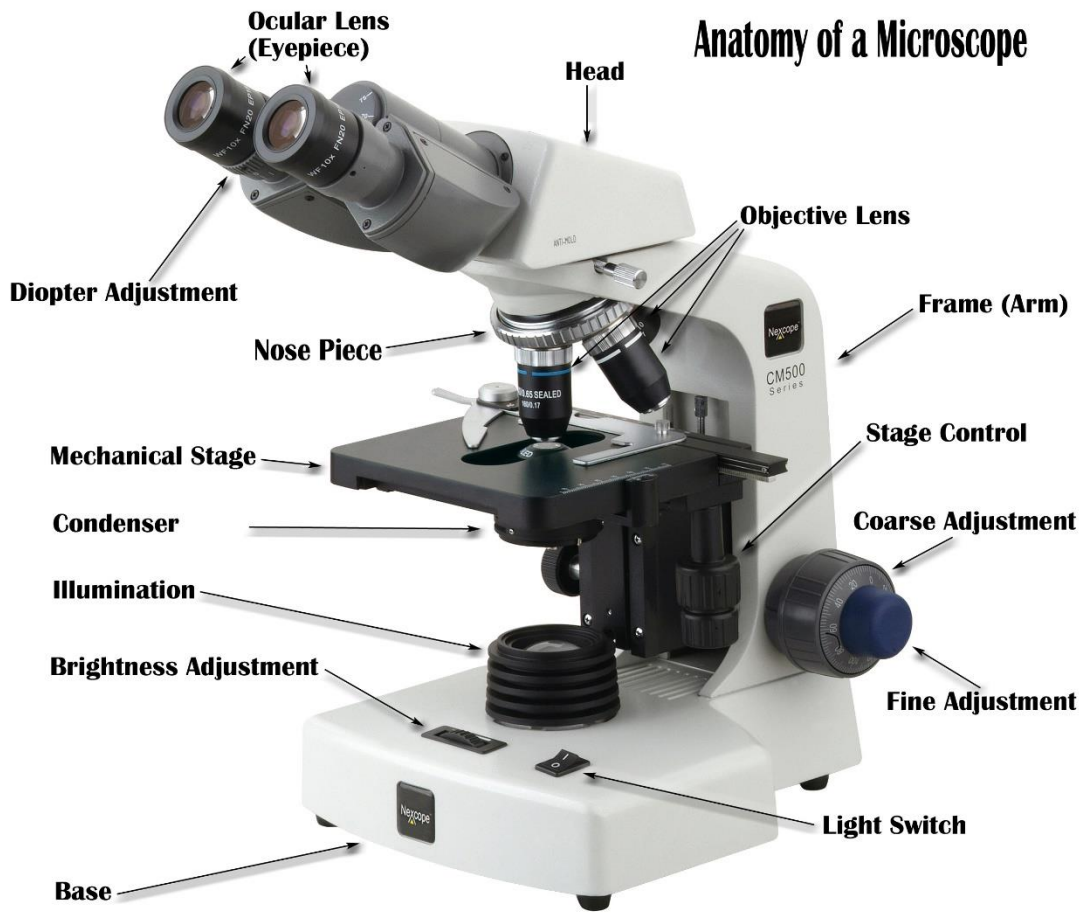
scientists as an invaluable tool of research and medical diagnosis as well as a vehicle for numerous medical revolutions.

In the following century, along with the general progress technology, the microscope had further technical improvements over its parts, such as the illumination, as well as new microscopy techniques, such as fluorescence microscopy and phase-contrast, greatly expanding its usage and capabilities. Moreover, the advances in knowledge and technology, though, gave birth to new kinds of microscopes including the electron microscope, the ultramicroscope and the scanning tunneling microscope (STM), all of which are able to cross the boundary of 200nm imposed on the optical microscope thus having the ability to view objects even down to the atomic level (STM). The last microscopes are beyond the scope of this thesis, in which we focus on the optical compound microscope.

With that said, the brief look at the evolution of microscopy is finished. In the following chapter, a modern compound microscope is going to be decomposed, and analyzed part by part.

1.3 Anatomy of a Modern Microscope

A modern compound microscope consists of several different parts, each having its own important role in the overall system operation. In this Chapter, a system breakdown is presented providing a detailed functionality description of the each corresponding part.



© OnFocus Laboratories

Figure 1.7: Parts of a modern compound microscope

Eyepiece (or Ocular Lens)

Eyepiece is set of lens that the user looks through to view the final magnified image of the object. It works in combination with objectives lens, as it will be analyzed later, in order to further magnify the image produced by the later and the magnification power is usually between 10x and 15x. The majority of modern microscopes, however, are bundled with a camera mount as well, so the user is able to attach a digital camera and view the specimen via the computer, having the opportunity to capture images.

The eyepieces are directly related to the term *field of view*, which describes the area of the object that can be seen when looking through the eyepiece. The field of view varies, depending on the magnification achieved, as well as the microscope and on properties of the eyepiece itself.

Diopter Adjustment

The functionality of this part is that it helps adjust the focus on each eyepiece and correct any vision difference between the eyes.

Head/Body Tube

It separates the eyepiece lens and objective lens and at the same time ensures the optics are aligned.

Objective Lens

The objective lens is the lens closest to the object, hence the name "objective". Light that passes through the object is gathered by this lens, which must have the capacity to reconstitute the light coming from the various points of the specimen into the various corresponding points in the image. The construction of the objective must be such so that it will be placed very close to the object in order to project a magnified image up into the body tube where it will be magnified further by the eyepieces.

A standard microscope has usually between 3 to 5 objective lenses that range in magnifying power from 4x to 100x.

Nosepiece

This is a rotating disk that objective lenses are attached. The user spins the nosepiece to select a different objective lens, thus giving the microscope different magnification capabilities.

Arm

The arm is a mechanical part, which connects the body to the base of the microscope making a stable device.

Stage

The stage is a platform that supports the slide being viewed. It has clips to hold the slides that the specimen is mounted. There is a hole in the center of the stage, which lets light that passes to illuminate the specimen.

Coarse & Fine Adjustment

These knobs help to bring the object in focus. Essentially, they move the stage up and down varying the distance between the specimen and the objective. Coarse adjustment executes a more intense move, so it is used for general focus while fine adjustment is used for perfecting the focus.

Condenser

The condenser is a lens designed to gather light from the illumination source and focus it onto the object. It may also include a diaphragm and/or filters, so the user can manage the intensity and the wavelength spectrum of the illumination. The role of the condenser is very crucial in high magnifications as it is a determinant factor of the actual resolution achieved by the objective lens.

Light Switch

It turns the illumination on and off.

Illumination

The illumination is responsible for providing sufficient light to the specimen. Modern light sources consist of halogen lamps and LEDs.

Brightness Adjustment

This knob adjusts the brightness by affecting the intensity of the illumination.

1.4 Principles of Functionality

1.4.1 Lens

Lens are the heart of the optical microscope. They are responsible for the magnification as well as every other optical phenomena experienced by the user and largely determine the overall quality and cost of the device. Hence, it raises the question: what exactly is a lens?

convex lens concave lens

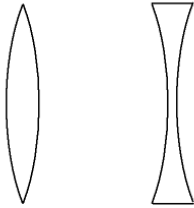


Figure 1.8: Geometric shape of convex & concave lenses

In general, a lens is defined as a transmissive optical device that focuses or disperses a light beam by means of refraction. [7] They are made of a transparent material, such as glass or plastic, which is shaped to a desired form. Usually lenses are spherical and they are classified by the curvature of the surface, which can be *convex*, *concave* or *flat*. [7] A lens is *biconvex* (or double convex, or just convex) if both surfaces are convex, just like the picture on the left, or *biconcave* if it is a concave lens. If one of the surfaces is flat, the lens is *planoconvex* or *planoconcave*. If both surfaces have the same radius of curvature, the lens is *equiconvex*. Microscopes take advantage of convex lenses, both biconvex and planoconvex, so these types of lenses are going to be analyzed.

A convex lens is characterized by the ability to converge a beam of light passing through it to a specific spot, a process commonly known as *focus*. [7] The distance from the lens to the spot is called the *focal length* of the lens, which is usually abbreviated f in the corresponding diagrams and equations. [7]

Below a biconvex lens is depicted showing how two beams of light converge to a specific spot behind the lens, the focal point:

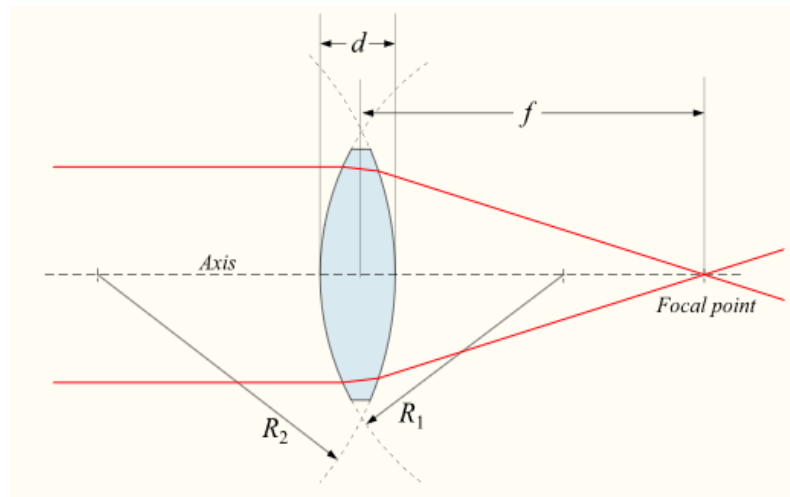


Figure 1.9: Beam path of a convex lens

Biconvex lenses have the same focal length when light travels from the back to the front as when light goes from the front to the back. [7]

The Lensmaker's equation is used to calculate the focal length of a specific lens, whether it is convex or concave:

$$\frac{1}{f} = (n - 1) \cdot \left[\frac{1}{R_1} - \frac{1}{R_2} + \frac{(n - 1) \cdot d}{n \cdot R_1 \cdot R_2} \right]$$

f is the focal length

n is the refractive index of the lens material

R₁, R₂ is the radius of curvature of the lens surface closest to the light source and farthest from the light source respectively

d is the thickness of the lens

If **d** is small compared to **R₁** and **R₂**, then the thin lens approximation can be made. For a lens in air, **f** is then given by the following, thin lens, equation:

$$\frac{1}{f} \approx (n - 1) \cdot \left[\frac{1}{R_1} - \frac{1}{R_2} \right]$$

Convex lenses are primary used to re-create an image of an object for various applications, including but not limited to cameras, microscopes or telescopes, each one based on different imaging properties of the lens as they are described below.

If the distance from the object to the lens is **S₁** and from the lens to the formed image is **S₂**, for a lens of minimal thickness, in air, the distances are related by the thin lens formula [7]:

$$\frac{1}{S_1} + \frac{1}{S_2} = \frac{1}{f}$$

Two kind of images are then produced by lens, *real* and *virtual*:

If an object is placed at a distance **S₁ > f** from a lens of focal length **f**, an image distanced **S₂** will be found according to formula above. If a screen is placed at a distance **S₂** on the opposite side of the lens, an image is formed on it that is smaller and reversed compared to the original object. This sort of image, which can be projected onto a screen or image sensor, is known as a *real image*. [7] The operation of a camera is based on this principle.

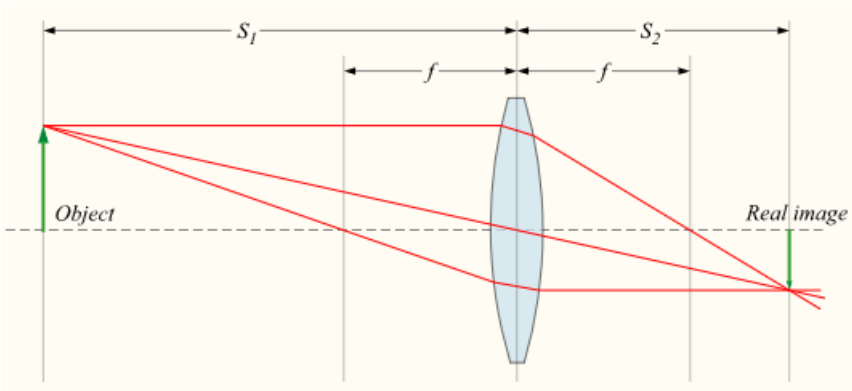


Figure 1.10: A real image produced by a convex lens

If an is placed at a distance $S_1 < f$ from a lens of focal length f , then a so called *virtual* image is produced, causing S_2 value to be negative. This indicates that the image formed is on the opposite side of the lens from where those rays are being converged [7]. Unlike real images, virtual images can not be project on a screen, but appear to an observer looking through the lens as if it were a real object at the location of that virtual image.

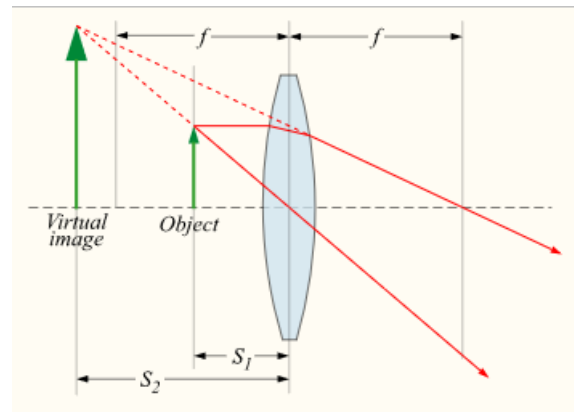


Figure 1.11: Virtual image produced by a convex lens

It then appears to a subsequent lens as if it were an object at that location, so that second lens could again focus that light into a real image, S_1 then being measured from the virtual image location behind the first lens to the second lens. This is exactly what the eye does when looking through a magnifying glass. The magnifying glass creates a (magnified) virtual image behind the magnifying glass, but those rays are then re-imaged by the lens of the eye to create a real image on the retina.

If the object is placed exactly at the focal length distance of the lens then no image is formed since the rays of light emerging from it will become parallel, a phenomenon known as the *object is imaged at infinity*. [7]

Lenses, of course, do not form a perfect image of an object and always introduces some degree of distortion, commonly known as *aberration* in optics. Several types of aberration affect the image quality. The two primal aberrations affecting a microscope's image quality still to this day are *Geometrical or Spherical Aberrations* and *Chromatic Aberrations*.

Spherical aberration occurs as a result of the shape non ideal spherical surfaces. It causes rays parallel to, but distant from, the lens axis to be focused in a slightly different place than beams close to the axis. This results as a blurring of the image.

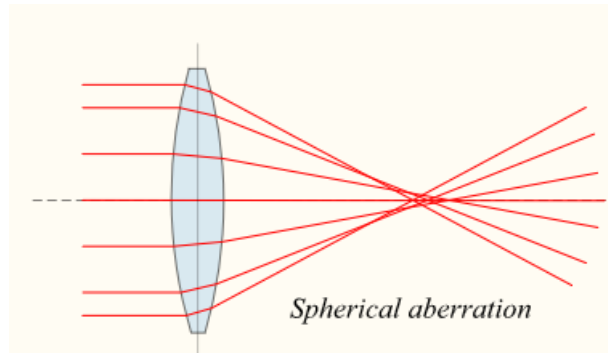
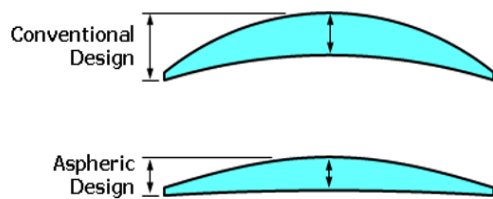


Figure 1.12: Spherical aberration of a convex lens

Lenses that are closer-to-ideal with non-spherical surfaces are now used, called aspheric lenses. Advances in technology have greatly reduced the complexity of the manufacturing cost for such lenses. In addition, these lens defects can be reduced by limiting the outer edges of the lens from exposure to light using diaphragms. Thus, spherical aberration can be minimized.



The next optical defect is a result of the fact that when light passes through a convex lens, the component wavelengths are refracted according to their frequency, a phenomenon known as dispersion. Thus, the lens fails to focus all the different wavelengths resulting in both different image size and focal point for each wavelength group. This is termed Chromatic Aberration.

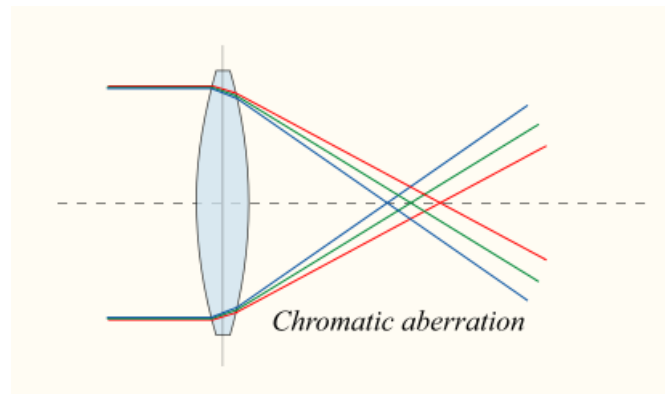


Figure 1.13: Chromatic aberration of a convex lens

It can be alleviated by using an *achromatic doublet* (or *achromat*), in which two materials with differing dispersion are bonded together to form a single lens. Although it does not provide a perfect solution, it reduces the amount of chromatic aberration over a certain range of wavelengths. A great improvement over achromat is the *apochromat*, a lens or lens system with greater correction, combined with improved spherical aberration correction.

1.4.2 Optical Path & Magnification

Compound microscopes incorporate two or more convex lenses in order to magnify the specimen. In the previous subchapter, the basic properties of convex lenses were analyzed

whereas in this one it will be shown how the combination of two lenses, the objective and the eyepiece, provide the user with the final magnified image.

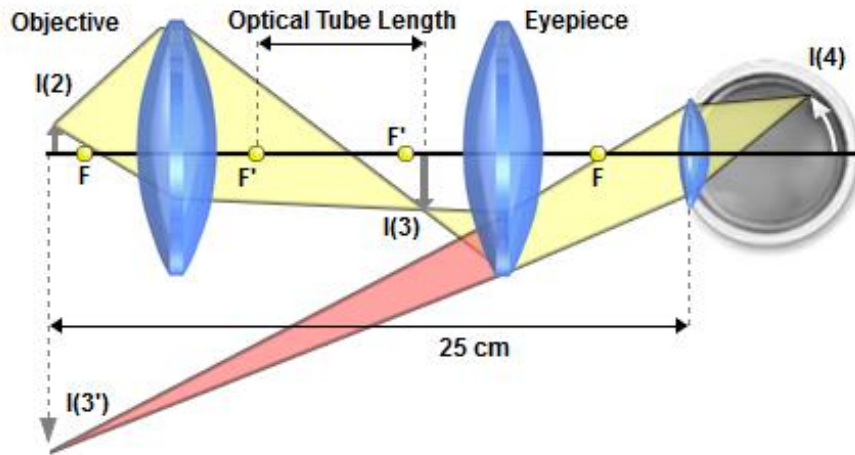


Figure 1.14: Optical path in the microscope

The objective lens of a microscope, which is the lens closest to the object being examined, gathers light, which passes through the specimen I(2), and projects a real and magnified image of the object to a fixed plane within the microscope that is called the *intermediate image* I(3). [8] The intermediate image is usually located about 10 millimeters below the top of the microscope body tube at a specific location within the fixed internal diaphragm of the eyepiece. [8]

Then, the eyepiece lens acts as a magnifying glass that further magnifies the real image formed by the objective thus creating the final, enlarged virtual image of the specimen I(3'). Consequently, the eye of the observer sees final magnified image as if it were at a distance of 25 cm from the eye I(4); hence the image appears as if it were near the base of the microscope. [8]

The image magnification is largely determined by the magnifying power of objective, which is predetermined while constructing. They typically have magnifying powers that range from 1:1 (1x) to 100:1 (100x), with the most common powers being 4x (or 5x), 10x, 20x, 40x (or 50x), and 100x. An important feature of microscope objectives is their very short focal lengths that allow increased magnification at a given distance when compared to an ordinary magnifying glass. [8] Eyepieces are also classified in terms of their ability to magnify the intermediate image. Their magnification are usually between 5x and 30x, with the most commonly used eyepieces having a value of 10x. [8]

Finally, the total magnification of the microscope is the product of the magnification values of the objective and the eyepiece. For instance, using a 10x objective with a 10x eyepiece produces a magnification of 100x. [8]

The primary reason that microscopes are so efficient at magnification is the presented two-stage enlargement that is achieved over such a short optical path, due to the short focal lengths of the optical components.

1.4.3 Numerical Aperture

Numerical Aperture, often abbreviated as N.A., is a property of the objective lens that empirically describes its ability to gather light and resolve specimen detail. In order to obtain a sharp image of the specimen, the objective must collect as much of diffracted light as possible thus higher N.A. means better resolution. [8] Because of that, N.A. also enables the comparison of two different objectives as well lens systems. [8]

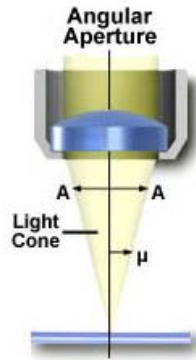


Figure 1.15: Numerical aperture

As it is depicted above, a longitudinal slice of the cone of light shows the angular aperture, a value that is determined by the focal length of the objective. The angle μ is one-half the angular aperture (A) and is related to the Numerical Aperture through the following equation: [8]

$$N.A = n \cdot \sin \mu$$

where n is the refractive index of the medium between the objective lens and the specimen.

By observing the equation, it is easily speculated that when the medium is the air (with a refractive index $n = 1.0$), then the numerical aperture is dependent only upon the angle μ whose maximum value is 90° . The \sin of the angle μ , therefore, has a maximum value of 1.0 (because $\sin 90^\circ = 1$), which is the theoretical maximum numerical aperture of a lens operating with air as the imaging medium, with the actual upper threshold being 0.95.

The image below shows how different values of the N.A. are related to higher light concentration by the objective lens, assuming that the medium in between is the air:

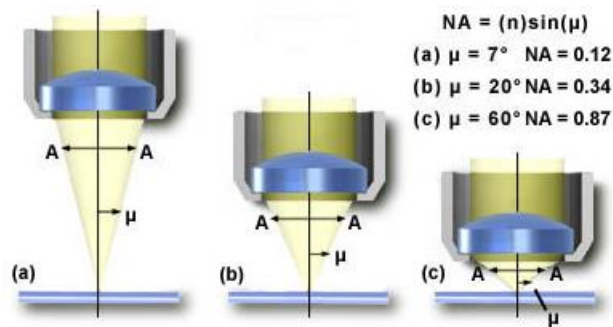


Figure 2.16: Different convex lenses and their corresponding N.A.

The way to increase the N.A. and cross the 0.95 limit imposed by the air, is to use a different medium between the objective lens and the specimen. The most common medium used for that purpose is the immersion oil, which typically has an index of refraction around 1.51. [8] Many objectives in the magnification range of 60x and higher are designed specifically for use with immersion oil. Lastly, correction of the aberration increases, up to a certain degree, the numerical aperture of an objective. [8]

As stated above, N.A. is directly related with the resolution of the acquired image. However, what is actually resolution?

Lens images an object point as a blurred spot surrounded by diffraction rings. This is called *Airy pattern*, and is caused by diffraction or scattering of the light as it passes through the specimen as well as the circular aperture of the objective. [8]

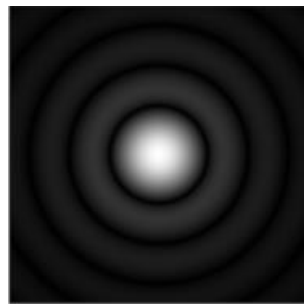


Figure 1.17: Airy pattern

The central disk of the Airy patterns is termed *Airy disk*, and it is surrounded by minimums and maximums. [8] The Airy disk is called the zeroth order maximum while the other following are first, second etc. [8] The resulting image at the eyepiece diaphragm level is actually a mosaic of Airy disks which we perceive as light and dark. Where two disks are too close together so that their central spots overlap considerably, the two details represented by these overlapping disks are not resolved or separated and thus appear as one. [8]

Thus, the resolution of a microscope objective is defined as the smallest distance between two points on a specimen that can still be distinguished as two separate entities. [8]

The image below depicts at (b) two Airy disks that can be resolved into separate entities. At (c), the distance of the two Airy disks is less than the width of these maximums, which results in a situation where the two disks are not resolvable. [8] The limit at which two Airy disks can be resolved into separate entities is determined the Rayleigh criterion. [8]

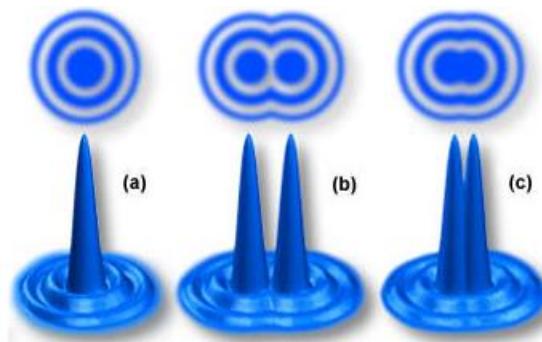


Figure 1.18: Distinguishable (b) and indistinguishable (c) Airy Disks

In order to achieve a detailed image, the objective has to project small Airy Disks, since smaller Airy Disks would provide more detail of the object. Lenses that have a high N.A. are capable of producing smaller Airy disks. The following image shows the correlation between the N.A. and Airy Disks:

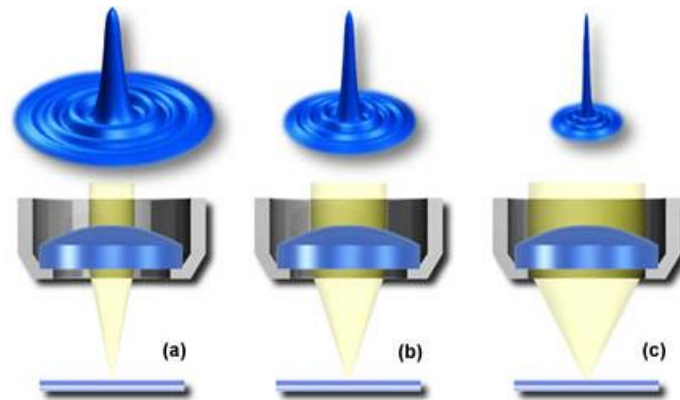


Figure 1.19: Convex lenses and their corresponding Airy Disks

As the light cone angle of an objective increases resulting in higher N.A., the size of the Airy disk decreases.

Consequently, an image may appear highly magnified by the lens but unsharp if the objective has not an adequate resolving power. [8] Additionally, the wavelength of light that is used to light the object is also a crucial factor that determines the overall resolution. [8] Since short wavelengths produce a higher resolution, the greatest resolving power is achieved with near-ultraviolet light, the shortest effective imaging wavelength. [8]

The equation that relates resolution R of an objective with N.A. and wavelength λ is: [8]

$$R = \frac{\lambda}{2 \cdot N.A.}$$

As it can be noticed, magnification is not a part of the equation meaning that the resolution is solely based on the N.A. property of the objective lens.

1.5 Positioning

Positioning is a non-standard microscope feature that helps the user to identify the coordinates of an area on the slide. This is very helpful in case the user wants to visit again a certain area in the future or to explore it another time. Usually, microscopes have rulers on horizontally and vertically on the stage in order to provide some kind of positioning, but the use of it is limited due to low accuracy achieved using naked eye.

The industry has developed solutions of high precision using piezoelectric effect, magnetic resonance and optical means for distance calculation as well as motorized solutions. While they are precise, their cost is prohibitive for the average user, hence they are incorporated only in costly microscopes targeting specific applications of microscopy and large providers.

The average cost of such device, which comes in the form of the microscope stage or stage add-on, is very high, usually exceeding 1500 € or more. This would consist of almost 1/3 to 1/10 of an average professional microscope. It is an obvious conclusion the medical professional cannot invest on such device, or the industry to provide low cost professional microscopes with positioning.

Pathologists often have a second microscope at home, examining samples privately. The way samples are examined is by visiting nearby areas until the whole sample has been scanned. This requires both time and energy from the user, who has to be focused constantly not to omit any areas of great significance.

A low cost, affordable positioning system would provide a great benefit by making their work less straining and much more efficient. Instead of worrying whether they have scanned the whole sample, the coordinates would direct the user, who can take note of the areas of interest and observe them sometime later if wanted to.

Chapter 2:

Introduction to Leukemia

2.1 Cell

The cell is arguably the cornerstone of all living organisms and that is why is often referred as the building block of life. It consists the most fundamental biological unit since it is the smallest entity able to replicate independently. [9] Since the discovering of their existence in the 17th century by Robert Hooke and Anton van Leeuwenhoek independently of each other [4] [6] , they have been fascinating the scientific community in the unique the way they build tissues cooperating to sustain life and their complex individual structure. This chapter aims to provide a quick overview of the interior of a cell directly related to the present thesis.

Components consisting a cell are called *organelles*. [9] They are specialized subunits within a cell that have a specific function. [9] As it is depicted below, a cell contains many different organelles, its one contributing in a different aspect.

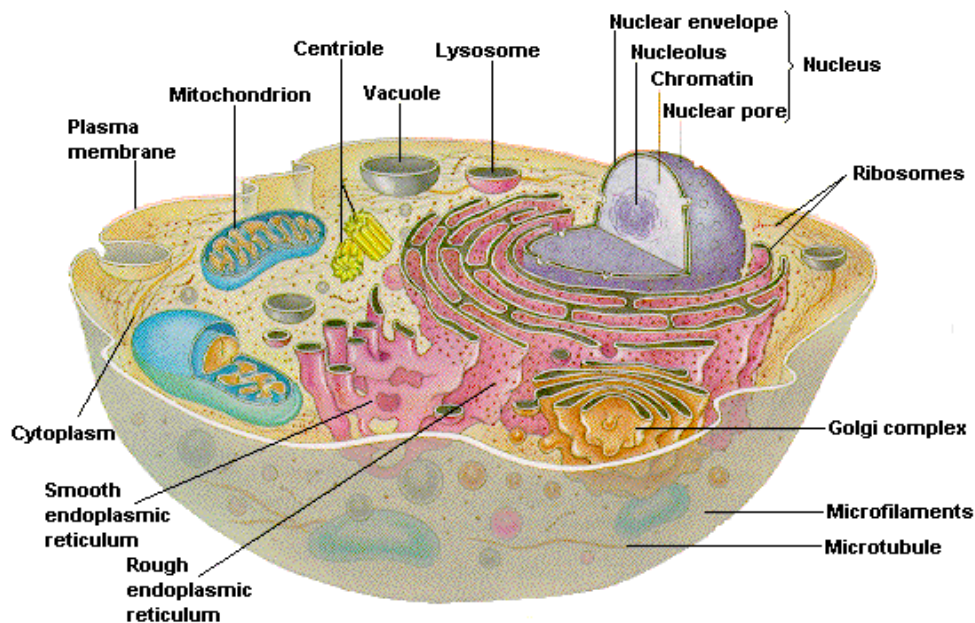


Figure 2.1: Inner Parts of the Cell

Cell/Plasma Membrane [9]

As states is name, it is a membrane that separates the interior of all cells from the outside environment. The basic function of the cell membrane is to protect the cell from its

surroundings, thus it is selectively permeable to ions and organic molecules , controlling the movement of substances in and out of cells.

Cytoplasm [9]

Cytoplasm is not an organelle itself, but the material inside the cell, excluding the nucleus where its contents are separated. It comprises cytosol, a gel-like substance enclosed within the cell membrane, and the organelles. Most cellular activities take place within the cytoplasm.

Nucleus [9]

This organelle has the role of the information processing as well as administrative center of the cell. It contains most of the cell's genetic material; the majority of its material consists of chromatin. Only advanced organisms have cell with a nucleus, and these type of cells are termed *eukaryotes*.

Chromatin and Chromosomes [9]

DNA has an enormous length of nearly 1.8 meters. In order to fit and function properly inside the nucleus, it is combined with various proteins and organized into a precise, compact structure, a dense string-like fiber. This is called chromatin.

Nucleolus [9]

The nucleolus is another organelle, inside the nucleus, with the purpose of manufacturer of ribosomes, which are the cell's protein-producing structures. A nucleus may contain up to four nucleoli (plural of nucleolus).

Mitochondrion [9]

A very important procedure of a cell is to convert oxygen and nutrients into energy. This is exactly what a mitochondrion does, serving this way as the main power generator of the cell. Apart from supplying cell with energy, it is involved in other tasks, such as signaling or cellular differentiation, as well as maintaining control of the cell cycle and growth. It is located in the cytoplasm. The number in a cell can vary, and it depends on the organism, tissue and cell type. Red blood cells have no mitochondria, whereas liver cells can have more than 2000.

Vacuole [9]

Vacuoles are membrane enclosed sections that are filled with water usually containing inorganic and organic molecules. In certain cases, they may contain solids that have been engulfed. Its structure varies according to the needs of the cell. In animal cells, they mainly assist in the larger processes of exocytosis and endocytosis, which is the extrusion and intrusion process of proteins and lipids from the cell respectively.

2.2 Blood

Blood is essentially a fluid that circulates inside the human body via the vascular system, carrying life necessary substances and oxygen delivered to the various cells. [15] Besides delivering, blood is responsible for bringing away waste products from all parts of the body. [15] The above make it extremely obvious that is a vital and irreplaceable part of the organism's well functioning mechanism. Nevertheless, its structure is quite simpler comparing to other organs inside the human body.

About half of blood is *blood plasma*, which is a fluid that comprises the blood's liquid medium. It contains proteins, glucose, mineral ions, hormones, carbon dioxide as well as the blood cells, which consist the other half of blood. [15]

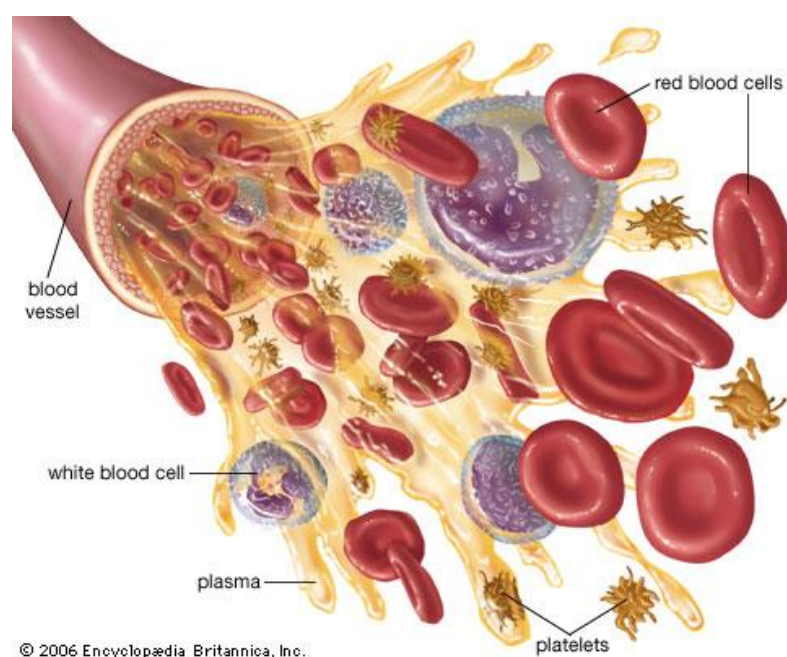


Figure 2.2: Artistic depiction of blood

All blood cells originate in the bone marrow, [11] which is the flexible tissue in the core of the bones. They derive from the *hematopoietic stem cells* or *hemocytoblasts*, which are cells that will eventually transform into any kind of blood cells through a process called *haematopoiesis*. [11] [15]

The blood cells are divided in three major categories:

Red Blood Cells or Erythrocytes [11]

Red blood cells (often abbreviated RBCs) are responsible for supplying oxygen from the lungs to the body's tissues and taking carbon dioxide from the tissues back to the lungs. They lack nucleus and many of the organelles, in order to accommodate maximum space for hemoglobin (the oxygen-transport protein). The color of the blood is attributed to this type of cells.

Platelets or Thrombocytes [11]

The function of these cells is to help form blood clots thus helping control bleeding. Platelets have no cell nucleus as well.

White Blood Cells or Leukocytes [11]

White blood cells (often abbreviated WBCs) are the line of defense of the immune system within the body and they are responsible for protecting it against diseases and intruders.

Out of the above categories, the last is of utmost importance since it is this type of cells that usually gives rise to leukemia.

2.3 Leukocytes

Leukocytes are invaluable cells of the immune system that serve as a protection shield within the body. Unlike erythrocytes and platelets, all white blood cells have nuclei. The normal white cell count is usually between $4 \times 10^9/L$ and $11 \times 10^9/L$, which is roughly translated as 4,000 to 11,000 per microliter of blood. [11]

They consist approximately 1% of the total blood volume, a number that indicates they are far less than the RBCs consisting of 40% to 45%. [11] Nevertheless, this small percentage makes a large difference to health since immunity depends on it. An increased number of leukocytes is termed *leukocytosis*, a normal immune response that reveals an indicator of disease. [11] However, it could be abnormal when the cause is neoplastic or autoimmune. A decrease below the lower limit is called *leukopenia* and states a weaker immune system. [11]

Another property of some white blood cells is the presence of tiny sacks in the cytoplasm containing enzymes that digest microorganisms. These sacks are termed *granules*, while the leukocytes containing them are called *granulocytes*. [11] The number of granules contained in a WBC varies depending on the type of cell. [11]

Leukocytes can be classified in two ways: by structure (granulocytes or agranulocytes) or by cell division lineage (*myeloid cells* or *lymphoid cells*). They will be classified below using the second approach:

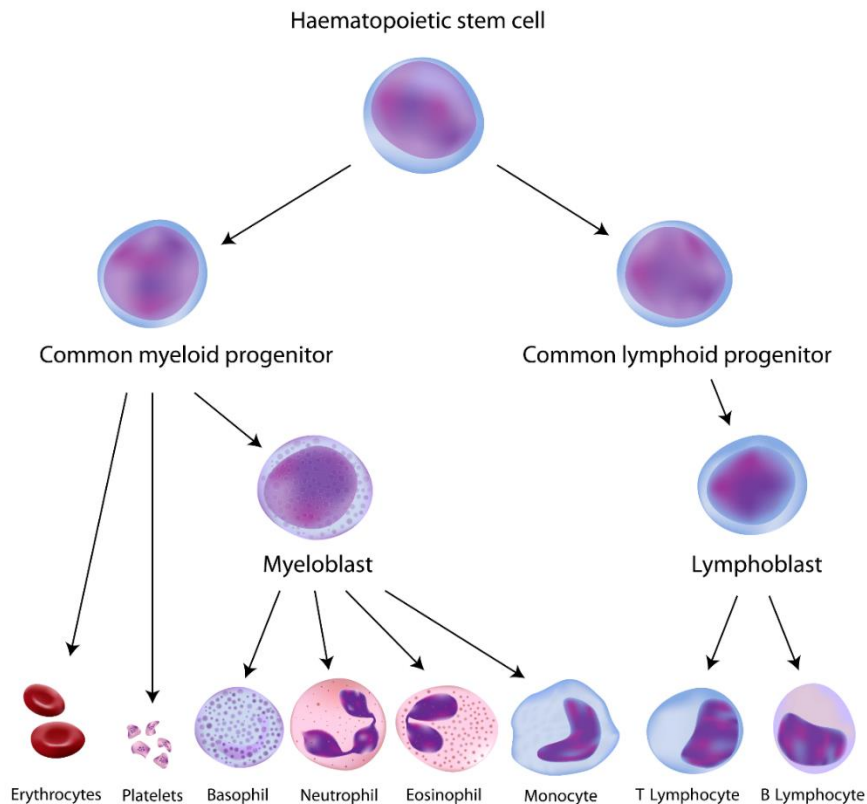


Figure 2.3: Classification of blood cells

Lymphocytes

Lymphocytes consist of about 30% all WBCs. They include natural killer cells (NK cells), which are not depicted above, T cells and B cells. They are the main type of cell found in lymph, which prompted the name lymphocyte and their size varies from 9 to 20 μm .

Natural Killer Cells: They are a part of the innate immune system (a subsystem of immune system that responds to pathogens in a generic way but does not provide long-lasting immunity) and play a major role in defending from both tumors and virally infected cells. [10] NK cells distinguish infected cells and tumors from normal cells by recognizing changes of a surface molecule.

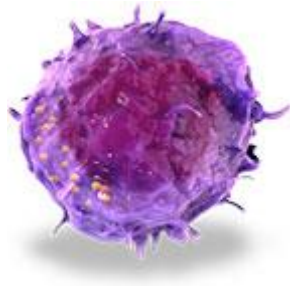


Figure 2.4: 3D perception of N.K. cell

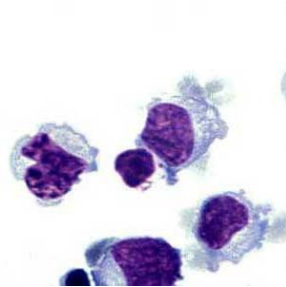


Figure 2.5: Stained N.K. cells

T cells (Thymus Cells): The name T cells derives from the fact they mature in the thymus (a primary lymphoid organ) from thymocytes (hematopoietic progenitor cells present in the thymus). [10] T cells play a central role in cell-mediated immunity, which is an immune system response that does not involve antibodies (proteins used by the immune system to neutralize pathogens such as bacteria and viruses). [10]

B cells: They function in the humoral immunity, an adaptive immune system response mediated by macromolecules found in extracellular fluids, by releasing antibodies and assisting activation of T cells. [10]

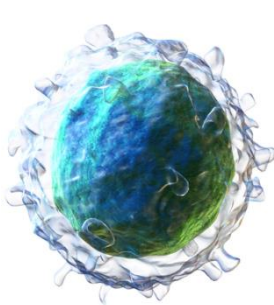


Figure 2.6: 3D perception of T cell

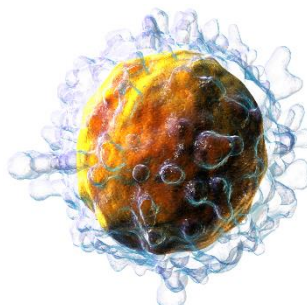


Figure 2.7: 3D perception of B cell

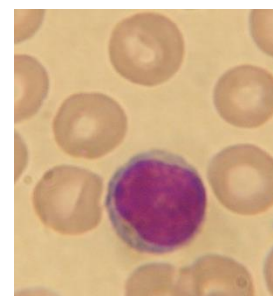


Figure 2.8: Stained lymphocyte

Myelocytes

Basophile granulocyte: Basophils represent 0.5% to 1% of WBCs. [10] Their diameter is between 12 and 15 μm . The central role of basophiles is to react in cases of inflammation as

well as chronic allergic diseases. [10] *Basophilia*, a condition in which the count of these cells rises dramatically, is seen in some forms of leukemia. They belong to the *polymorphonuclear* cells (along with eosinophil and neutrophil), named after for the nucleus' multilobulated shape.

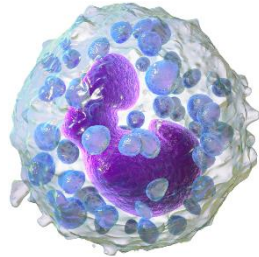


Figure 2.9: 3D perception of Basophile

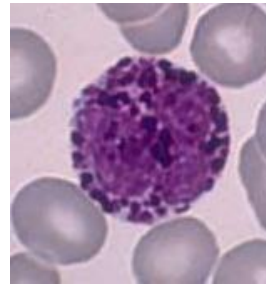


Figure 2.10: Stained Basophile

Neutrophil granulocyte: Neutrophils represent the largest share of WBCs, having a large percentage of 40% to 75% of WBCs [11] while their size is between 10 and 12 μm . They are characterized by their high agility, since they can enter parts of tissue that are inaccessible to other cells. The function of these cells is to respond quickly during the beginning phase of inflammation, usually caused by bacterial infection, environmental exposure and some cancers. [10] Low neutrophil counts, termed *neutropenia*, has been linked with some kinds of leukemia.

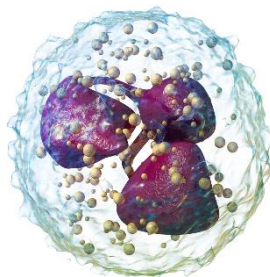


Figure 2.11: 3D perception of Neutrophil

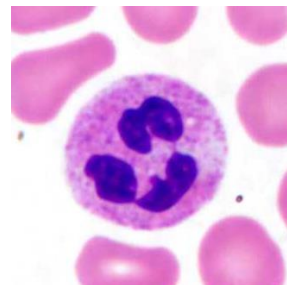


Figure 2.12: Stained Neutrophil

Eosinophil granulocyte: Eosinophils consist a relatively small percentage of WBCs, usually around 1% to 6% of all WBCs, [10] having a size between 12 and 17 μm . Their functionality is to fight against parasites as well as certain infections and modulate allergic inflammatory responses. [10] They are, also, involved in the control mechanisms associated with allergy and asthma. They are linked with Acute Eosinophilic Leukemia, which is a rare subtype of leukemia characterized by 50 to 80 percent of eosinophilic cells in the blood and marrow.

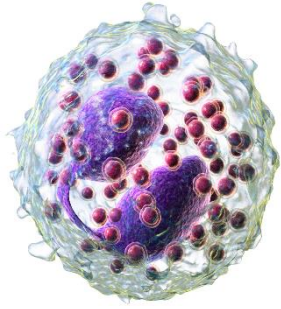


Figure 2.13: 3D perception of Eosinophil

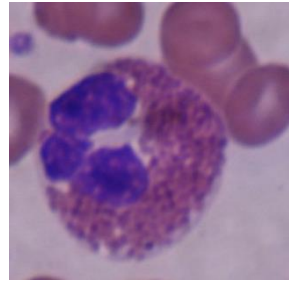


Figure 2.14: Stained Eosinophil

Monocyte: Monocytes consist around 5% of WBCs and they are the largest type of leukocytes, with a varying size between 15 and 30 μm . They are a type of phagocyte so they perform phagocytosis (essentially “eating” microbes), and respond to inflammations. [12] Moreover, they help adaptive immunity so the immune system has a memory of that specific pathogen and react better in a future encounter. [12] Monocytes are linked with Acute Monocytic Leukemia, distinct subtype of Acute Myeloid Leukemia.

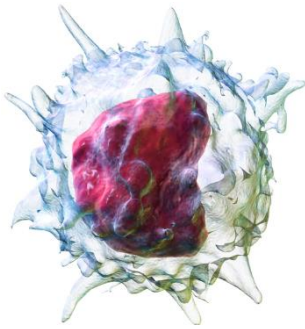


Figure 2.15: 3D perception of Monocyte

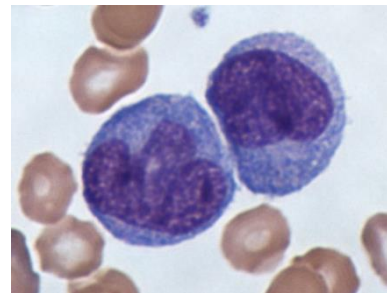


Figure 2.16: Stained Monocyte

2.4 Leukemia

Leukemia is a group of cancers that originate from the bone marrow, which produces abnormal leukocytes. These cells, which are not fully developed, are termed *leukemia cells* or *blasts*. As these dysfunctional cells proliferate, they crowd out the healthy blood cells and result in a situation where it is harder for the body to respond to various challenges such as fighting infections as well as getting oxygen to the tissues. [13] Leukemia accounts for the majority of cancers affecting childhood. [14]

The higher numbers of blasts results in a lack of blood platelets. Hence, people with leukemia may easily become bruised, bleed excessively, or develop pinprick bleeds. Additionally, immune system may be unable to respond properly to an infection or it may start attacking other body cells. This leads to experiencing frequent infection that may pose a life threat. Finally, the red blood cell deficiency leads to anemia, which may cause dyspnea and pallor. [13]

Different forms of Leukemia may be classified based on the rate the disease progress. Hence, there are two major categories, *Acute* and *Chronic*. [13]

Acute leukemia usually develops quickly meaning that the number of leukemia cells increases rapidly. People with acute leukemia may feel very tired, bruise easily, and get infections often. Chronic leukemia usually develops slowly. There may not be any symptoms, and the first sign of the illness may come from a routine blood test. [13]

The second classification is based on the type of leukocytes involved, thus there are two classes: *Myeloid* and *Lymphoid*. The former type of Leukemia starts in myeloid cells while the latter in lymphoid cells. [13]

Although there are many types of leukemia, 4 out of them from the most common types. [13] These are:

- *Acute Myeloid Leukemia (AML)*: It affects myeloid cells and grows quickly. Leukemic blast cells collect in the bone marrow and blood.
- *Acute Lymphoblastic Leukemia (ALL)*: It affects lymphoid cells and grows quickly. As in AML, leukemic blast cells usually collect in the bone marrow and blood.
- *Chronic Myeloid Leukemia (CML)*: It affects myeloid cells and usually grows slowly at first. Blood tests reveal an increased number of leukocytes. The abnormal blood cells function properly and there may be a small number of blasts in the bone marrow.
- *Chronic Lymphocytic Leukemia (CLL)*: It affects lymphoid cells and usually grows slowly. Blood tests show an increased number of leukocytes. The abnormal cells function almost as the normal white blood cells.

According to National Cancer Institute of the U.S. there were approximately 60,140 new cases of Leukemia in 2016, which comprise 3.6% of all new cancer cases. Additionally, there were 24,400 estimated deaths because of leukemia, which comprise 4.1% of all cancer deaths. Approximately 1.5% of men and women will be diagnosed with leukemia at some point during their lifetime, based on 2011-2013 data. In 2013, there were an estimated 333,975 people living with leukemia in the United States alone. Leukemia is the 10th most

common cancer in U.S. The percentage of surviving 5 years or more is estimated to be around 59.7%.

ALL accounts for approximately 75% of all childhood types of leukemia. By contrast, the most common types of leukemia in adults are AML and CLL, followed by ALL and CML.

Based on the above facts, the severity of the disease is easily concluded. A great amount of the global population is threatened and battling against this lethal cancer as these lines are written. Out of the 60.140 people that were diagnosed with the disease in 2016, almost 24.000 of them are going to pass away in the following 5 years. Considering that, the urge of more advanced technological equipment at doctors' disposal is apparent.

2.5 Diagnosis & Goals

Diagnosis of leukemia is not a straightforward standard procedure. On the contrary, it includes numerous different diagnostic tests and is characterized by uncertainty. Usually, detection of leukemia begins with an abnormal routine test or some signs and symptoms noticed by the patient that suggest medical attention. Based on the above information, the medical doctor may ask for further investigation beginning with health history and physical exam. The doctor will look for physical signs of leukemia, such as pale skin from anemia, swelling of lymph nodes, and enlargement of the liver and spleen.

In the unfortunate event that the person has strong signs of the disease, blood tests are following. It is common that even the blood tests are unable to show whether the person has leukemia or not, especially in cases where the disease is in early stages or in remission. In order to perform a blood test, the doctor takes a blood sample from the patient and in many cases a sample from bone marrow as well. The samples are placed on slides and stained and a microscope is used to examine the samples.

The specialist tries to locate areas of interest on the samples using a low magnification and when those areas are found a higher magnification is used to have a better perspective of the area and an even higher to examine it. Afterwards, the doctor tries to classify the visible leukocytes according to structure and abnormality, based on his knowledge, experience and references. This is repeated several times in order to extract a diagnosis. Sometimes, an additional blood count test is performed where the number and kind of blood cells is measured thus helping the doctors to establish a more accurate diagnosis. Many times though, the determination of the leukemia type fails which results in wrong treatments, deterioration of the symptoms and, ultimately, decease. [15]

The described procedure for leukemia diagnosis raises two fundamentals objections:

1. The diagnosis is prone to human error despite the capability and excellence of the doctors since it is based on the experience, mentality, psychology and optical physical limitations. Hence, the diagnosis is mainly subjective and qualitative, which may give rise to ambiguous diagnosis and disagreement between the medical professionals.
2. A lot of valuable time is spent on searching and identifying the critical areas on blood and marrow samples while that lost time could be spent in a more productive way regarding the diagnosis.

This thesis proposes an integrated optical microscopy system that aims to deal with the above by providing the doctor with quantitative objective measurements and a navigational system, thus assisting in a better diagnostic procedure.

2.6 Staining

Staining is a universally accepted and employed auxiliary technique in the field of microscopy that aims at enhanced contrast in the microscopic image. In biology, specifically, it is used to highlight structures in biological tissues, facilitating this way the examination of the latter by applying a certain stain or dye. Stains may provide structural details, like shape or size, as well as compositional, such as available organelles or proteins, thus making it an invaluable tool for the researcher. It is usually based on the electrostatic interaction between the dye and target molecules.

Regarding hematology, a thin drop of blood is placed onto the slide and then a standard staining process is applied, depending on the illness and sample. There are numerous dyes available for application onto the smear, but the one of interest in this thesis is the *May-Grünwald Giemsa*, the most common stain used in staining of blood smears, which contains Eosin Y (acid), Methylene Blue (base) and Azure B (base). The resulting solution, as will be further explained, is able to highlight various features of the cell making it possible for the observer to distinguish and evaluate numerous cell characteristics, as shown below:

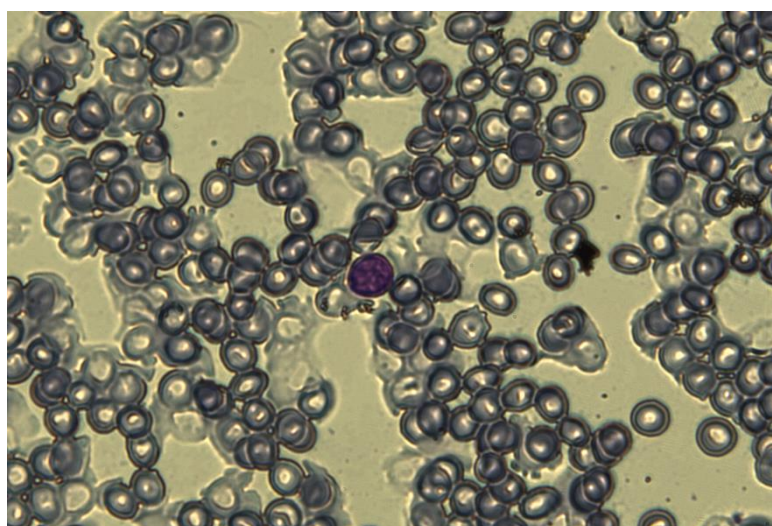


Figure 2.17: Various blood cells stained with the May-Grünwald Giemsa stain

The spectral absorbance of each substance was measured in 7 different concentrations, using the methods described in detail in [18], and were later used for the development of the system.

2.6.1 Eosin Y

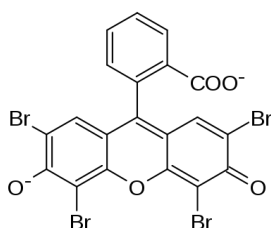


Figure 2.18: Chemical structure of Eosin Y

Eosin Y (chemical formula: $C_{20}H_6Br_4Na_2O_5$) is a fluorescent acidic compound which binds to and forms salts with basic compounds like proteins that contain amino acid residues, such as Arginine and Lysine, and stains them dark red or pink. Structures that stain readily with eosin are termed *eosinophilic*. [11]

On nucleus, it stains chromatin while on cytoplasm it stains positive charged hemoglobin parts, a protein found in Red Blood Cells, as well Neutrophil and Eosinophil granules (more on that in the following chapter). [11]

Below is the spectral absorbance in 7 different concentrations:

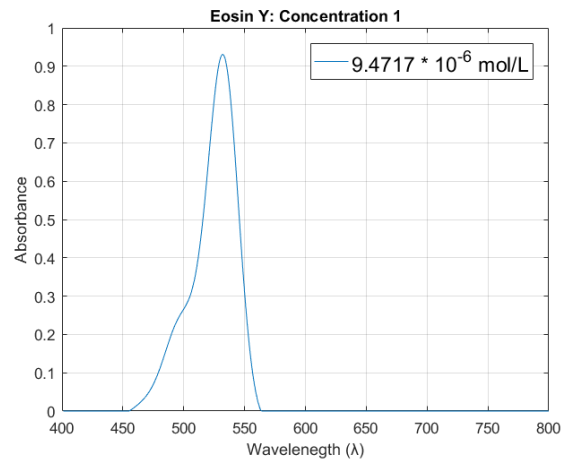


Figure 2.19: Eosin Y Diagram 1

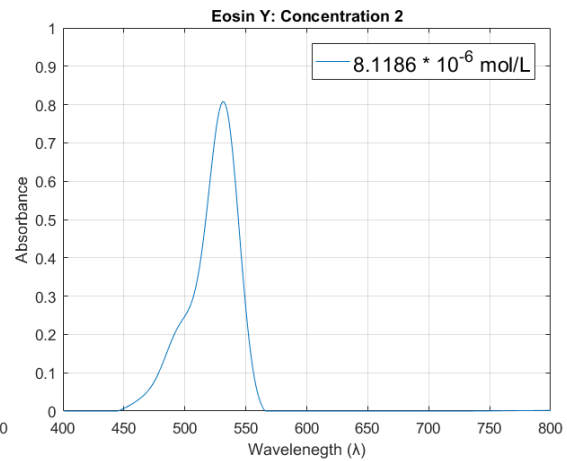


Figure 2.20: Eosin Y Diagram 2

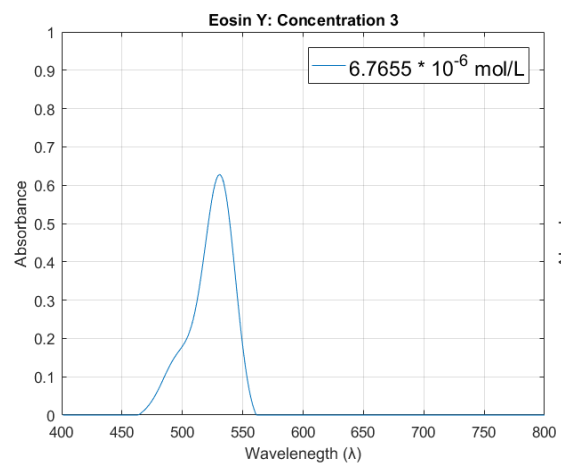


Figure 2.21: Eosin Y Diagram 3

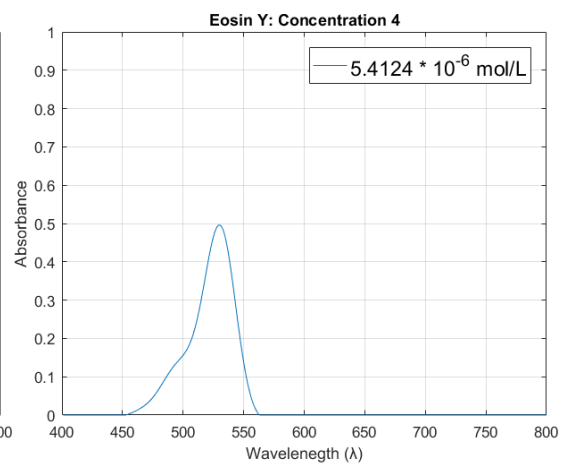


Figure 2.22: Eosin Y Diagram 4

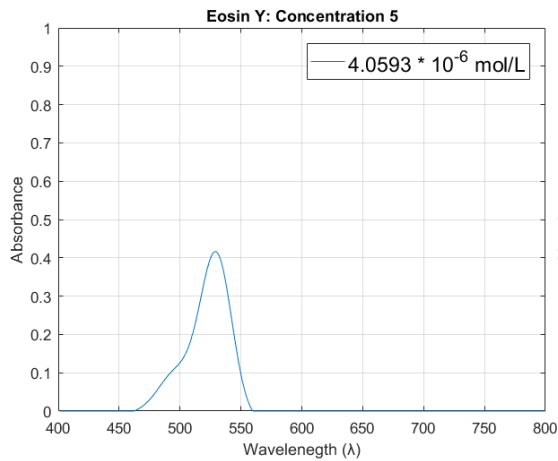


Figure 2.23: Eosin Y Diagram 5

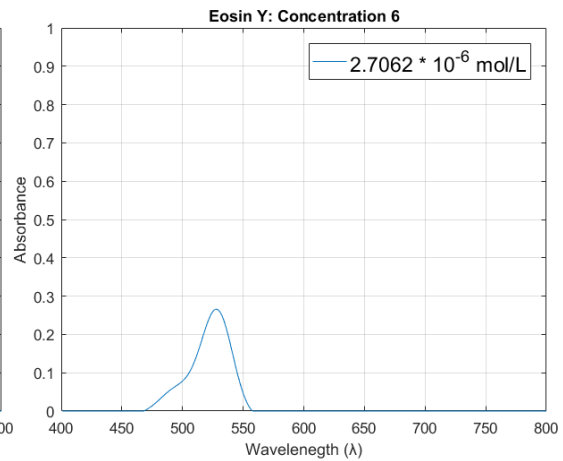


Figure 2.24: Eosin Y Diagram 6

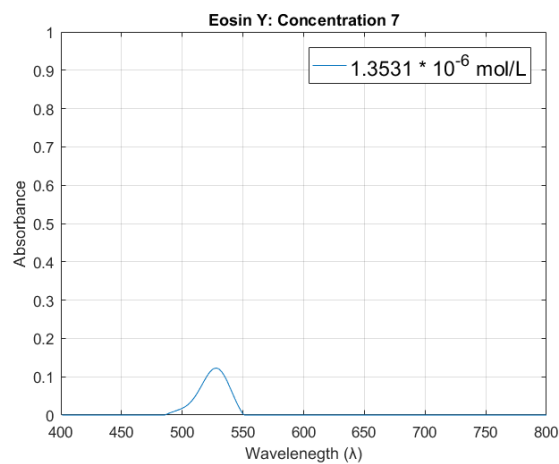


Figure 2.25: Eosin Y Diagram 7

As noticed, different concentrations have different spectrum.

2.6.2 Methylene Blue

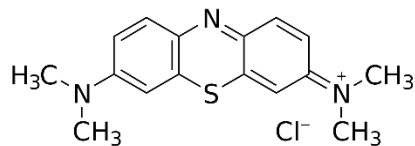


Figure 2.26: Chemical structure of Methylene Blue

Methylene Blue is a heterocyclic aromatic chemical compound and is usually attracted from the basophil parts of the cell. [11] The chemical composition of this compound is C₁₆H₁₈ClN₃S. It stains the DNA and RNA on nucleus as well as some proteins, and RNA on nucleoli. [11] On cytoplasm, it stains various proteins, cytoplasmic RNA and basophil granules as well as negative charged Neutrophil granules. [11]

Below is the spectral absorbance in 7 different concentrations:

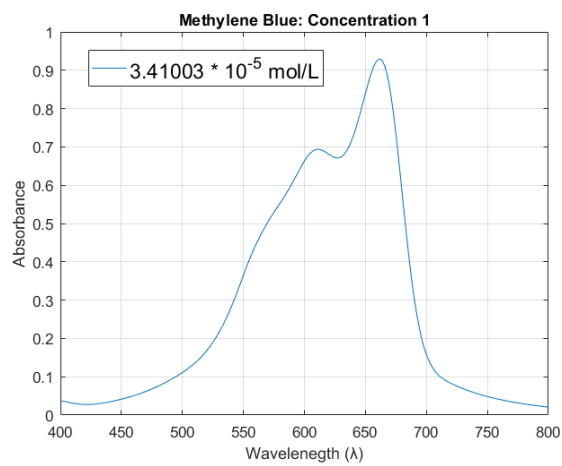


Figure 2.27: Methylene Blue Diagram 1

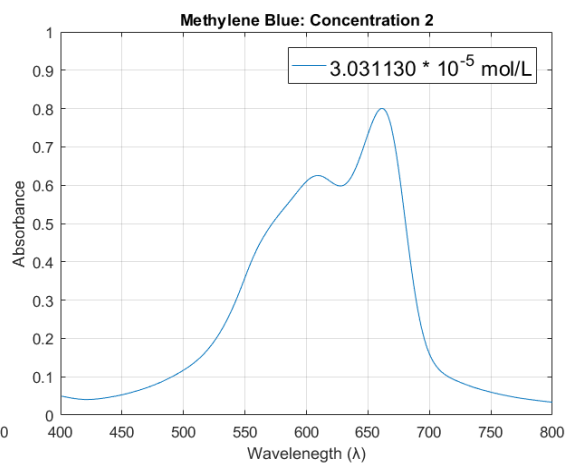


Figure 2.28: Methylene Blue Diagram 2

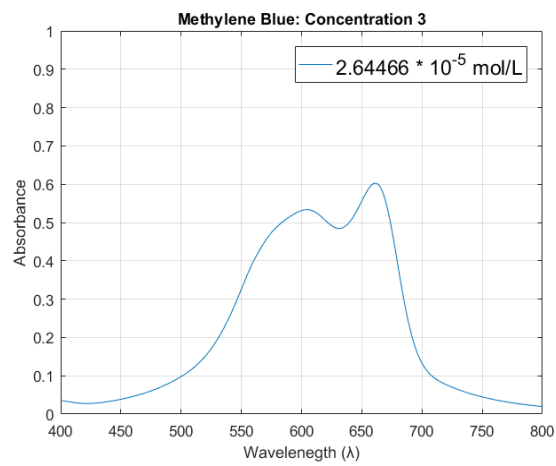


Figure 2.29: Methylene Blue Diagram 1

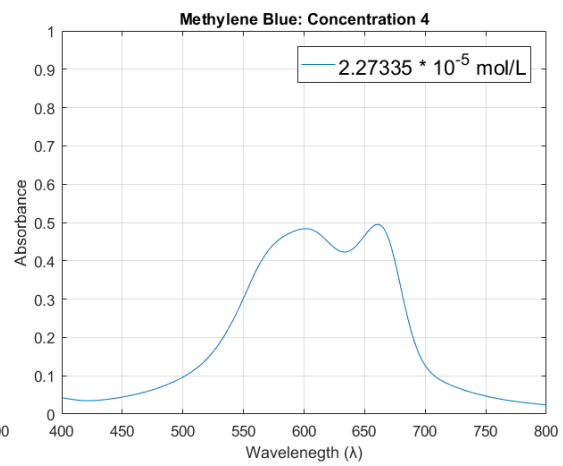


Figure 2.30: Methylene Blue Diagram 2

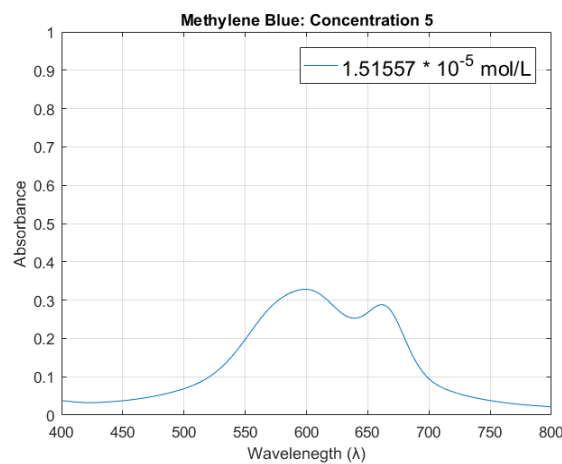


Figure 2.31: Methylene Blue Diagram 5

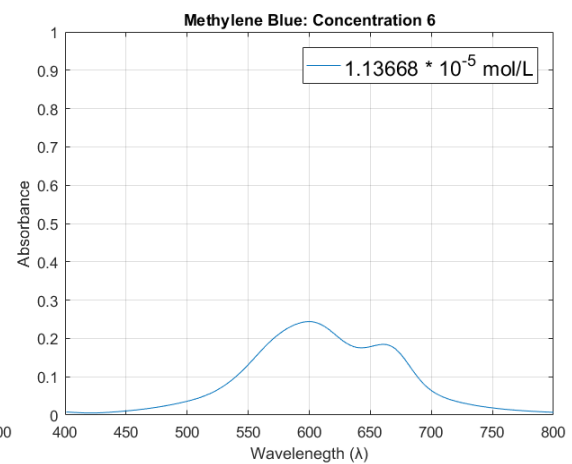


Figure 2.32: Methylene Blue Diagram 6

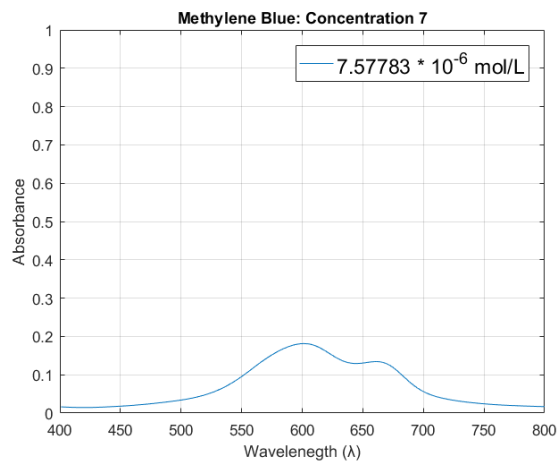


Figure 2.33 Methylene Blue Diagram 7

Again, it is easily observed that different concentrations correspond to different spectrum.

2.6.3 Azure B

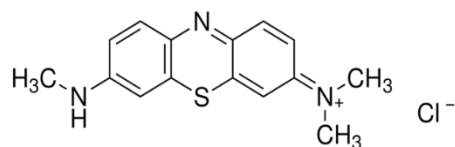


Figure 2.34: Chemical structure of Azure B

Azure B is a methylated thiazine dye formed by oxidation of Methylene Blue, with the chemical formula $C_{15}H_{16}ClN_3S$. On nucleus, it stains nucleic acids DNA & RNA, and RNA on nucleoli. [11] On the cytoplasm, it stains cytoplasmic proteins and RNA, as well as Basophil Granules and negative charged Neutrophil granules. [11]

Below is the spectral absorbance in 7 different concentrations:

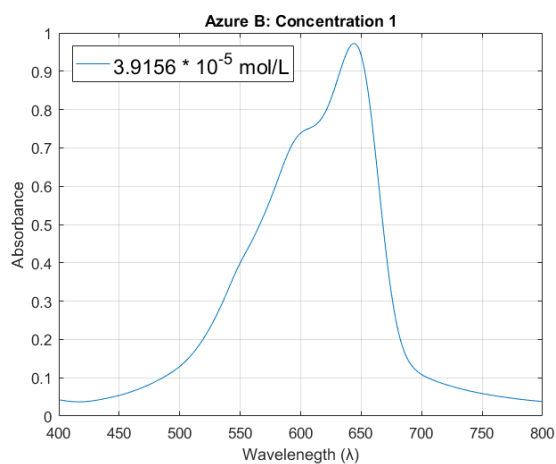


Figure 2.35: Azure B Diagram 1

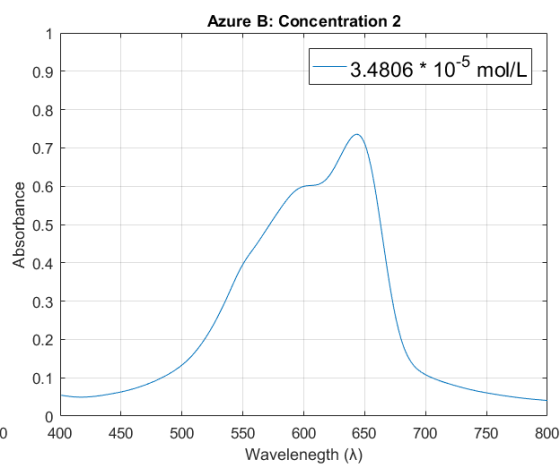


Figure 2.36: Azure B Diagram 2

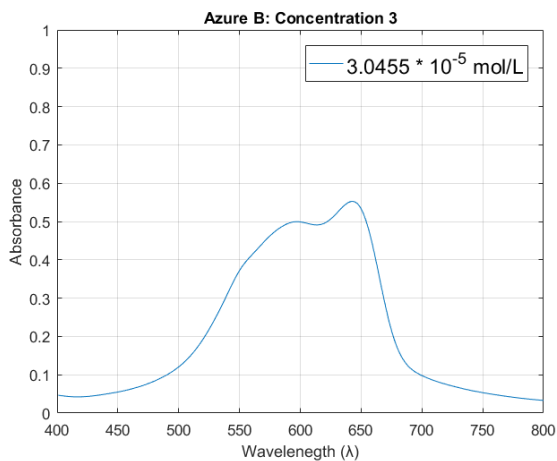


Figure 2.37: Azure B Diagram 3

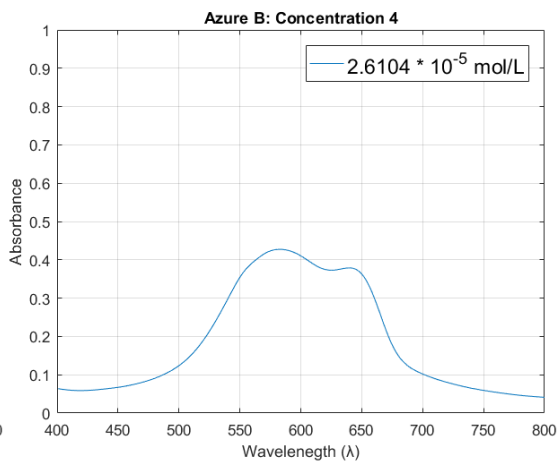


Figure 2.38: Azure B Diagram 4

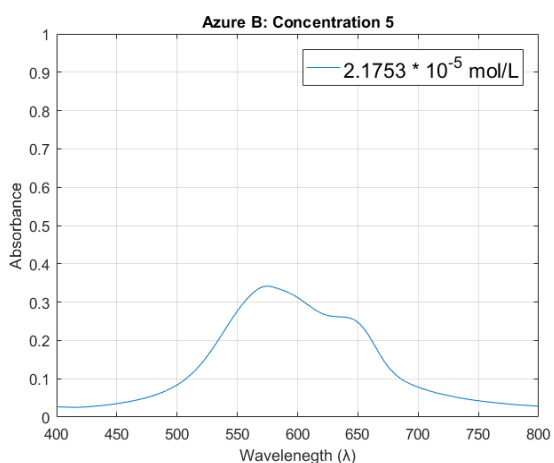


Figure 2.39: Azure B Diagram 5

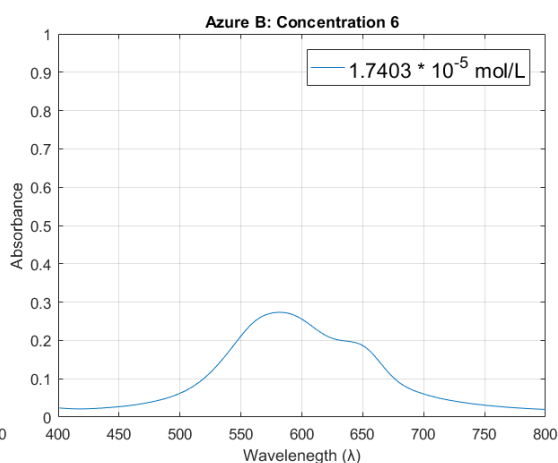


Figure 2.40: Azure B Diagram 6

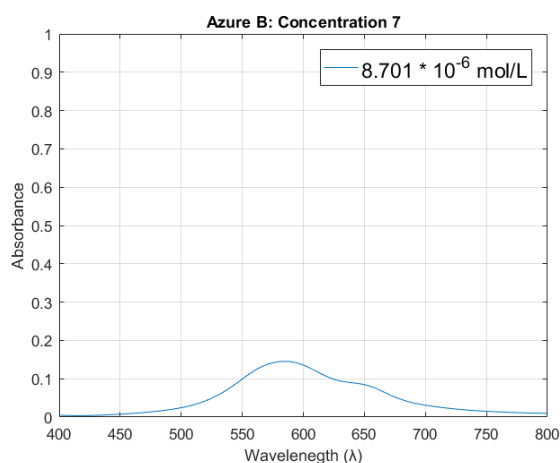


Figure 2.41: Azure B Diagram 7

Once more, it is easily speculated that different concentrations correspond to different spectrum.

Chapter 3:

Proposed Hardware

3.1 Introduction

Since its initial conception and creation, the optical microscope has come a long way. Nevertheless, since the 19th century, it has mainly evolved technically by vastly improving the components comprising it, while the overall design per se has not experienced a new breakthrough. This becomes obvious by comparing the following two microscopes. The left is more than 100 years old while the right is just a few years:



Figure 3.1: 19th century microscope



Figure 3.2: Modern microscope

Profoundly, the modern microscope produces a better, higher quality image. However, both follow the same designing guideline. They have the ocular piece, multiple objective lenses for higher magnification, condenser lens and a light source, which consist of a mirror for the old one whereas in the modern has been replaced with an electrical. While new forms of microscopy have emerged during time and new forms of microscopes have been brought to existence in order to accompany them, the optical microscope has remained quite stagnant.

To the contrary, a new microscope has been designed and developed by Professor Costas Balas and lab members. It aims to introduce novel and unique features that will enhance the user experience, utility and practice of microscopy in the field of research. Additionally, a great effort has been made so the overall cost of the instrument is reasonably low, compared to microscopes of the same category and the features they offer.

Therefore, in this chapter, a brief overview of this custom microscope will be provided focusing on the hardware aspect of the positioning subsystem, which consists the author's contribution in the microscope. Later, in Chapter 6, it will be discussed how the data obtained by that are utilized to benefit the user.

3.2 Microscope Overview

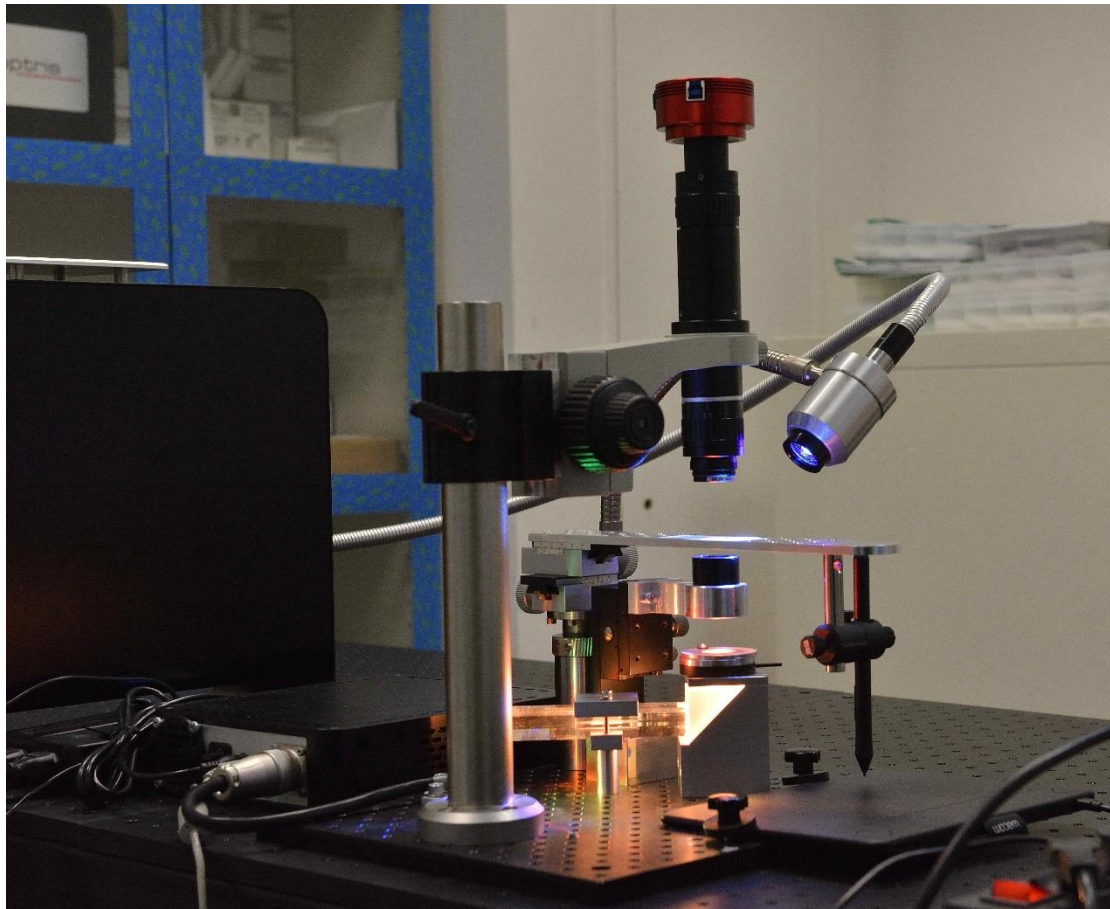


Figure 3.3: The custom microscope

Compared to the standard optical microscope, the first noticeable difference is the absence of multiple objectives as well as the ocular piece. The proposed microscope is purely digital, which means the image is only viewed using a screen, via a high-resolution digital camera, hence replacing the traditional eyepiece.

There are several reasons that contributed to the omission of the latter. The applications of this microscope, primarily, require viewing, as well as processing, images in multiple different wavelengths opposed to the standard microscope that has a single light source. Additionally, it is used for fluorescence microscopy, thus using LASER that could damage vision, and, lastly, the image view on a HD screen is a far more relaxed experience for the user than the eyepiece.

As stated above, the microscope also lacks multiple objective lens. This is because a single, parfocal lens has replaced those lenses. The type of this lens stays in focus despite changes in magnification and/or the focal length. Therefore, contrary to the standard microscope, it offers a continuous range of magnification rather than a fixed set, and is controlled by an ordinary knob. Consequently, the user is able to provide accurately the right amount of magnification considered necessary for the specimen being examined. Obviously, there is a focus error produced by the lens that is so small it can be omitted.

More often than not, microscopes have a square stage with side clips to hold the slide. Instead of this, the microscope developed in the lab has a rectangle stage with a fixed position for the slide to be placed. This offers a tight, secure place for the slide.

Beside the parfocal lens, another major difference that exists is the light source. Whereas most microscopes provide a typical white LED or halogen lamp for the specimen illumination, the custom microscope provides its own light source, which offers not only the typical white LED but also 7 more wavelengths: the visible 470 nm, 505 nm, 520 nm, 590 nm, 630 nm, 690 nm and the infrared 940 nm. The intensity control of each LED is achieved by using a microcontroller that is communicated via serial port.

The aforementioned wavelengths are used, as it will be explained in the next chapter, for the analysis of blood samples in order to improve the accuracy of leukemia diagnosis. Nevertheless, this extension is of very high significance since it enables the user to investigate samples regardless of blood in different wavelengths across the spectrum, which may extract invaluable information for the observed object. Furthermore, it creates a prospect for new applications targeting different samples to be developed in the future, long after the microscope has been shipped to an end user, thus extending its capabilities and utility.

Additionally, the light source provides LASERs for fluoresce microscopy, which is beyond the scope of the present thesis, but is an important aspect of modern microscopy as well as research per se. For more information regarding the light source, please consider reading [16] and [17].

Finally yet importantly, the microscope includes a positioning subsystem, giving the user the ability to locate his position on the slide, knowing the current magnification and navigate, as it will be further explained in chapter 5, into desired locations.

In conclusion, the overall instrument is an invaluable tool for the researcher, offering numerous features that extend its usage far beyond leukemia diagnosis. Consequently, it is not limited only to a single application and general usage, as users can individually apply it to their own field of research.

3.3 Positioning Subsystem

The positioning subsystem consists of two main parts: firstly, the magnification and, secondly, the actual location on the slide. These two are interdependent since knowing one without the other cannot provide an accurate position mapping on the slide. Thus, the two questions that are going to be discussed in this subchapter are:

- a) How the magnification is known every time.
- b) How are the spatial coordinates, which consists of two entirely different problems.

3.3.1 Magnification

The knowledge of magnifications is achieved by incorporating a linear potentiometer in the form of a knob. The potentiometer knob is attached on the magnification adjustment knob via a strap. Therefore, when the user changes the magnification using its corresponding knob, it moves the potentiometer knob as well, thus changing the resistance and, consequently, the output voltage. The latter is connected to a 10-bit analog to digital converter (ADC) of the light source microcontroller, which converts it into a number between 0 and 1023. Hence, the microcontroller serves two purposes: control the intensity of each LED or LASER and provide the current value of the potentiometer. By asking periodically the microcontroller for its specific ADC value, the current position of the knob is always known.

In order to get the current magnification, though, the output of the ADC has to be calibrated to specific magnifications. This was done as described below:



Figure 3.4: Magnification values on the parfocal lens

The magnification knob of the parfocal lens has specific values written on it, so the user is informed about the magnification at specific points. Therefore, the first step was to store the output number of ADC for those known magnifications that resulted on the table below:

Magnification	ADC
0.6	284
0.8	307
1	322
1.5	352
2	375
2.5	397
3	416
3.5	435
4	452
4.5	468
5	483

Figure 3.5: ADC value for known magnification

The value of the lowest magnification is 284 while the value of the highest is 483, which means that there are 198 points in between and 200 totally. Moreover, the difference of the first and last magnification is 4.4 and when divided by 200 results to 0.022, which means an accuracy of second significant digit is viable.

Next step was to calibrate the output of the ADC data. This was done by employing the curve-fitting applet of MATLAB as it is profound the magnification is not linear. Initially, polynomial equations in various degrees were used. The extracted equation did describe the behavior of the magnification approximately and not entirely accurately based on the above table. For example, the result of the equation for the number 322 would be 0.992 or 1.0115. This is depicted below.

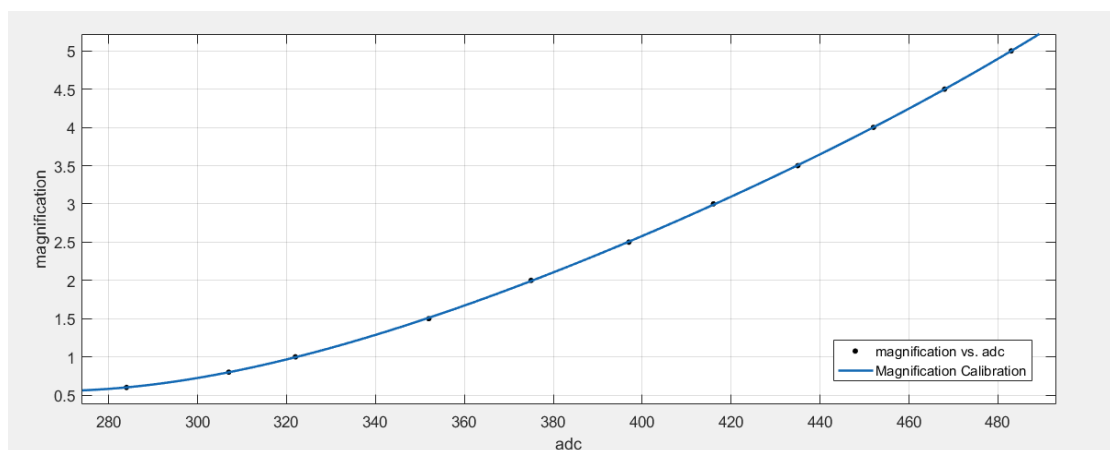


Figure 3.6: Polynomial fitting for magnification calibration

So, smoothing spline was used alternatively which fitted a curve more accurately. Due to the nature of spline, instead of an equation, a look up table (LUT) of 200 points was acquired, describing the magnification with the desired accuracy.

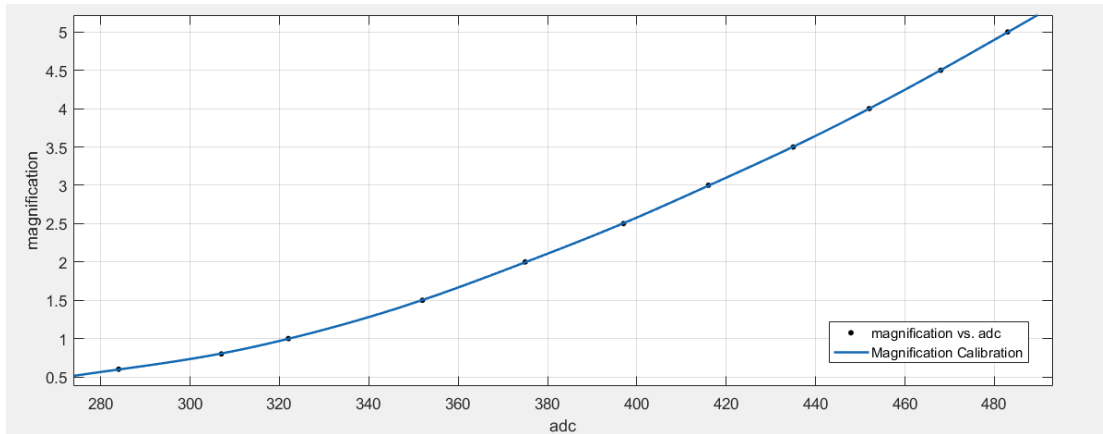


Figure 3.7: Smoothing spline for magnification calibration

It is well known that a table of one dimension is accessed using an index while specifically in this case the index has values ranging from 0 to 199. In order to get the correct index, the lowest ADC value has to be subtracted from the current ADC value.

For example, the 0.6 magnification has 284 as its ADC value, which is also the lowest possible value. So when 284 is acquired from the ADC, the difference $284 - 284$ is performed that results to 0, which is the correct position in the LUT. Another example is if 322 is acquired from the ADC. The difference $322 - 284 = 38$, so the 38th position in the LUT contains 1x as the magnification.

The above method has the advantage that only the lowest value possible has to be known in order to get the correct magnification values. Thus, the potentiometer has to be calibrated only once and in case the strap is detached for some reason, next time only the lowest value has to be known for correct functioning. It also enables a minimal effort from the end user to calibrate the magnification values.

3.3.2 Spatial Coordinates

Spatial coordinates define the exact position on the slide. Therefore, a need for a device that offers these coordinates and not only displacement values, like the optical mouse, emerged.



Figure 3.8: A graphics tablet

This device is the graphic tablet, also known as pen tablet, drawing tablet or simply digitizer, which is an input device that enables a user to hand-draw images with a special pen-like stylus, similar to the way a person draws images with a pencil and paper. It is also used as a way to get handwritten signatures. There are various technological ways to manufacture a digitizer, and the one used in the microscope belongs to the *passive* tablets category.

Passive tablets make use of electromagnetic induction technology. There is an underlying grid, where horizontal and vertical wires of the tablet operate as both transmitting and receiving coils. The tablet generates an electromagnetic signal, which is received by the LC circuit in the stylus. The wires in the tablet then change to a receiving mode and read the signal generated by the stylus. This

way, the position of the stylus on the tablet is determined. It is not mandatory for the stylus to contact the surface; it can function if it is very close. Additionally, passive tablets do not require additional power supply for the stylus, something that would raise the manufacturing complexity of the microscope.

The pen tablet incorporated in the positioning system is a Wacom Intuos, which satisfies the specifications set for the positioning subsystem:

- Passive stylus, in order not to perplex the overall system design by using wires.
- Proximity functioning, which serves not to wear out the stylus tip over time.
- Adequate displacement sensing, so the digitizer can capture slight movements.
- Adequate repetitiveness, so that the user can visit again a specific location without much hassle. Deviations are to be expected.
- Reasonable price.

The control of a digitizer can be achieved in two ways: via Windows libraries, as Human Interaction Device (HID), or via a special API, called WinTab, which is an API for digitizers developed from 1991 to 1998 by LCS/Telegraphics and from 1998 until now by Wacom. It is an interface implemented by all digitizers regardless of the manufacturer, therefore an implementation is enough for all the digitizers to be used. Consequently, if a better digitizer is found in the future, it can replace the current one without changing anything in the software. Therefore, the communication was done using the WinTab API.

The pen tablet is placed under the stage of the microscope while the stylus is attached on it, hence when moving the stage the stylus is moved as well.

A C++ class was developed based on WinTab, which configures the tablet not interfere with the computer mouse and generate events when the location of the stylus changes containing the X-Axis and Y-Axis data. The generated event is captured by the software and displays the values, enabling the user to know the spatial coordinates of the slide based on the digitizer.

Displacement and accuracy tests were performed on the digitizer by the author, in order to determine the actual capabilities of the device and conclude if its usage is appropriate for the positioning subsystem. The experiments were organized using the custom microscope and a SL5 Cell Finder Target Reticle. It is a special slide, that has a grid precisely printed on it and the distance between each dot, letter and line is known:

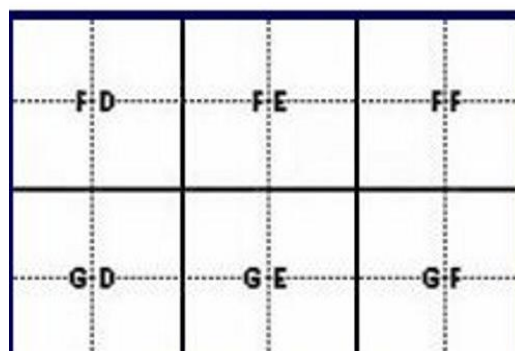


Figure 3.9: Part of the grid of SL5 Cell Finder

To determine the actual distances for each experiment, the image was magnified up to a specific magnification, depending on the test that would be performed. An image was then captured, and since the distance between two objects on the slide is known, the division of that distance with the pixels of the image consisting it reveals the relation between pixel and distance. For example, the length of a dot is 10 μm according to the specifications. If an image is captured at 4x magnification, then a dot is depicted using 80 pixels. Thus, if the length is divided by the number of pixels, results in approximately $0.12 \frac{\mu\text{m}}{\text{pixel}}$ and the number of pixels now shows the actual distance.

Firstly, the displacement sensitivity was measured; the slightest move detected by the digitizer. The manufacturer claims to have 2540 lines per inch (LPI) so it can theoretically detect motion of approximately 10 μm .

The image was magnified to 5x and using the above method results in $0.09 \frac{\mu\text{m}}{\text{pixel}}$. An image was taken, then the slide was moved and upon a change in coordinates a second image was taken. The two images were then compared to determine the actual distance that the digitizer changed its coordinates. The experiment was conducted for three different stylus positions, 15 times each for X-Axis and Y-Axis. One very close to the digitizer, one in a medium distance from the surface and another one far. The results are presented below:

Pen Close to Digitizer: Almost touching surface					
X-AXIS			Y-AXIS		
#	Pixel	μm	#	pixel	μm
1)	320	28,8	1)	1020	91,8
2)	250	22,5	2)	1240	111,6
3)	180	16,2	3)	320	28,8
4)	1250	112,5	4)	250	22,5
5)	1180	106,2	5)	1330	119,7
6)	270	24,3	6)	340	30,6
7)	370	33,3	7)	300	27
8)	1060	95,4	8)	380	34,2
9)	1410	126,9	9)	290	26,1
10)	500	45	10)	800	72
11)	260	23,4	11)	180	16,2
12)	170	15,3	12)	220	19,8
13)	1020	91,8	13)	1120	100,8
14)	200	18	14)	350	31,5
15)	290	26,1	15)	1120	100,8
Min	170	15,3	Min	180	16,2
Max	1410	126,9	Max	1330	119,7
Mean	582	52,38	Mean	617,33	55,56

Figure 3.10: Displacement sensitivity measurements (close to surface)

Pen Far from Digitizer: 7.42 mm over the surface					
X-AXIS			Y-AXIS		
#	Pixel	µm	#	pixel	µm
1)	430	38,7	1)	380	34,2
2)	800	72	2)	280	25,2
3)	280	25,2	3)	580	52,2
4)	220	19,8	4)	310	27,9
5)	140	12,6	5)	480	43,2
6)	280	25,2	6)	270	24,3
7)	620	55,8	7)	780	70,2
8)	400	36	8)	600	54
9)	480	43,2	9)	520	46,8
10)	630	56,7	10)	590	53,1
11)	420	37,8	11)	920	82,8
12)	840	75,6	12)	610	54,9
13)	720	64,8	13)	570	51,3
14)	580	52,2	14)	200	18
15)	890	80,1	15)	310	27,9
Min	140	12,6	Min	200	18
Max	890	80,1	Max	920	82,8
Mean	515,33	46,38	Mean	493,33	44,4

Figure 3.11: Displacement sensitivity measurements (far from the surface)

Pen Middle Range from Digitizer: 2.17 mm over the surface					
X-AXIS			Y-AXIS		
#	Pixel	µm	#	pixel	Mm
1)	280	25,2	1)	960	86,4
2)	210	18,9	2)	810	72,9
3)	1120	100,8	3)	690	62,1
4)	420	37,8	4)	900	81
5)	230	20,7	5)	550	49,5
6)	310	27,9	6)	450	40,5
7)	950	85,5	7)	190	17,1
8)	860	77,4	8)	460	41,4
9)	1190	107,1	9)	1260	113,4
10)	960	86,4	10)	960	86,4
11)	260	23,4	11)	280	25,2
12)	1160	104,4	12)	370	33,3
13)	260	23,4	13)	170	15,3
14)	350	31,5	14)	1230	110,7
15)	1140	102,6	15)	830	74,7
Min	210	18,9	Min	170	15,3
Max	1190	107,1	Max	1260	113,4
Mean	646,67	58,2	Mean	674,00	60,66

Figure 3.12: Displacement sensitivity measurements (medium distance from the surface)

It is profound the best results are attained with the stylus tip as close as possible on the surface. The average error of 50 μm and the worst error of 129 μm , means that the user has to move 5 or 13 cells respectively in order to get the movement detected, which is an acceptable displacement sensitivity.

Moving on, the other test was about repetitiveness. The 4x magnification was employed, which results in $0.12 \frac{\mu\text{m}}{\text{pixel}}$ and with the stylus as close as possible to the surface. A random location was chosen on the slide and a note of the coordinates as well as an image was taken. Then, the location was changed and tried to trace it back based on the noted coordinates. When getting as close to the original coordinates, a picture was taken again. The original and last picture were compared, hence the repetitiveness deviation was measured.

Again, three experiments were conducted. The first was to visit nearby locations then try to trace the original, the second to visit further locations while the third to visit very far. The results are presented below:

Short Distance - Nearby Locations				
	X-AXIS		Y-AXIS	
#	pixel	μm	pixel	μm
1)	300	36	220	26,4
2)	530	63,6	120	14,4
3)	260	31,2	10	1,2
4)	160	19,2	30	3,6
5)	520	62,4	180	21,6
6)	680	81,6	840	100,8
7)	130	15,6	900	108
8)	380	45,6	860	103,2
9)	250	30	50	6
10)	50	6	150	18
11)	220	26,4	740	88,8
12)	10	1,2	40	4,8
13)	120	14,4	820	98,4
14)	700	84	30	3,6
15)	50	6	10	1,2
Min	10	1,2	10	1,2
Max	700	84	900	108
Mean	290,6667	34,88	333,33	40

Figure 3.13: Repetitiveness measurements (nearby)

Medium Distance - A few blocks away				
	X-AXIS		Y-AXIS	
#	pixel	μm	pixel	μm
1)	600	72	150	18
2)	50	6	800	96
3)	300	36	40	4,8
4)	210	25,2	150	18
5)	70	8,4	10	1,2
6)	560	67,2	950	114
7)	500	60	60	7,2
8)	190	22,8	150	18
9)	450	54	400	48
10)	80	9,6	150	18
11)	100	12	140	16,8
12)	120	14,4	120	14,4
13)	200	24	180	21,6
14)	550	66	200	24
15)	250	30	820	98,4
Min	50	6	10	1,2
Max	600	72	950	114
Mean	282	33,84	288,00	34,56

Figure 3.14: Repetitiveness measurements (medium)

Long Distance - Other side or so				
	X-AXIS		Y-AXIS	
#	pixel	μm	pixel	μm
1)	150	18	800	96
2)	250	30	700	84
3)	500	60	220	26,4
4)	400	48	340	40,8
5)	400	48	600	72
6)	500	60	180	21,6
7)	450	54	280	33,6
8)	700	84	340	40,8
9)	440	52,8	700	84
10)	250	30	220	26,4
11)	550	66	800	96
12)	470	56,4	100	12
13)	550	66	800	96
14)	500	60	150	18
15)	550	66	500	60
Min	150	18	100	12
Max	700	84	800	96
Mean	444	53,28	448,67	53,84

Figure 3.15: Repetitiveness measurements (long)

Based on the data above, the worst-case scenario is the last case: moving far from the initial location and then trying to trace it back, which produces an average error of 53 μm. The greatest error is around 90 μm, which means the user will land more or less 9 cells away of the original location.

The amounts of error is acceptable considering the cost, the purpose of the device and the overall usage of the subsystem. Although it cannot provide coordinates so accurately compared to its more expensive counterparts, it is a decent, low cost way for the user to sense the position on the slide.

In chapter 5, a novel way for visiting locations of interest based on the aforementioned positioning system I going to be discussed.

Chapter 4:

System Algorithms

4.1 Introduction

The heart of the system, or more accurately the mind, consist of three main algorithms. The first is the analysis algorithm, which, as it will be described, performs the analysis of the spectral data acquired by the camera in combination with the custom light source. The other two algorithms are complementary to this one. The second is a background light extraction algorithm that enables a dynamic analysis of the sample, as the analysis algorithm was developed originally to function in fixed light intensity. The last algorithm isolates the WBCs. Besides helping the doctor to identify them, it reduces the analysis time by excluding unnecessary data from the acquired samples.

In this chapter, a thorough description and implementation philosophy is provided for the aforementioned algorithms.

4.2 Data Analysis

4.2.1 Description

The analysis algorithm is applied to blood and bone marrow samples that are stained with the May-Grünwald Giemsa stain. Multiple spectral images of the area of interest are captured and then the analysis is performed. Upon application, it provides the user with the amount of concentration, expressed in mol/L, of each substance that comprises the stain (Azure B, Methylene Blue and Eosin Y) for every point (pixel). Hence, it produces a quantitative, objective measurement that the medical professional can evaluate. A pseudo-color map generated based on the substance and the amount of concentration as well as a generic pseudo-color map of the three, further assists the doctor.

The first step of the algorithm is to acquire the spectral data, which consist of 6 grayscale images (one for each spectral band) known as the spectral cube. The 6 bands that the spectral images are captured and comprise the dataset are: 465 nm, 505 nm, 530 nm, 600 nm, 640 nm and 685 nm.

The acquired images are used to calculate the absorbance for each band by applying the Beer-Lambert law for each pixel in every image:

$$A = 2 - \log_{10}\left(100 \cdot \frac{I}{I_0}\right)$$

where I is the pixel value and I_0 is representing the value that *the pixel would have if the sample was not present* (thus, it will always be true that $I \leq I_0$). The Beer-Lambert law has a few reformulations and the above formula, which is the least famous, uses the percentage of the transmittance in order to calculate the absorbance.

Upon completion of the process, the images' dimensions are reformed from Width = w and Height = h to Height = $w \cdot h$ and Width = 1, essentially resulting in 6 single column matrixes with $w \cdot h$ number of rows. Then these matrixes are concatenated to form a single matrix that has dimensions $(w \cdot h) \times 6$, so each image consists of a matrix column, starting from the smallest to the greatest wavelength. Another column with the same row dimensions is then added in the beginning consisting only with number 1 for each row. Thus, the final matrix has dimensions $(w \cdot h) \times 7$.

The above wavelengths were selected via a calibration process based on:

- The absorbance spectrum of each substance (provided in subchapter 2.6).
- The absorbance spectrum of various mixtures of them.
- The fact that different spectrums of the substances are linked with different concentrations.

Using those spectra, a training set was formed and was used for calibration of the PLS (Partial Least Squares) algorithm, resulting in:

- A 7x3 weights matrix called *beta matrix*.

- The wavelengths that were be used for the above process, thus the bands used in the system.

When the beta matrix is linearly multiplied with the aforementioned matrix that was created using the acquired data, it produces a new matrix with dimensions $(w \cdot h) \times 3$. Each column of the new matrix is a prediction of the concentration of each substance for every pixel expressed in mol/L. The first column is for Eosin Y, the second is for Azure B and the last is for Methylene Blue.

Each column of the new matrix is separated to a single matrix of dimensions $(w \cdot h) \times 1$ and then reformed to a matrix of h rows and w columns, as the dimensions of the acquired spectral image data. Finally, using the calculated predictions of the concentrations, 7 pseudo-color maps are generated, 2 for each substance and 1 general.

For an in depth analysis of the analysis algorithm, the theory supporting the PLS prediction and how the training sets are formed to train PLS, consult [11] and [18].

4.2.2 Algorithm Steps

1. Capture spectral images at 465 nm, 505 nm, 530 nm, 600 nm, 640 nm and 685 nm.
2. Apply Beer-Lambert Law to each image.
3. Reshape images from Width x Height to a matrix $(\text{Width} \cdot \text{Height}) \times 1$.
4. Create a matrix with dimensions $1 \times (\text{Width} \cdot \text{Height})$. Every element is initialized to the value 1.
5. Concatenate the above matrixes with the Ones matrix first and the rest in ascending order based on the wavelength to form a new matrix with dimensions $(\text{Width} \cdot \text{Height}) \times 7$.
6. Multiply linearly this matrix with the *beta matrix*.
7. The result is a new matrix with dimensions $(\text{Width} \cdot \text{Height}) \times 3$.
8. Separate each row to a new matrix, with dimensions $(\text{Width} \cdot \text{Height}) \times 1$.
9. Reshape those matrixes back to the original image dimensions.
10. Each pixel of the new matrices corresponds to the concertation of Eosin Y, Methylene Blue and Azure B.
11. Create 2 pseudo color maps for each substance and a mixed proportions map that contains all of them.
 1. If the concertation of a pixel belongs to a specific range, paint the corresponding pixel of the substance's pseudo color map with a specific color. This consists the formation of the first 3 pseudo color maps of each substance.
 2. If the concentration of a pixel is over a certain threshold, different for each substance, then multiply the concentration with 255 otherwise set it to 0. Then, store the value in a specific channel of the corresponding pixel of the substance's pseudo color map. For Eosin Y, store the value to the red channel of the pseudo color image, while for the Azure B and Methylene Blue to the green channel accordingly. This consists the formation of the other 3 pseudo color maps, called mono maps.
 3. Merge the red channel of Eosin Y mono map, the green channel of Azure B mono map and the blue channel of the Methylene Blue mono map in order to form the proportions map.

A more detailed algorithm explanation is provided in Annex A, in the form of pseudo code. Below is an example of the application of the analysis algorithm, depicting the spectral images and the final pseudo color maps.

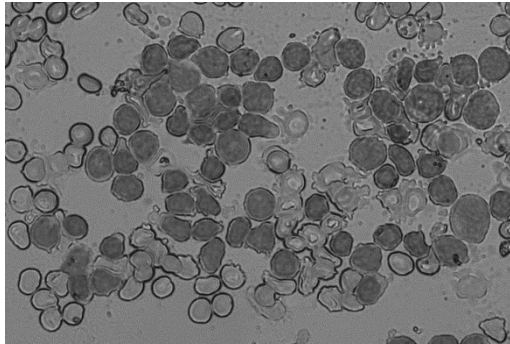


Figure 4.1: Image at 465 nm

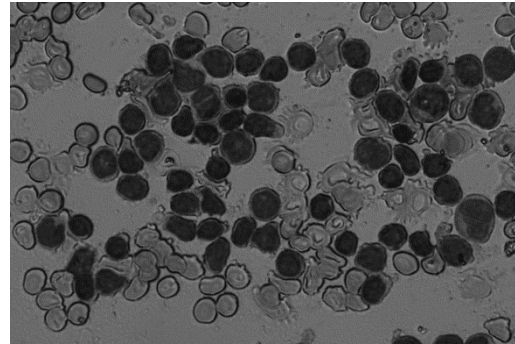


Figure 4.2: Image at 505nm

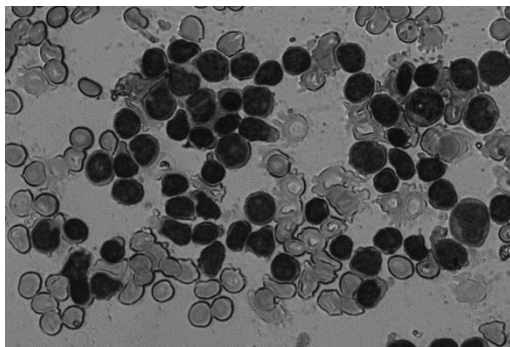


Figure 4.3: Image at 530 nm

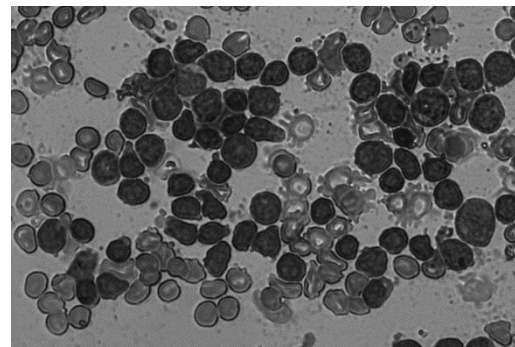


Figure 4.4: Image at 600 nm

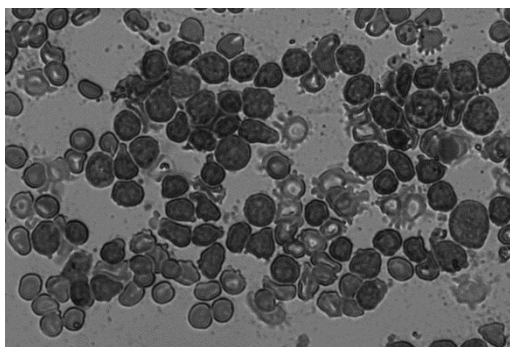


Figure 4.5: Image at 640 nm

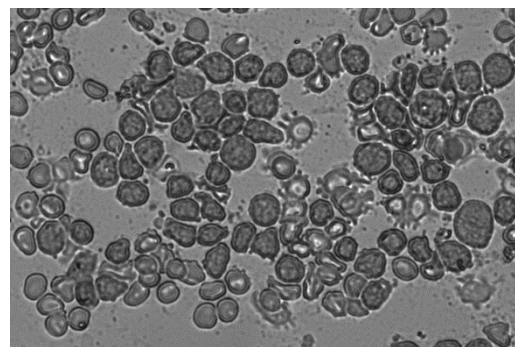


Figure 4.6: Image at 685 nm

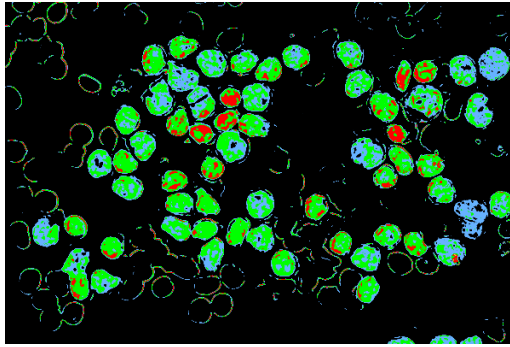


Figure 4.7: Eosin Y Pseudo-color Color Map

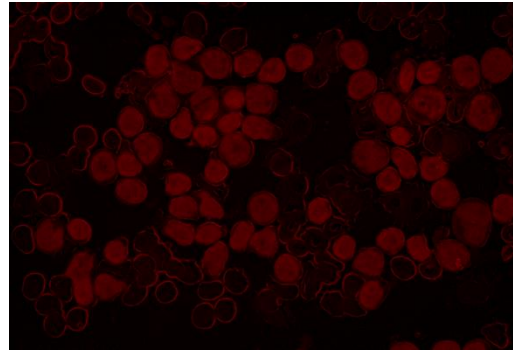


Figure 4.8: Eosin Y Pseudo-color Mono Map

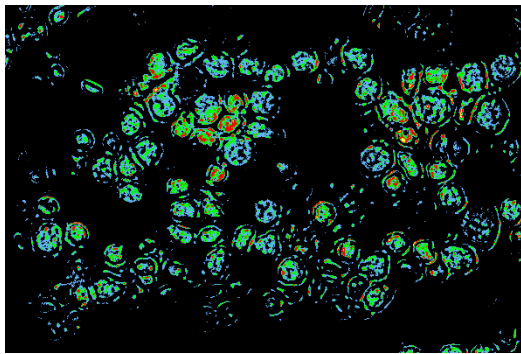


Figure 4.9: Azure B Pseudo-color Color Map

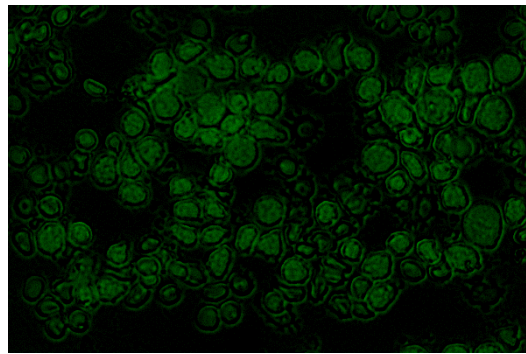


Figure 4.10: Azure B Pseudo-color Mono Map

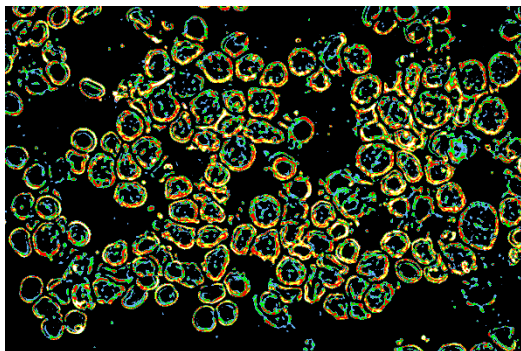


Figure 4.11: Methylene Blue Pseudo-color Color Map

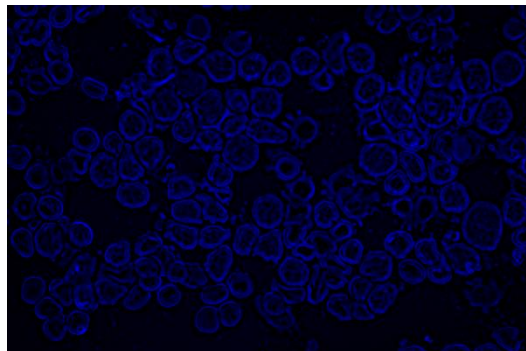


Figure 4.12: Methylene Blue Pseudo-color Mono Map

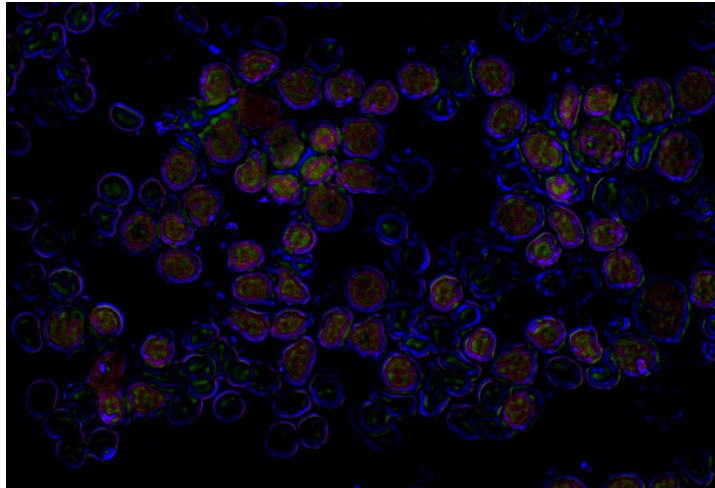


Figure 4.13: Proportions Map of the three substances

In the last map, Eosin Y consists of the red channel of the RGB image, Azure is the green channel while Methylene Blue is the last. Thus, the general proportions map is formed and different concentrations will result in different colors at a specific point. For example, blueish areas have higher concentration of Methylene Blue while greenish areas of Azure B. A point where there are high concentrations of two or three substances will have a mixed color appearance thus indicating the existence of them.

4.2.3 C++ Implementation & Optimization

The first implementation of the algorithm was made using on OpenCV (Open Computer Vision) library. This was because the library is well optimized, open source (released under BSD License) and provides linear algebra capabilities. Hence, it allows a quick implementation. OpenCV was compiled with Open MP support and SSE 3, SSE 4 and SSE 4.1 extensions using MinGW as the preferred compiler.

Although it provided a quick implementation, it had three major disadvantages:

- The memory usage was excessive due to the amount of data.
- The code was perplexed because of the different image formats. More specifically, the RGB representation of the image had to be converted to BGR because of Open CV and then backwards as well as the different datatypes.
- The footprint of the overall software grew up significantly because of library. In addition, ideally, it would be better a dependence on third party libraries to be avoided unless necessary.

The second implementation of the algorithm was made with the above three in mind, as long as it would provide an equal or greater speed of execution.

A careful inspection of the algorithm revealed that whole process was repetitive for each group of pixels. Therefore, instead of doing the process as described above, it could be done for each group of pixel from start to the end rather than proceeding step by step for all pixels.

For example, it is possible to take the first pixel of each spectral image and do the whole process: convert to absorbance, predict the concentration of the substances and then

determine the pseudo-color for that specific pixel in the final maps. Then follows the second pixel, the third etc, until arriving at the final maps pixel by pixel. This loop has to be done $w \cdot h$ times.

The above implementation greatly reduces the code as well as the complexity since it was much more straightforward. Moreover, it reduces the memory usage dramatically since only temporary variables are used to store intermediate results until arriving to the final pseudo color maps.

A comparison of the two algorithms follows in charts:

System Reference:
Intel i7 Core-6700HQ x64 2.60 GHz | DDR4 8GB | 6.439.680 pixels

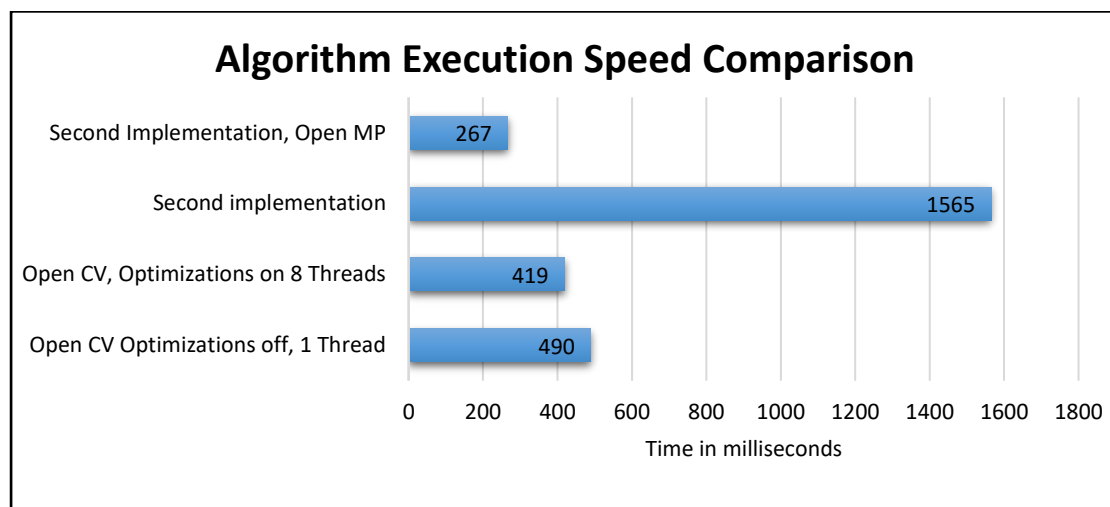


Figure 4.14: Data analysis algorithm implementations execution speed comparison

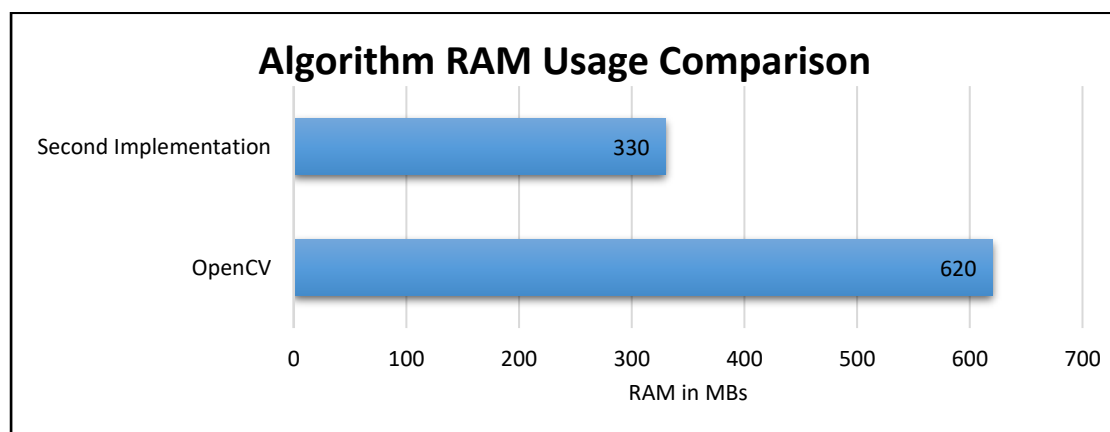


Figure 4.15: Data analysis algorithm implementations RAM usage comparison

The second implementation is much slower than the Open CV because of the heavy optimizations of the latter, however using Open MP for the second results in an almost twice as fast execution. This is because each loop is independent of the other so it favors

parallelism as the cores are utilized efficiently. The algorithm could be further optimized by employing SIMD instructions.

A reasonable question that arises is if the end user's computer does not contain multiple cores then Open CV would perform better. Although this is true, there are three arguments against it:

- Firstly, single core CPUs are becoming rare nowadays. Modern computers employ at least 2 cores, more commonly 4, so that would result in speeds equal or close to Open CV performance.
- Secondly, the software targets high end computers and is developed with that in mind.
- The third and most important argument is that the, as it will be shown in the following chapters, a WBC mask was developed. This mask isolates WBC as these cells are of greatest interest and analysis is only performed on the corresponding pixels and not on the whole image as above. Hence, it favors the usage of the second implementation since it enables to skip pixels that are excluded by the mask, which is impossible using the Open CV implementation. This reduces time even more, between 30 to 250 ms depending on the amount of pixels. Worst case scenario is that the whole image has to be analyzed, thus an upper bound of 250 ms.

Considering the mentioned arguments, the second implementation was established as the way the analysis would be made.

4.3 Background Light Extraction

4.3.1 Description

The first step upon acquiring the spectral images, as seen in the previews chapter, is to convert them from transmittance to absorbance using Beer-Lambert Law,

$A = 2 - \log_{10}(100 \cdot \frac{I}{I_0})$, for every pixel. A careful inspection of the equation reveals that:

- I corresponds to the intensity of the light on a particular surface and in this case the cells on the slider, which is translated as the intensity of the camera pixel.
- I_0 corresponds to the intensity of the initial incident light on that surface, which in this case is the intensity of the LED light.

It is obvious that the ratio $\frac{I}{I_0}$ is of great significance for the analysis process. In order to maintain constant results despite changes in lighting, then the above ration has to be constant and this means that those changes must affect both I and I_0 .

While developing the system, the need of knowing the incident light on the cells every time the analysis process was going to occur quickly emerged. This is equivalent with the so-called “background” of the area of interest, which was named after that due to the existing space between cells. That space makes incident light look like a background.

Since the analysis is performed using optical means (microscope and camera), the intensity of the incident light (background) is relative. This is because it is not strictly defined by intensity of the LED light source (where in that case would be constant and absolute, thus only one set of values would be enough to determine it). It is heavily influenced by a series of factors such as the camera, shutter speed, zoom, gain, lens, alignment of the microscope and many others.

A simple example would be the following: Consider a scenario where the slider is removed from the stage, so user only sees the background on the screen. If shutter speed is fluctuated then although the background is constant from the LED source perspective, it varies greatly from the camera perspective, consequently affecting and alternating the results dramatically.

Provided that the LED light source has been calibrated for the camera to be flat in every wavelength, then it can safely be assumed that, from the camera perspective, the background intensity of each wavelength is the *same* thus there is no need to find a different background for every LED.

While in an experimental state, the hematological analysis had been designed to functions only in a constant, strictly defined background intensity. More specifically, it was assumed that the incident relative light for each spectral image captured by the camera:

- a. Had a specific given intensity value of 180.
- b. That intensity was the same for every point of the area (pixel on camera).

During the integration of the system by analyzing samples in work like conditions, the following incidents occurred, all of which could be potentially eliminated by knowing the incident light:

- Static and hypersensitive system

Every change in the setup which would affect the lighting (e.g. shutter speed, zoom in/out, camera) would alter the ratio $\frac{I}{I_0}$ since the nominator would be different but the denominator would not change accordingly, thus different results. This is because I_0 was constant and equal to 180, while I , the intensity of the pixel, would be different even for minor changes. However, always knowing the background before the analysis takes place allows the system to be dynamic and adjustable in the corresponding changes without being affected, up to a certain degree, by those. If prior to the analysis the background has been extracted, the aforementioned ratio is almost constant all time.

- Lighting Inhomogeneity

This is a phenomenon where the incident light is not distributed the same across the sample area to be analyzed due to lens, a misalignment and other factors. Consequently, the results were considerably different from what should be in various places of the area. This happened because the intensity of background light is varies across the area. Hence, if the background is known, the lighting differences of each place are taken into account via the correct I_0 resulting in a correct ratio.

All the above clearly stated the need to develop a method for extracting the background every time an analysis is going to take place. Many different approaches were tried until arriving in the final form of the algorithm. They will be discussed below.

4.3.2 Spectral Image at 530 nm

The first approach of the problem was by using the spectral image at 530 nm because the greatest absorbance happens at this wavelength so there is a contrast enhancement between cells and background. The main concept was to remove all cells by setting the corresponding pixels to zero so only the background is preserved. Afterwards, the space of those cells would be filled by interpolation. Although some early implementations were done followed by their results, the idea was quickly abandoned since in cases where the population of the cells is dense the above would be doomed to failure.

Furthermore, it became obvious that the background extraction is not possible using the visible spectrum so a decision was made to develop the procedure using near infrared light. The cells exhibit an interesting property at those wavelengths that could be taken advantage, which is that they do not interact with light essentially becoming featureless and transparent. Hence, there is enough information to extract the background, as it can be seen below:

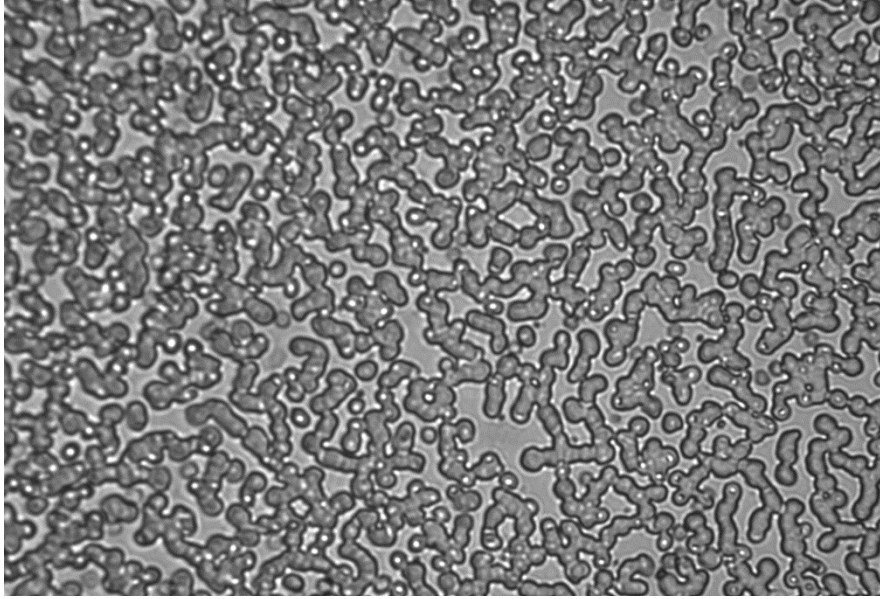


Figure 4.16: Infrared image of blood sample

4.3.3 Infrared Using Interpolation/Cubic Spline

The first approach of the problem using the infrared image was by taking a spatial profile across various lines and it was assumed that the background is the curve that fits to the profile, maintaining its “shape”. Below is a typical spatial profile of the infrared is presented:

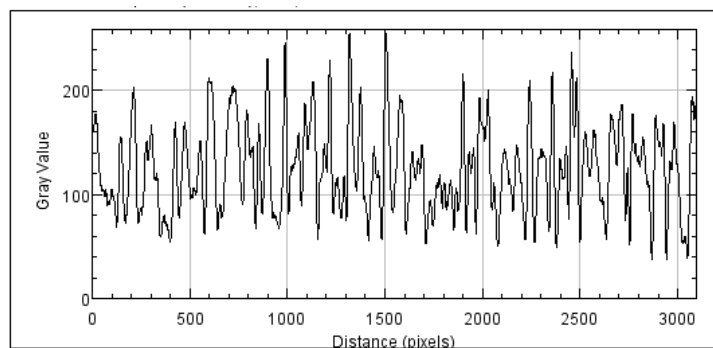


Figure 4.17: Spatial profile across an infrared image

By observing it, it was assumed that the highest peaks are the background, so the first version of the algorithm was:

1. Detect the peaks over a threshold (initially 170), storing the intensity (y) and position (x), thus a point (x,y).
2. Perform interpolation (latter using cubic spline) so the points in between are calculated.
3. Repeat the above steps for every line of the image.
4. Apply some sort of smoothing, like mean filtering or the same procedure vertically.

If the method proved to be successful, then an algorithm for detecting the appropriate peak values would be developed.

First, an algorithm for peak detection over a certain threshold was developed using C++. Below, the former infrared image is presented where the pixels/peaks of each line are colored black and would be used on the above procedure:

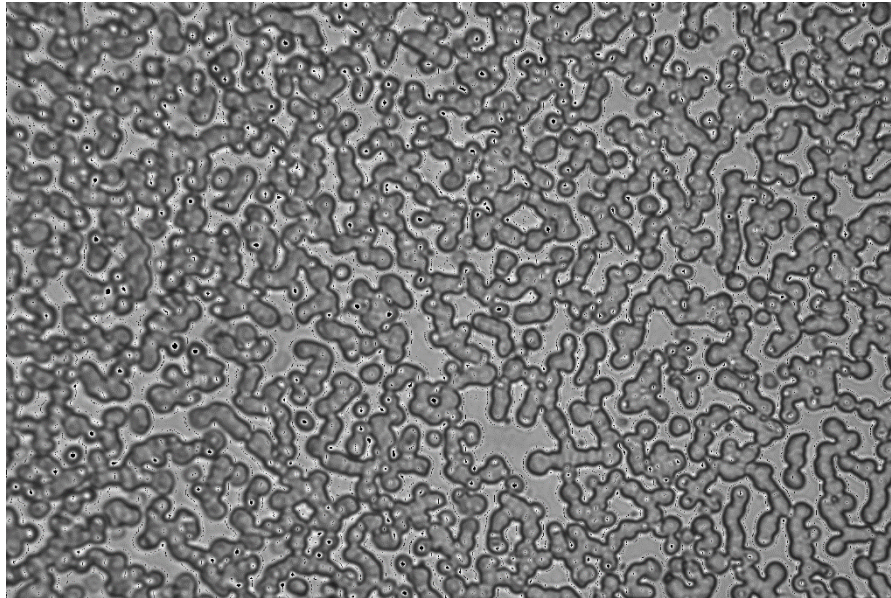


Figure 4.18: Peaks colored black on the infrared image

Afterwards, a simple interpolation was applied and later spline was used by employing two different algorithms (alglib, tkspline). It is worth noticed that spline did not differ much than simple interpolation in the current situation. By applying Linear Spline, the following image is generated:

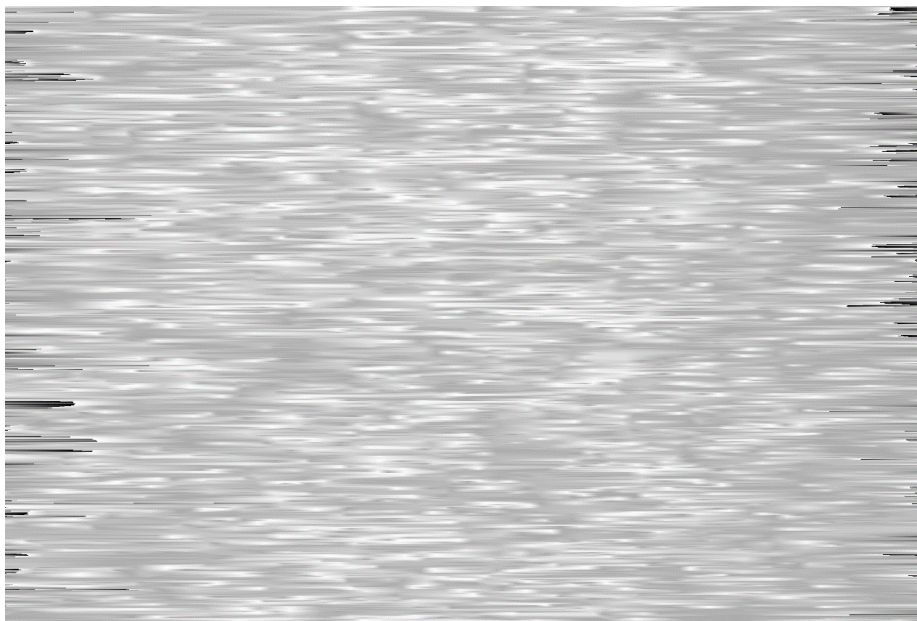


Figure 4.19: Application of Linear Spline

Two methods for image smoothing were applied on the previous image:

- A. A mean filter, starting from 10x10 up to 80x80, which had the best results. Below the previous image is presented after application of 80x80 mean filter:



Figure 4.20: Application of 80x80 mean filter

It is obvious that beside the fact the features of the original are visible, the image is way too bright comparing to the infrared one and does not conclude to the background light.

- B. The same procedure was followed vertically, aiming to smooth the image. The result was:

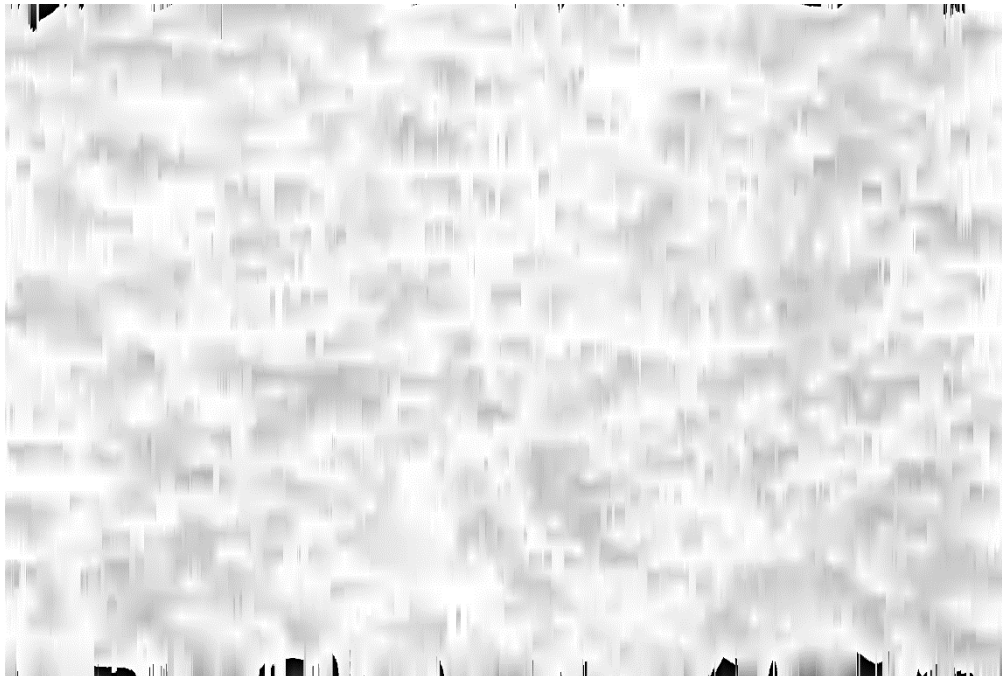


Figure 4.21: Application of vertical spline for smoothing

The conclusion was:

- The high peaks do not necessarily represent the actual intensity of the background. It is observed that some sort of focusing is aided by the nucleus that caused the final image to be much brighter than it really is.
- Taking into account that optics follow a Gaussian like distribution, something not taking into account earlier, the research was steered towards Gaussian curve fitting.

4.3.4 Gaussian Curve Fitting

For this new direction of the project, the MATLAB tool of curve fitting was extensively used. Following a similar way of thinking as above, it was attempted to fit a Gaussian curve into a “window” of the peaks: instead of detecting peaks over a certain threshold, peaks were detected between ranges, e.g. between 140 and 180, in order to avoid very high values which do not represent background values. When those points are detected, a curve would be fitted.

Although the results were far better than the previous attempt, they were not satisfying and far from the wanted result. While in some lines fitting was successful, it’s a failure on many others and thus the background could not be extracted.

Then Gaussian fitting was applied on the whole line, without any peak detection. The results of this attempt were very satisfying as the curve was like the “shape” of the spatial profile, which was the ultimate goal. The problem that had risen was that although the shape was fine, the intensity was lower:

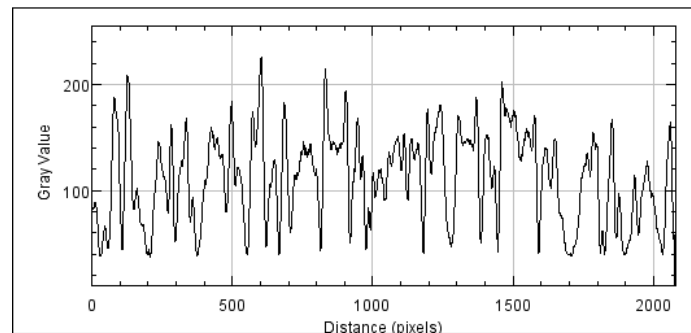


Figure 4.22: Spatial profile across the infrared

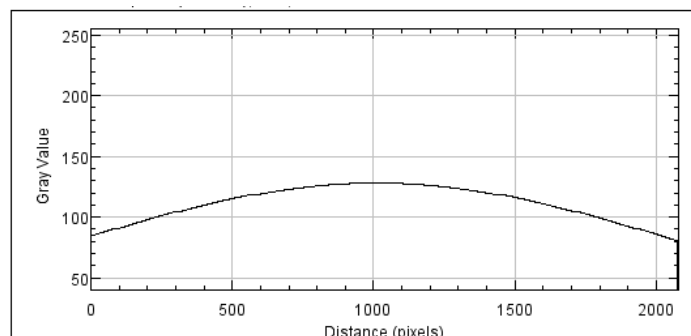


Figure 4.23: Spatial profile across the resulted image, same line

The following solution was proposed:

- Find the mean value of the line.
- Store all points whose intensity is over that value.
- Fit the curve using those points.

By using this, it was speculated that the both shape and overall intensity would be preserved at the same levels of the spatial profile. In order to smooth the image, the same procedure was applied again vertically to all points this time.



Figure 4.24: Final image using Gaussian fitting both vertically and horizontally

The final result as well as the following spatial profile reveal that in a random line of the image, the extracted background follows a Gaussian like curve and is in the same levels as the infrared. These properties are to be expected by the optics.

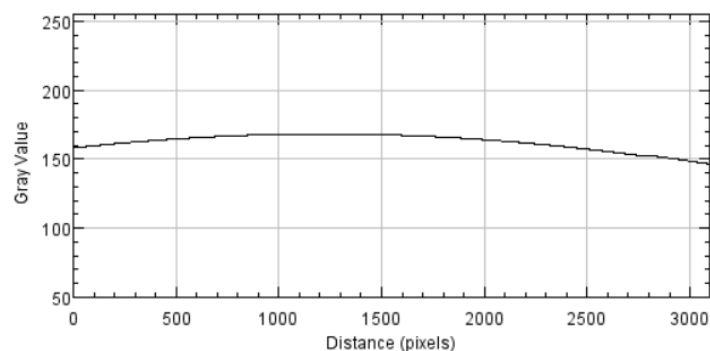


Figure 4.25: Spatial profile across the extracted background image

Due to time performance issues of the Gaussian fitting, new ways of curve fitting were explored that would potentially give similar results in a better time. The curve that stand out was the polynomial of 2nd degree, but the results were not as good as Gaussian.

4.3.5 Extensive Testing

In order to ensure the legitimacy of the algorithm, an extensive test was performed. More specifically, a lot of samples were taken using infrared from many different areas of cells and in different magnifications. Thus, the algorithm was tested in multiple varying and difficult situations.

Two samples that reveal the difficult situations of testing are those below:

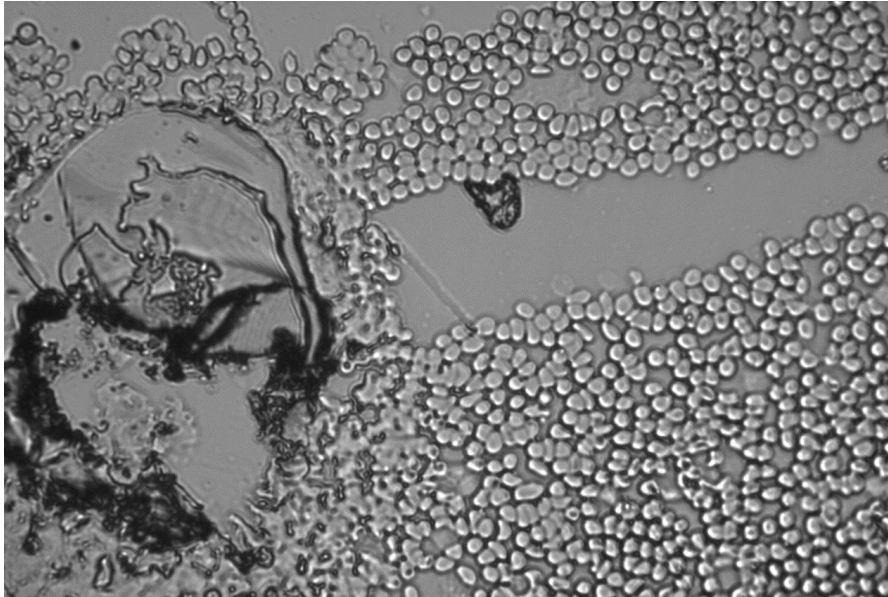


Figure 4.26: Uneven distribution of cells accompanied with dirt on one side

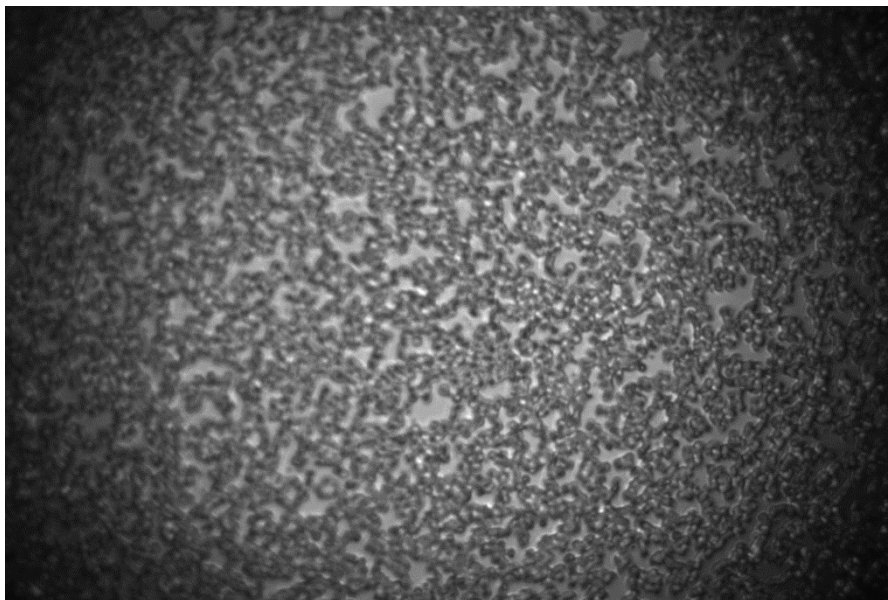


Figure 4.27: Very low magnification

After the algorithm was applied in all samples and the results were checked, samples of low magnification revealed some interesting insights for the improvement of the algorithm.

The first observation was that fitting should be performed vertically first and then horizontally, contrary to the way it was done until now. This helps to preserve the brightness in the center and dark on the side. The second observation was that Gaussian fit horizontally and vertically resulted in “spreading” of the light to areas that should be darker.

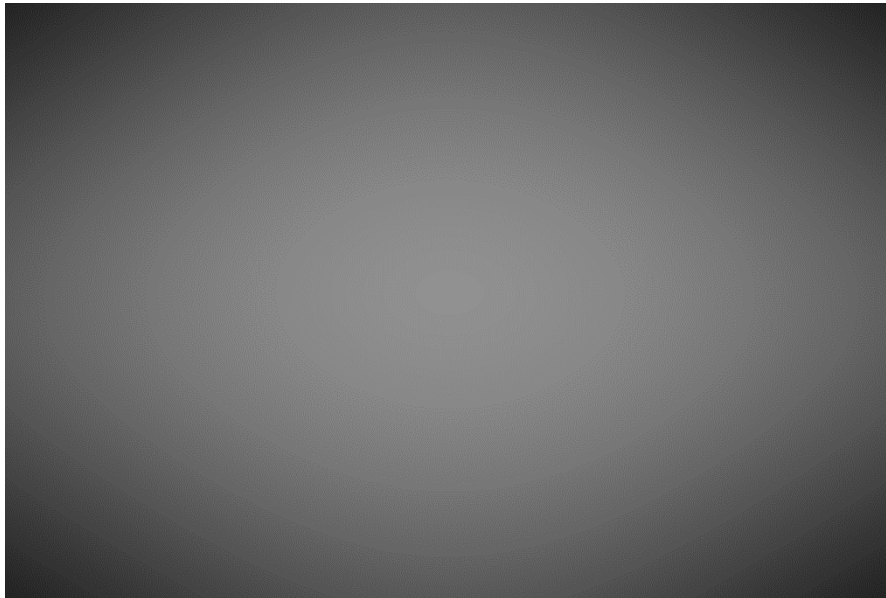


Figure 4.28: The above background should be darker on the sides

Therefore, it was decided that the second fit performed would be a polynomial of 2nd degree instead of Gaussian, which is a “steeper” curve and helps maintain the dark sides.

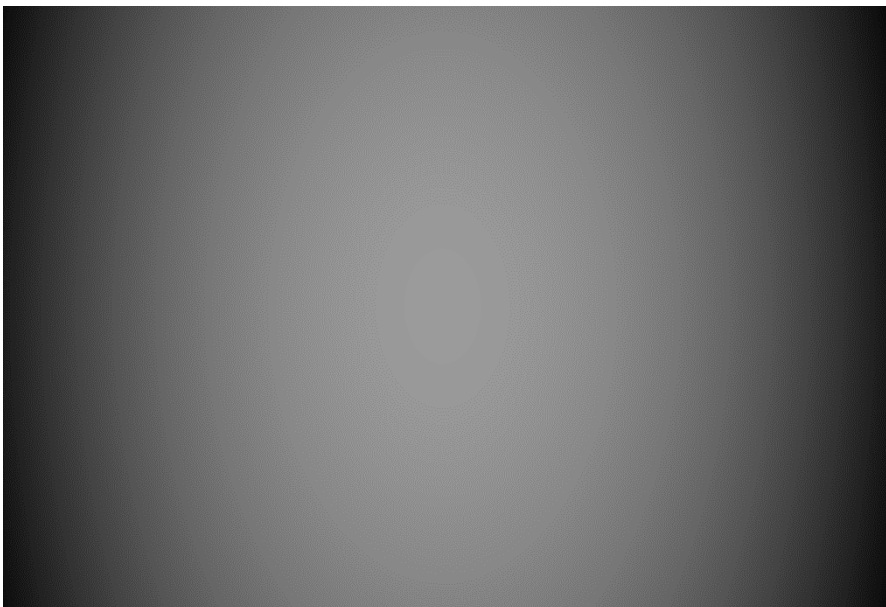


Figure 4.29: The resulting background is now darker on the side

By dividing the original image with each extracted background above, it results in a better flat field correction in the second case.

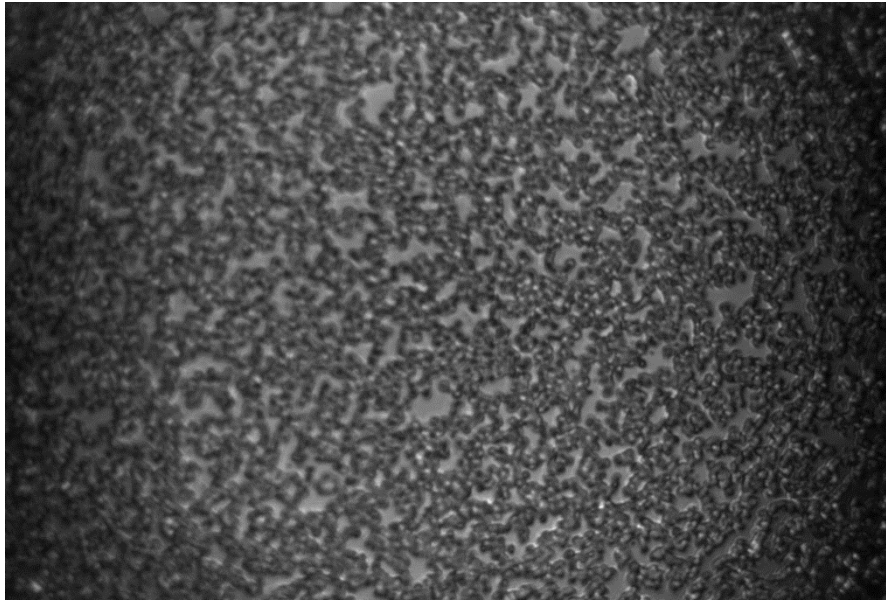


Figure 4.30: Image divided using Gaussian - Gaussian background



Figure 4.31: Image divided using Gaussian - Polynomial background

All the samples were tested again using the combinations below in order to conclude the final form of the algorithm:

- Vertical Gaussian – Horizontal Polynomial 2nd Degree
- Vertical Gaussian – Horizontal Gaussian
- Vertical Polynomial 2nd Degree – Horizontal Polynomial 2nd Degree
- Vertical Polynomial 2nd Degree – Horizontal Gaussian

After comparing the results of each algorithm, the final combination was Vertical Gaussian - Horizontal Polynomial 2nd Degree because:

1. In high magnification had almost identical results as Gaussian – Gaussian.
2. The results were better in lower magnifications.
3. The overall procedure was much faster

4.3.6 C++ Implementation

For the implementation in C++, the library *Alglib* was employed. The aforementioned library offers the proper functions for non-linear least square fitting, which is used in the Gaussian fitting part, and polynomial fitting. The commercial version is optimized and offers an overall speed boost to the process.

It should be warned that the value of the parameter *diffstep* (non-linear fitting, *alglib*) must not be lower than 10^{-6} , because it causes an undetermined behavior of the fitting procedure due to rounding errors. Thus, the results are not stable and vary each time, which caused much worry until discovered first.

4.3.7 Final Algorithm

Although the C++ implementation increased the execution speed compared to MATLAB, unfortunately the execution time was still prohibitive. Even using the optimized version of *alglib*, the time would vary between 35 and 40 seconds.

In order to increase the execution speed, it was decided not to perform the Gaussian in every vertical line of the image, but omitting a certain number in between using some step. Experimentally, it was discovered that the best tradeoff between speed and results was for a step of 50. More specifically, the first fit is performed of the first vertical line, then 50, then 100, 150, 200, etc. As side effect, the polynomial fitting is faster as well, since the point samples in every line are fewer, resulting in an overall speed boost.

The final time of execution is now expected between 0.7 and 2 seconds, which permitted the incorporation of the algorithm into the hematology project. Below, a case is presented where the first background extracted has the whole procedure applied whereas the second has a step of 50.

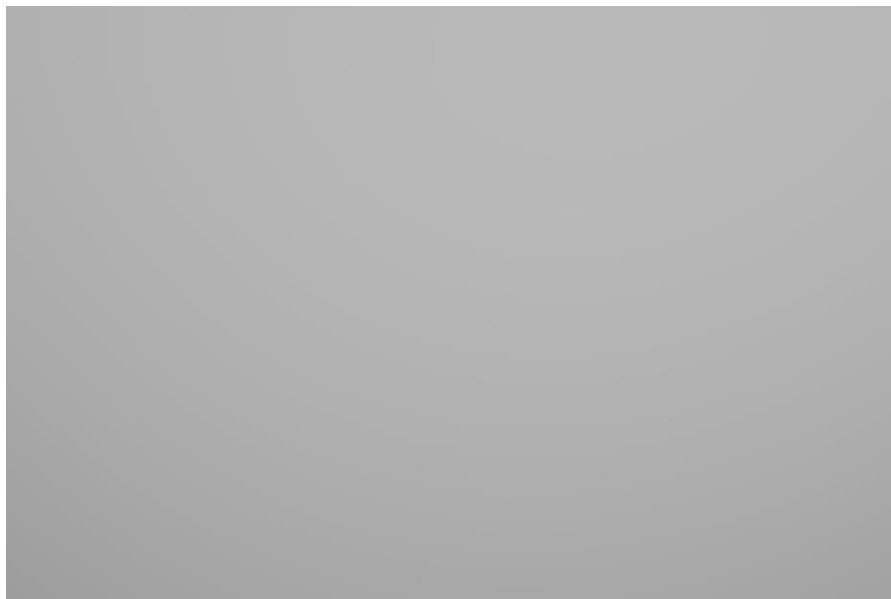


Figure 4.32: Extracted background without step



Figure 4.33: Extracted background using a step of 50

4.3.8 Algorithm Steps

1. Grab infrared.
2. Create intermediate and final images, which are empty.
3. For the columns of the infrared from 1 to width with step 50:
 - 3.1 Calculate mean value of the column.
 - 3.2 Find pixels (position, intensity) where $\text{intensity} \geq \text{mean value}$. (Position takes values from the range [1, height] while intensity from the range [0, 255]).
 - 3.3 Gauss fitting using those pixels.
 - 3.4 Using the generated curve, get the values of pixels from 1 to height and store the values to the corresponding position of the intermediate image. (Therefore, the intermediate image would have values in 1, 51, 101, 151,... , and would be black in between)
4. For each row of the intermediate image, perform a polynomial 2 fit using only non-zero values. Using the generated curve, get the values of the pixels from 1 to width and store them to the corresponding line position of the final image.
5. The final image is the extracted background.

4.3.9 Example of Analysis

Here is presented an analysis using extremely different illuminance of the same area, before and after the assistance of the background extraction algorithm.

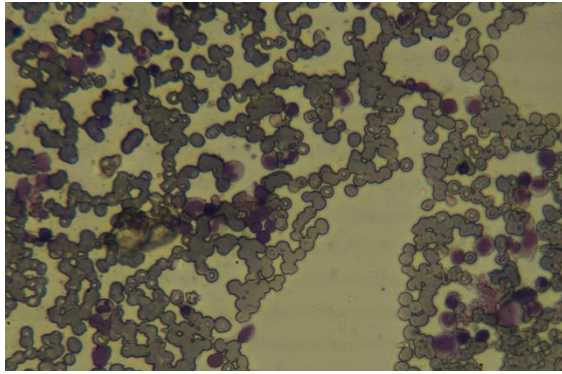


Figure 4.34: Example case in normal light

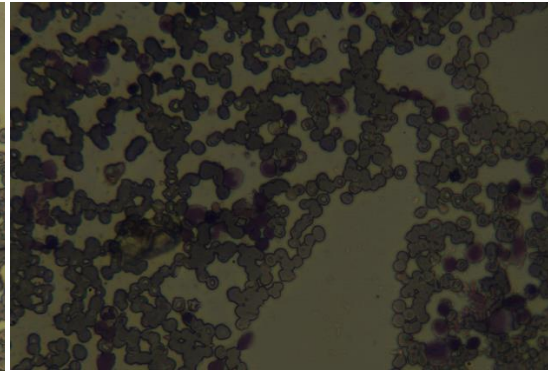
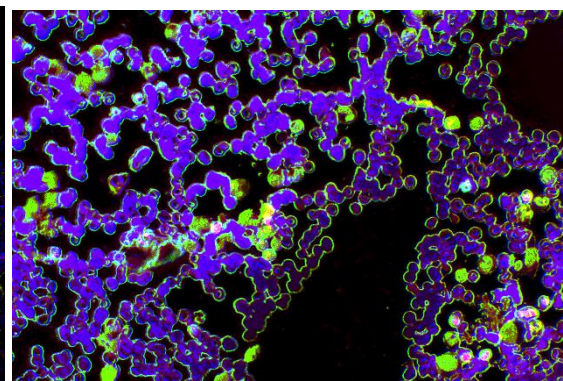
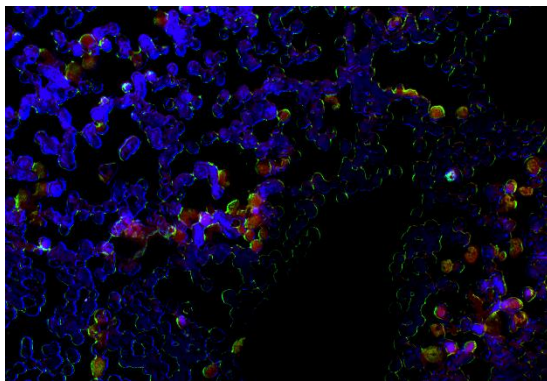
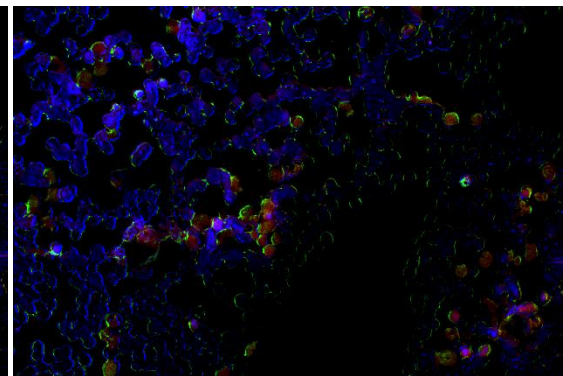
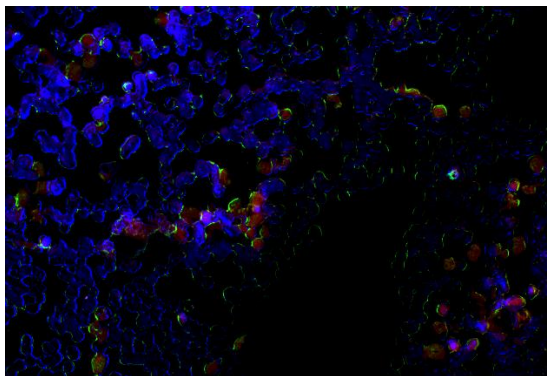


Figure 4.35: Example case in low light



Figures 4.36 & 4.37: Proportion maps without background extraction for normal and low light



Figures 4.38 & 4.39: Proportion maps with background extraction for normal and low light

It is obviously stated by observing the above case that background is critical for the correct application of the analysis algorithm.

4.4 WBC Isolation Mask

4.4.1 Description

When diagnosing blood samples for leukemia, doctors are focused on the leukocytes as the failed transformations of them are responsible for the disease. Consequently, they reveal crucial information via their number, shape, size, and stain color that the medical professional has to interpret in order to determine the type and severity of the disease. However, apart from leukocytes, the sample contains erythrocytes, platelets and even dust, which are stained as well and impose an extra barrier into the already difficult work of diagnosis.

For these reasons, lab member Marios Kastrinakis developed a WBC detection and isolation algorithm. It takes advantage of the color image of the area of interest that is about to be analyzed. After careful and multiple examinations, it was decided that this is the best approach since leukocytes are stained in specific colors and, at the same time, spectral images do not contain enough information to precisely distinguish them from the other type of cells.

The algorithm detects WBCs in the area of interest by employing various image-processing techniques and it takes precedence over the data analysis algorithm. It takes as input the magnification, which is provided by the previously described mechanism in Chapter 3.3.1, and outputs a binary mask that is then applied to all the spectral images isolating in this way the leukocytes. Since everything but the leukocytes are now excluded, the analysis algorithm is only analyzing this parts of the area, thus greatly reducing the time of analysis as stated in the end of Chapter 4.2.3.

Prerequisites for the correct functioning of the algorithm are:

- The area of interest has to be properly focused.
- The user provides enough lighting but not over a certain limit.

A thorough explanation of the algorithm, its philosophy and limits will be provided by Marios Kastrinakis in his forthcoming Master thesis.

4.4.2 Algorithm Steps

Phase 1:

1. Acquire color image.
2. Split image channels.
3. Add red and blue channel pixel wise.
4. Multiply each green channel pixel by 2.
5. Divide pixel wise the sum resulted from step 3 by each pixel resulted from step 4.
6. Get the min and max values that emerged from the last step.
7. If the difference of max minus min is smaller than $2.2204e-16$, then proceed using the image from step 5 as is. Otherwise:
 1. Subtract min value from each pixel of step 5.
 2. Multiply each pixel by 255.

3. Divide each pixel by the difference of max value minus min value.
8. Apply Maximum Entropy Threshold to the image emerged from step 7, resulting in a binary image.

Phase 2:

9. Clone the binary image of step 8.
10. Fill connected components of the clone with value 255.
11. Invert the values of the clone.
12. Perform a bitwise OR operation between the clone and cloned image.
13. For every BLOB of the image of step 12, check if its area is smaller than a threshold. If so, remove it.

Phase 3:

14. If magnifications is over 20, then apply OTSU Threshold to the green channel of the color image else apply Triangle Threshold. A binary image will emerge.
15. Invert all pixels of the last image.
16. For every BLOB of the image of step 15, check if its area is smaller than a threshold. If so, remove it.

Phase 4:

17. Find the contours of the last image.

Phase 5:

18. Create an empty image, which is going to be the final mask.
19. Isolate every BLOB of the step 13 image and for each:
 1. Perform bitwise AND with the contours image.
 2. Find the sum of all elements of the resulted image.
 3. If the sum is below a certain threshold, dilate the BLOB using an ellipse and repeat 18.1 - 18.3.
 4. Merge the dilated blob to the final image.

A more detailed algorithm explanation is provided in Annex B, in the form of pseudo code. Below is an example of the application of the analysis algorithm, depicting the spectral images and the final pseudo color maps.

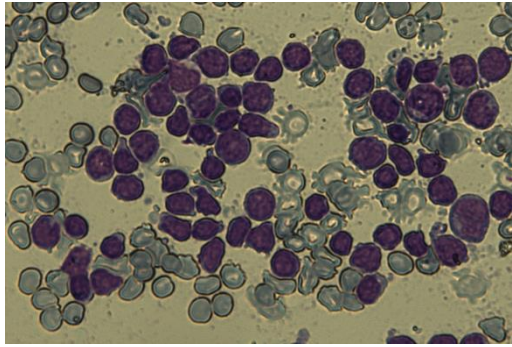


Figure 4.40: Color Image

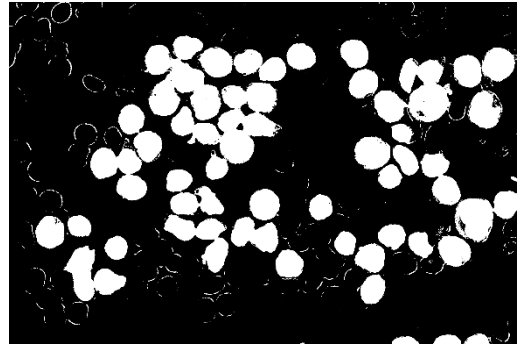


Figure 4.41: Phase 1

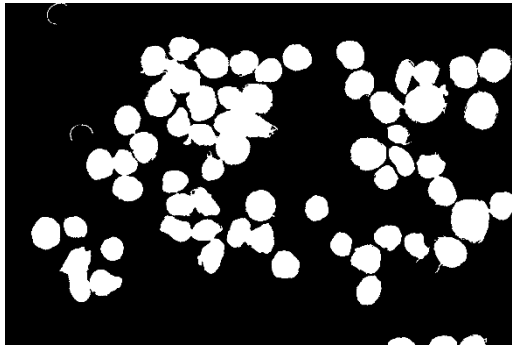


Figure 4.42: Phase 2

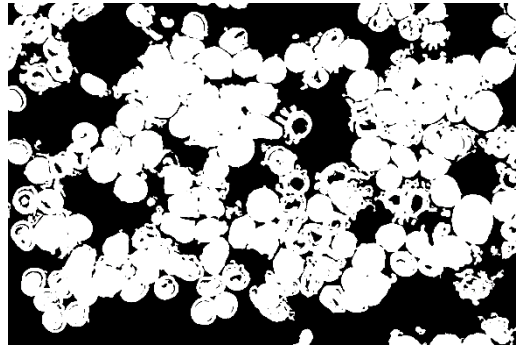


Figure 4.43: Phase 3

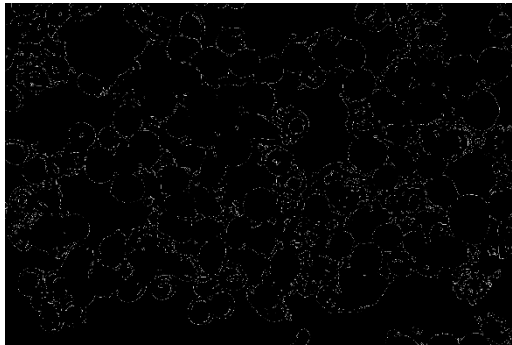


Figure 4.44: Phase 4

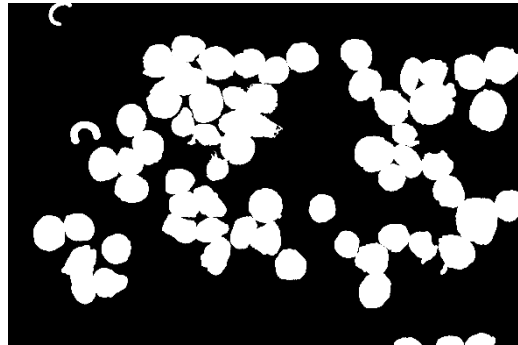


Figure 4.45: Phase 5 (Final)

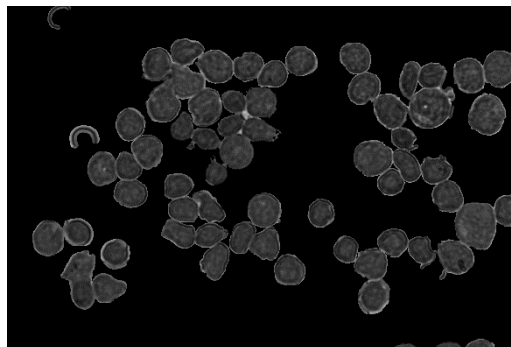


Figure 4.46: Final Mask Applied on the Original Image

4.4.3 C++ Implementation & Optimization

The algorithm was implemented using OpenCV library in combination with OpenCVBlobsLib, an open source library released under GNU License that is built on top of OpenCV, extending the capabilities of the latter to include BLOB (Binary Large Object) support.

OpenCV is an amazing tool, proving the developer with a wide variety of features and optimizations. Hence, the transition of an algorithm from an experimental environment such as MATLAB (which is where it was originally developed) becomes a lot less difficult than it would be not so long ago. However, it has no support of BLOB yet, something which is obvious that the isolation algorithm uses extensively. So, it is worth mentioning C++ BLOB libraries are scarce, even in a proprietary form, as it is a very special subcategory of image processing. A lot of search was done in order to track such libraries and only that one had the necessary features. Thus, the existence of that library proved to be critical as without it the task of implementing the algorithm would be extremely time consuming at best and impossible at worst.

Due to its heavy image processing and dynamic nature (different amount of WBCs each time), it has a variable complexity and has proved to be very time consuming under certain circumstances. Although OpenCVBlobsLib has optimizations options, this is not enough and execution time may vary from few hundreds of milliseconds to tens of seconds. The bottleneck is easily spotted on step 5. Thus, a careful re-design of the implementation or the isolation algorithm itself had to be done some time in the future, incorporating parallelism or/and smarter ways to boost the speed.

The first step was redesigned in a single loop, employing Open MP and local variables, which gave a speed boost of 30 milliseconds. The 5th step was redesigned as well to get only the ROI of the images containing the white blood cell, the contours and the final when the dilation is performed. It gave a massive amount of speed boost. In some cases, the execution time would even reach 30 seconds while the same case now will perform as fast as 900 milliseconds.

Chapter 5:

User Interface

5.1 Qt

Qt (pronounced as “cute”) is a cross-platform application framework written in C++. It is used for developing multi-platform applications and graphical user interfaces (GUIs). An application developed using the Qt framework can be easily ported to different operating systems as well as mobile platforms. Besides its practical GUI development abstraction, it offers a wide range of capabilities, such as image read/save, image preview, image manipulation, strings management, timers and many others, thus extending its capabilities far beyond the GUI development.

The elements of interactions, such as buttons or sliders, are termed widgets. In Qt, the communication between widgets or objects is facilitated by the use of signals and slots. A *signal* is emitted when a particular event occurs or a certain line of code is reached and a *slot*, which is a function, is called in response to that particular signal. Although Qt widgets have many handy pre-defined signals and slots, the developer is free to add more according to the needs of the application. Signals and slots can take any number of arguments of any type and they are completely type safe. Moreover, any number of signals can be connected to a single slot, and a signal can be connected to as many slots as needed. It is also possible to connect a signal directly to another signal, which will emit the second signal immediately whenever the first is emitted. Lastly, slot functions can be used as common functions.

Many compilers are supported, including the GCC C++ compiler and the Visual Studio suite. In the present project, the GCC is used as the dominant compiler, although the project has been compiled under the Visual C++ too. Qt 5.5.0 x64 has been used as the basis of the project and MinGW 5.1.0 x64 as the default compiler.

5.2 Initial Screen

Upon executing the application, the user is prompted to select the *patient's folder*. In this folder all future analysis and screen captures are going to be saved. Then, the screen depicted below appears:



Figure 5.1: Initial Screen

Four buttons exist on the left, all of which are stylized standard QPushButtons. The blue button on top enables the user to switch the patient's folder anytime. The red button, directly below the blue one, enters the "View Mode" while green button enters the "Acquisition Mode". Finally, the red button at the bottom shuts down the application.

In the center, where the intro image is depicted using a QLabel, lies a stacked widget. Every time a button is pressed, the page of the stack is changed accordingly. If the same button is pressed again while in a mode, the user returns to initial screen.

5.3 View Mode

By pressing the view mode button, the application leads the user to the following screen:

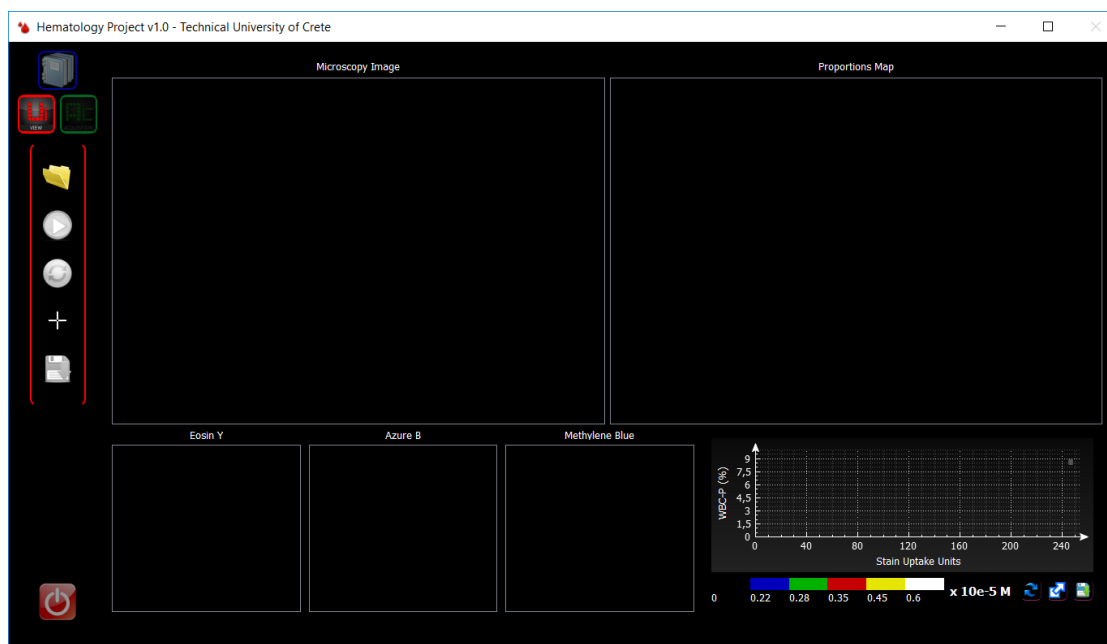


Figure 5.2: View Mode

As it is depicted, there are 2 main image viewers, 3 thumbnails and an empty diagram. The main viewers are custom viewers that inherit from `QGraphicsView` class and implement the handling of mouse events as well as other custom methods. The same applies to the 3 thumbnails.

On the left, there are 5 buttons (`QPushButtons`) with only the first activated. Upon clicking it, the user is prompted to load a folder containing the data of a previous analysis. If the folder contains the necessary images named appropriately, the color image is loaded and displayed; otherwise, an error message pops up. Additionally, if the user has saved the produced maps of that case before, then they are loaded and displayed as well.

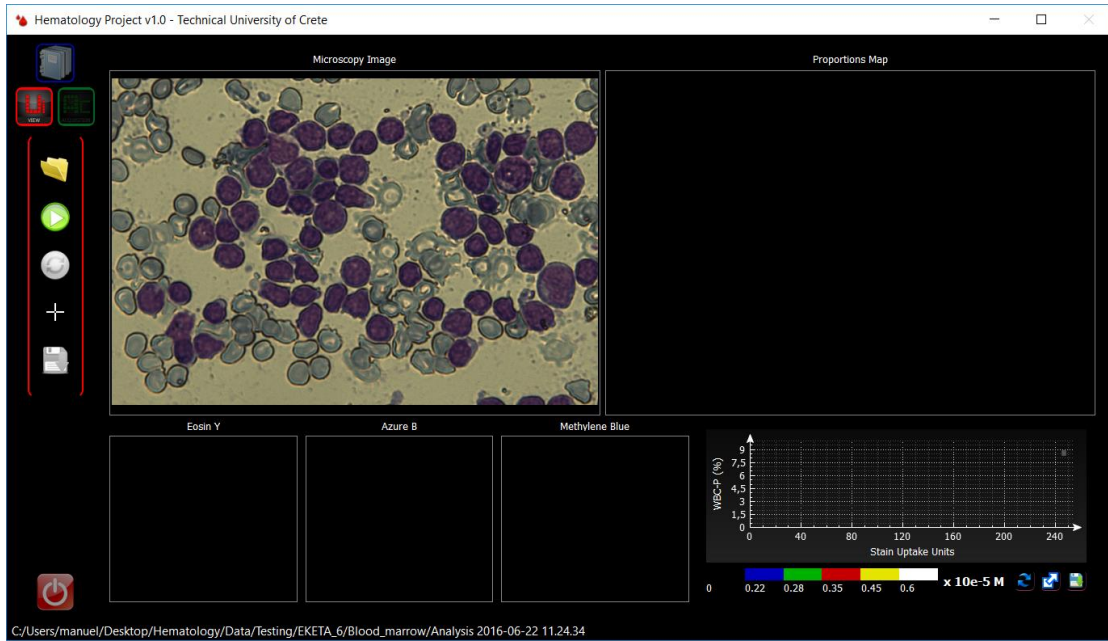


Figure 5.3: Loaded case on the View Mode

When a valid case is loaded, the analyze button is enabled. In addition, the path of the folder is written at the bottom, informing the user the exact path. By pressing the analysis button, the algorithms process the data and generate the pseudo color maps. The maps are then loaded to the corresponding viewers while the rest of the buttons are enabled.

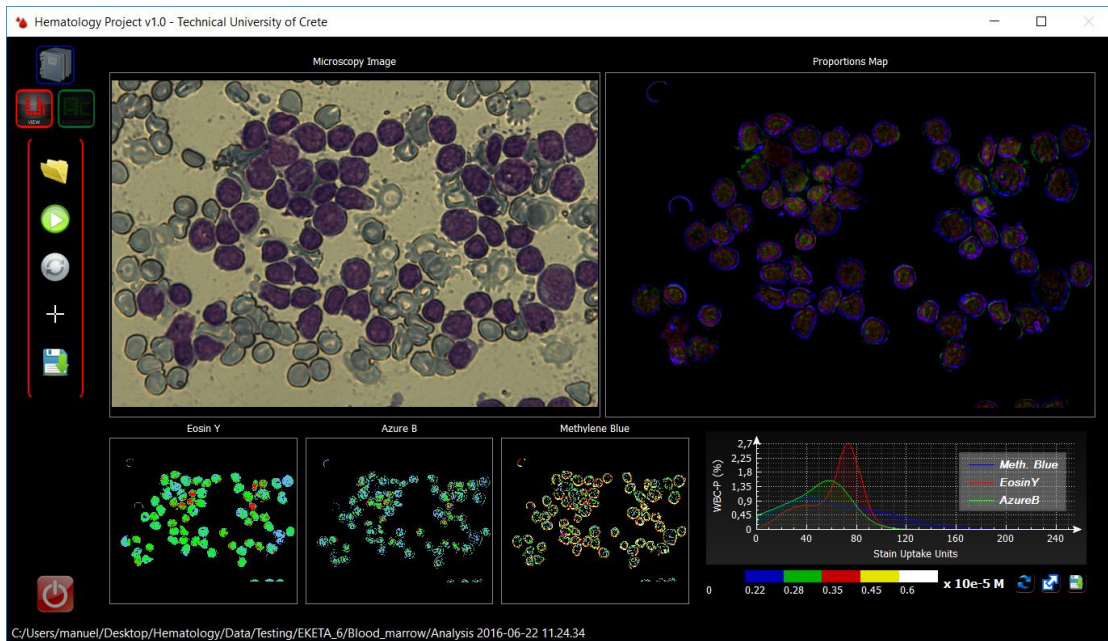


Figure 5.4: Analysis performed

The button below the analysis button is named “switch”, and changes the substance pseudo color maps to their monochrome counterparts and reverse.

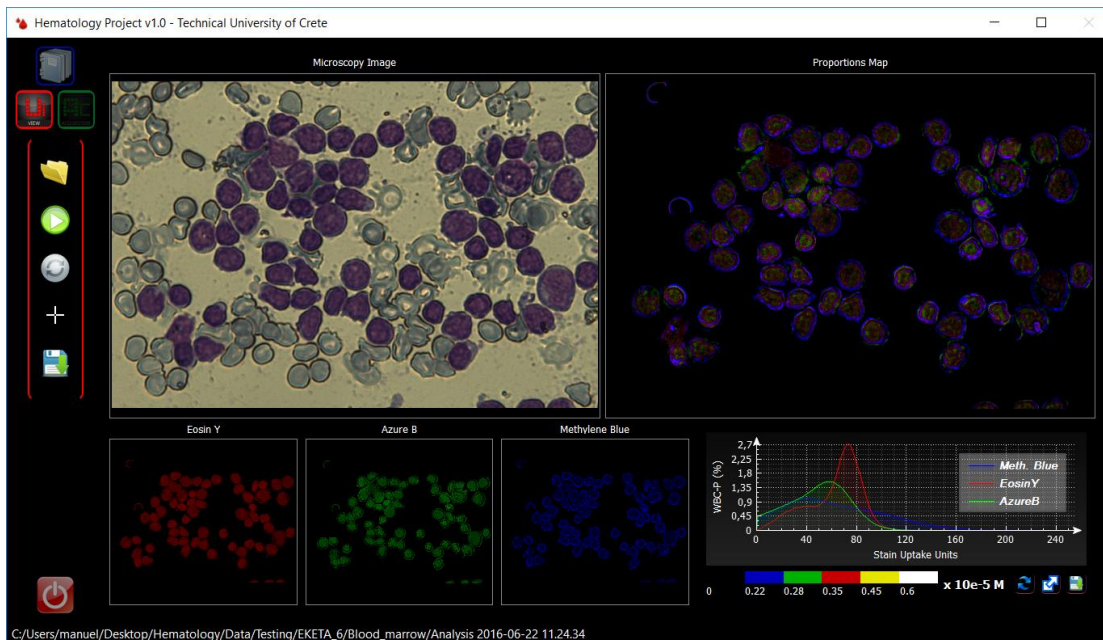


Figure 5.5: Switch button changes to monochrome maps

The cursor below the switch button enables the “multi cursor” feature. When pointing somewhere on a viewer, a cursor appears in every window pointing to the same spot on the displayed image. This is achieved by implementing a mouse move event, getting the coordinates of the mouse on the image and emitting a signal to the other view objects containing that data. The slot function then gets the data and places a pixmap of a cursor into the very same spot. Thus, the effect of multi cursor point to the same spot is done. When clicked again, the feature is disabled. It is a very useful way to help the user compare the same area or points in every displayed map.

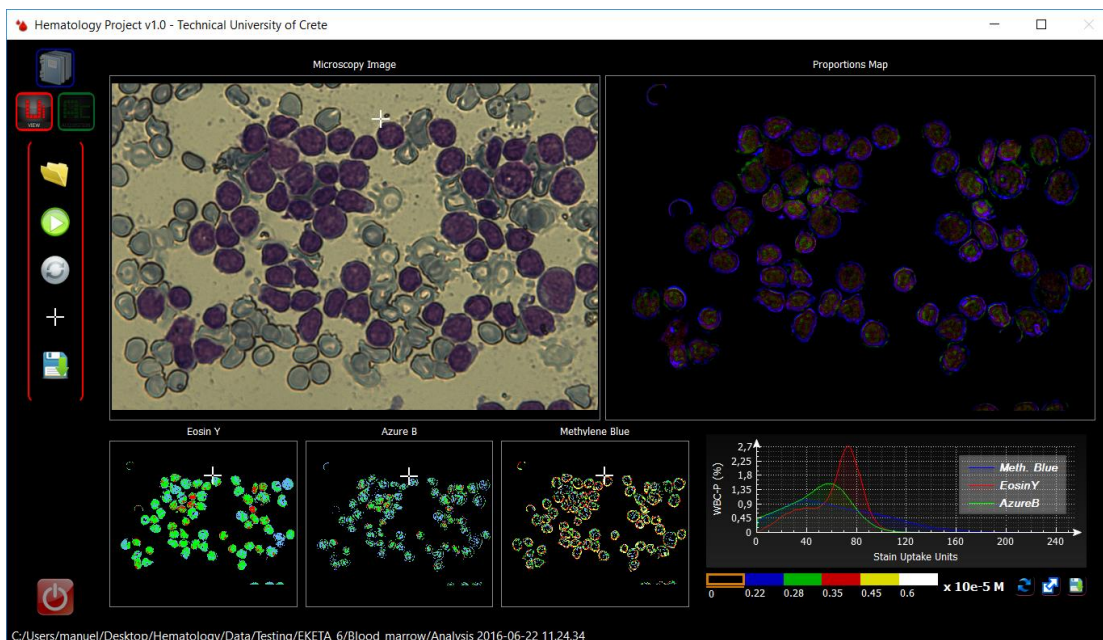


Figure 5.6: Multiple cursors pointing to the same spot

The last button saves the generated maps to the folder of the case, the same that contains the spectral images. Therefore, next time the case is loaded the maps do not have to be generated again; they are automatically displayed instead.

When zooming in/out and moving an image, all viewers respond to it concurrently by employing a similar mechanism as described above for the multi cursor.

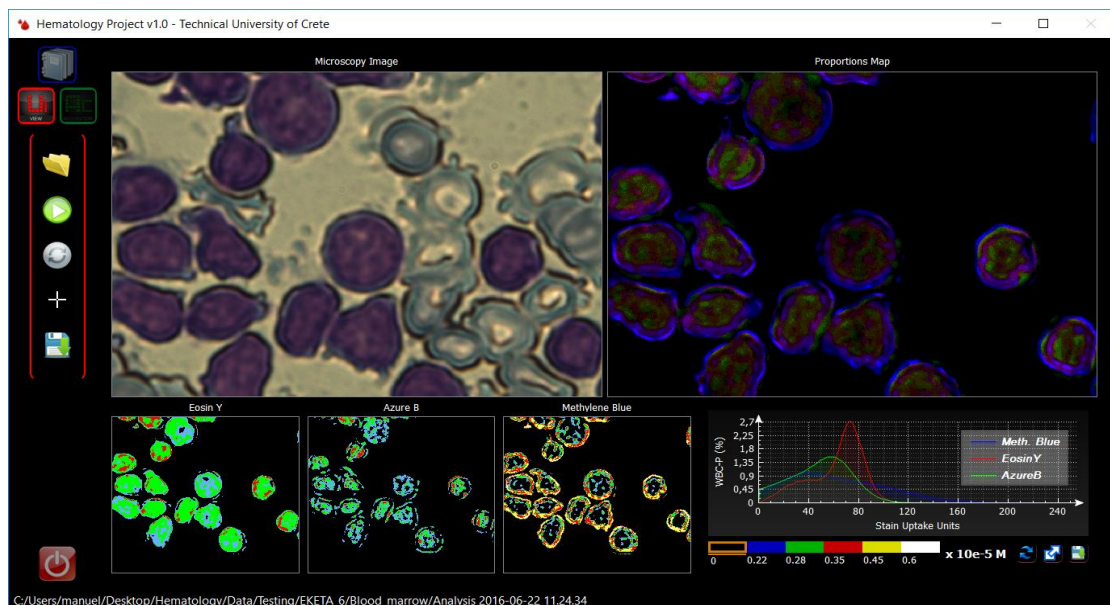


Figure 5.7: Zooming will cause zoom in all viewers

If a thumbnail is clicked a signal is emitted containing the ID of the thumbnail and its image is placed on the secondary main viewer on the left of the microscopy image. That thumbnail is then highlighted, as well as the corresponding curve on the plot. When clicked again, the proportions map returns.

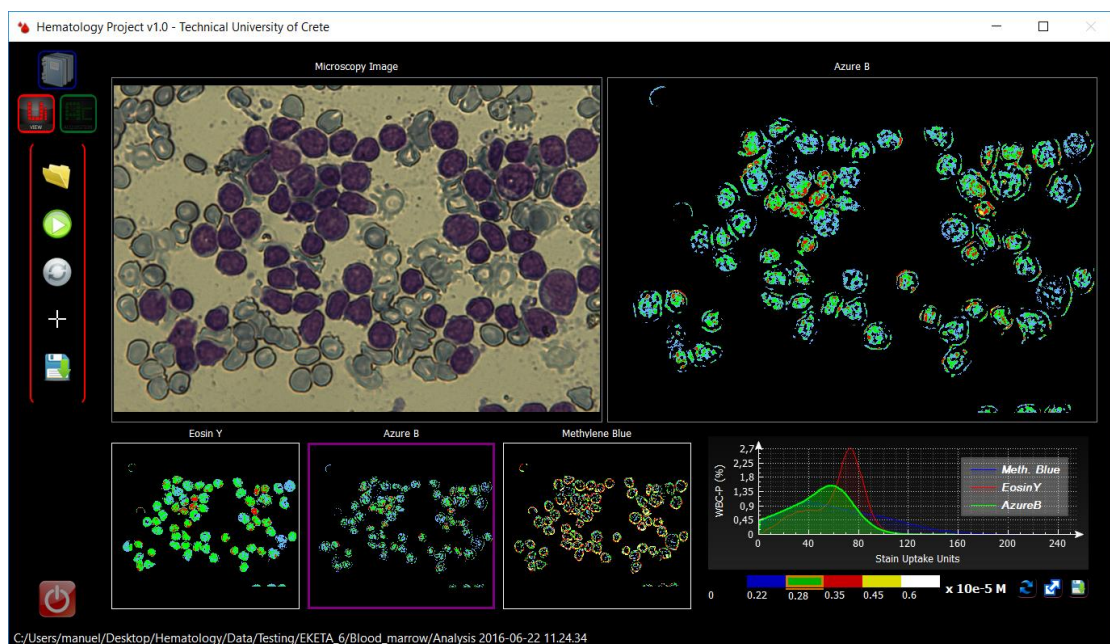


Figure 5.8: Azure B thumbnail highlighted and displayed in the second main viewer

If a viewer is double clicked, its image fills the entire screen. This is accomplished by turning to a different page on the stack widget, which has a standard viewer, and loading the image there. If double clicked again, the user returns to the view mode.

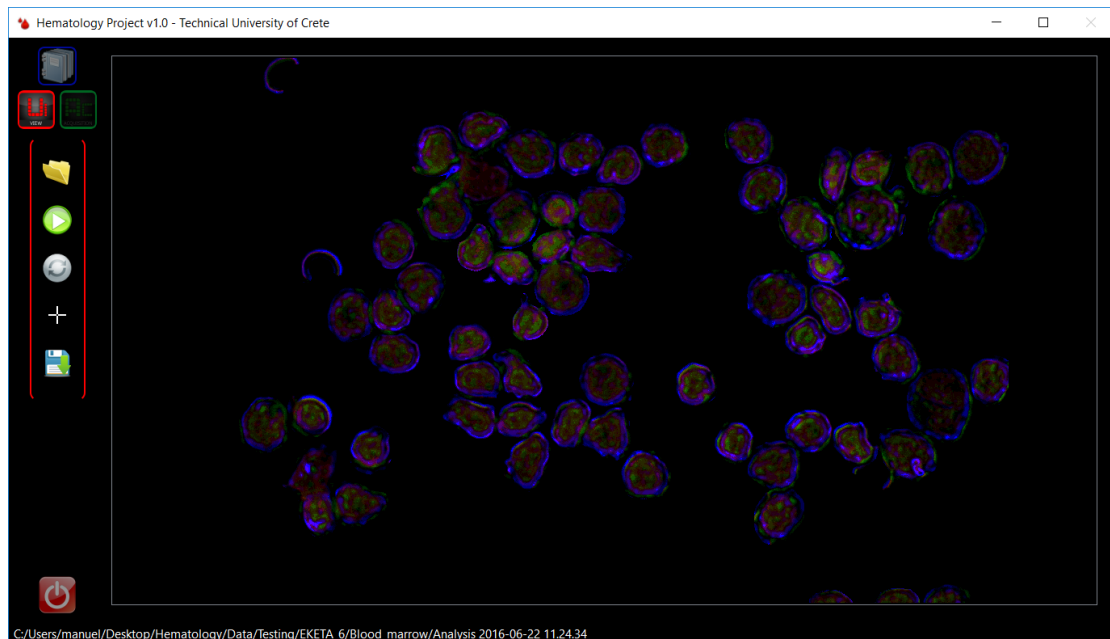


Figure 5.9: Proportions map double clicked

Lastly, there is the stain plots widget. It can be expanded by clicking the arrow pointing right.

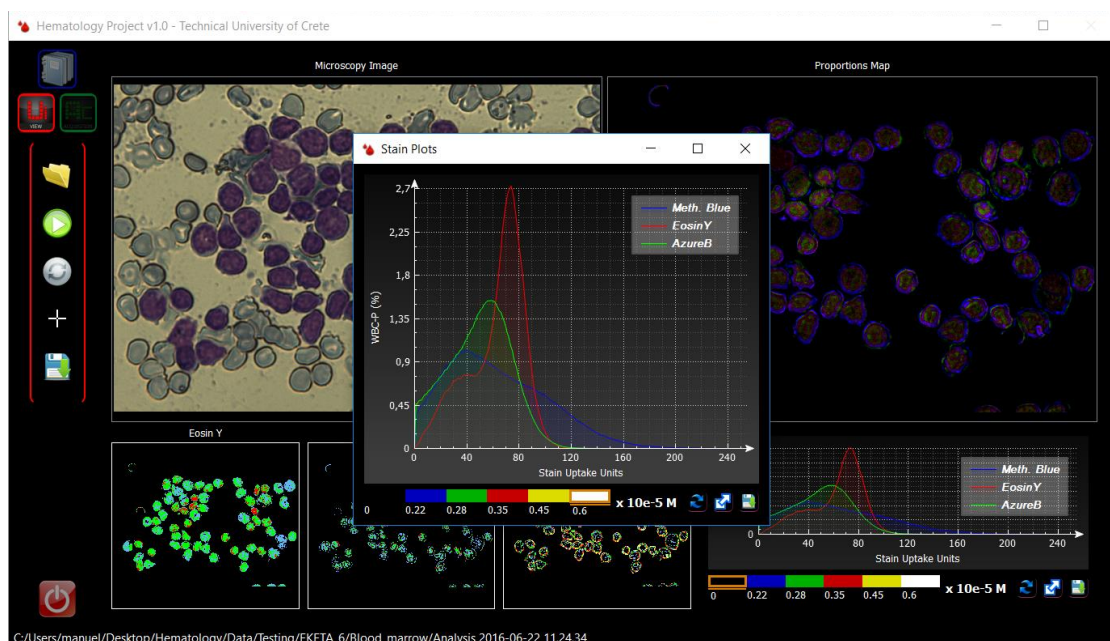


Figure 5.10: Expanded plot widget

It essentially provides information about the distribution of concentrations of the different substances. Firstly, the histogram of each channel of the proportions map is generated. Then, the number of the total active pixels, which is determined by the WBC mask, divides each histogram. Thus, it results to the above plots for each substance.

For example, the green line that consists of Azure B is examined. A histogram of the green channel of the proportions map, which is the same as the green channel of the Azure B monochrome map, is generated. The WBC mask indicates if a specific pixel is active or not, so its value is taken into account when making the histogram; otherwise, it is omitted. When the histogram is completed, it is divided by the total amount of active pixels. Then, the non-zero values of the histogram are plotted and connected together, resulting in the above lines.

Lastly, the user has the ability to zoom in/out and save the lines in MS Excel format.

5.4 Acquisition Mode

A series of events begin when the user presses the acquisition button. First, the light source controller is initialized, if it has not already. Then, a command is sent to light the white LED and a timer starts which polls, with a frequency of 10 Hz, the microcontroller, asking for the current magnification value. Afterwards the digitizer is initialized, if not already, and, finally, the camera, using the default or the last shutter and gain values. Upon initializing the camera, a thread is started, which grabs the data from camera and sends them, via a signal, to the Acquisition Mode viewer slot where they are depicted.

The Acquisition Mode consists of the following window:

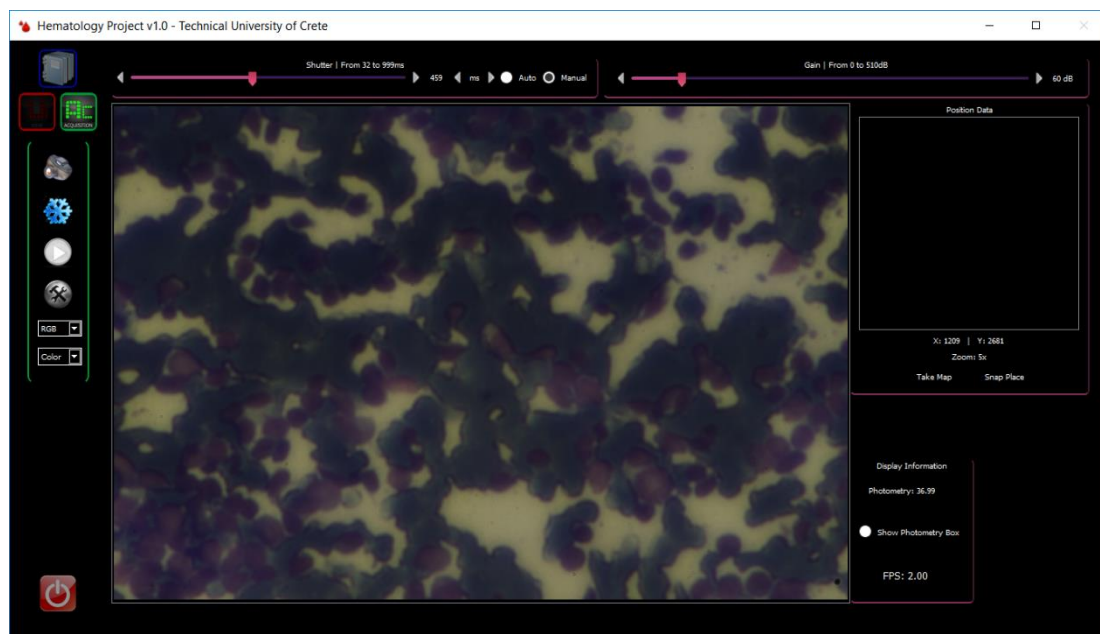


Figure 5.11: Acquisition Mode

On top, two standard sliders affect the shutter and gain values of the camera respectively. Furthermore, the shutter setting has “Auto” and “Manual” choices, via radio buttons. When set to auto, the camera changes its exposure automatically. A timer provokes a slot periodically that gets the current shutter value and updates the slider.

There are 4 buttons and 2 combo boxes on the left. The first button captures an image and saves it under a folder named “Captured Images” inside the patient’s folder. If the folder does not exist, it is created. The name of the captured image is the current date and time.

Below is the freeze button. In order to start analyzing an area, the user has to freeze the image first and then the analysis button is activated.

The button below analysis is the “Options”, which presents the user with various camera options if clicked. The options available are:

- Change of resolution: The user selects the desired resolution out of a fixed set of resolutions.
- Image flip: It flips the image vertically, horizontally or both. It is useful when viewing specific samples that require correct orientation.

- Gamma correction: Affects the gamma parameter of the camera.
- White Balance: This has three settings: “manual”, “auto” and “default”. The first setting gives user the freedom to change the slider values, thus configuring the white balance as desired. The second activates the automatic white balance mode of the camera. In this mode, a timer starts and updates periodically the values on the sliders by asking the camera about the current values, so the user is notified. Finally, the default radio button sets the white balance at the default, optimal values as determined in the laboratory.

The user has to click the options button to return in the previews screen on the Acquisition Mode.



Figure 5.12: Camera configuration

Moving on, there are two combo boxes. Those boxes affect the image grabbed by the camera: what is captured and how is displayed.



Figure 5.13: Selecting camera channel for live preview

The first combo box lets the user determine the channel displayed. Instead of the standard RGB, the user can select to view and of the consisting channels of the image. The second box lets the user change the wavelength of illuminance.

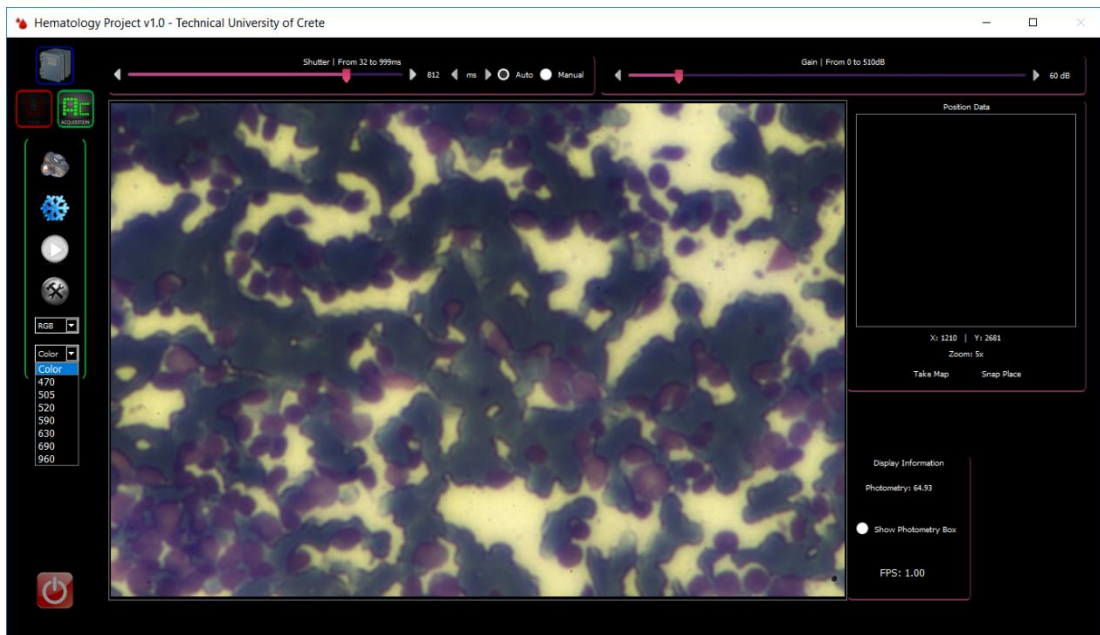


Figure 5.14: Selecting a different wavelength for the illuminance

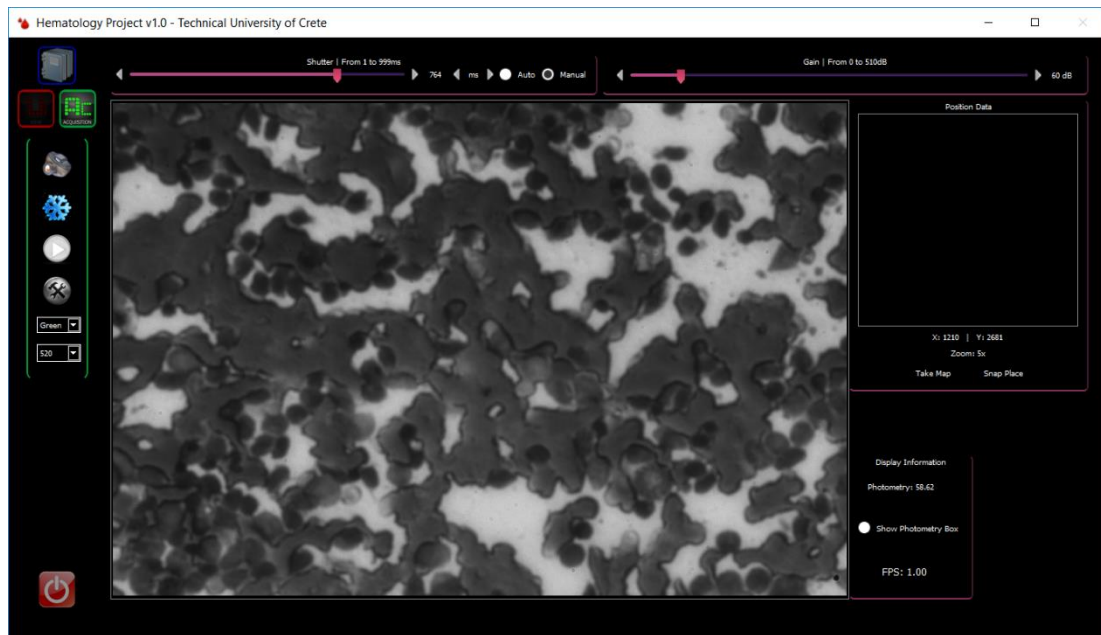


Figure 5.15: Illuminance switched to 520 nm

Finally, when right area has been located, the freeze button has to be clicked. The various options are then hidden while the analyze button is activated.



Figure 5.16: Freeze button pressed

The user then presses the analyze button and the analysis begin. A new thread is created which starts capturing the images in different wavelengths. Upon capturing, the image is displayed on the screen and the current wavelength is written on the right.

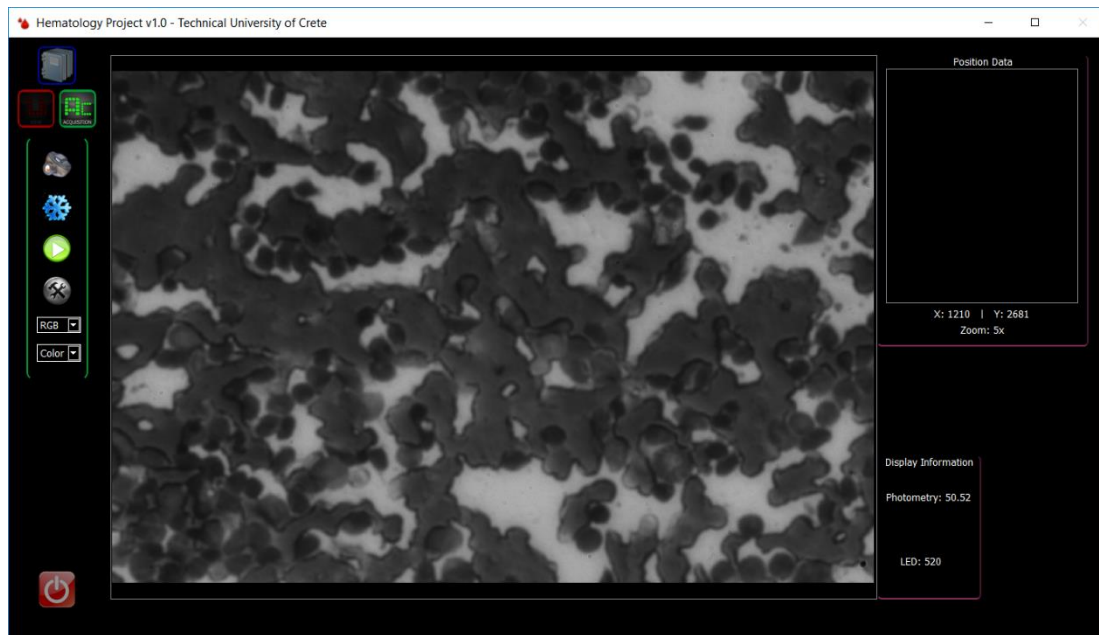


Figure 5.17: Analysis is performed and currently the image acquired at 520 nm is displayed

When the process is completed, the algorithms analyze the captured data and the application switches to view mode, displaying the color image and the generated maps as described in the previews subchapter. Meanwhile, another thread starts silently in the background, saving the captured images inside the patient's folder as well as the WBC mask and the extracted background. These data can then be used in the future for regenerating the maps.

5.5 Positioning & Navigation

The user is provided with a positioning system to further assist the detection of the areas of interest. As it is depicted, on the left of the viewer exists another smaller viewer and beneath it the X-Axis and Y-Axis values given by the pen tablet as well as the current zoom value.

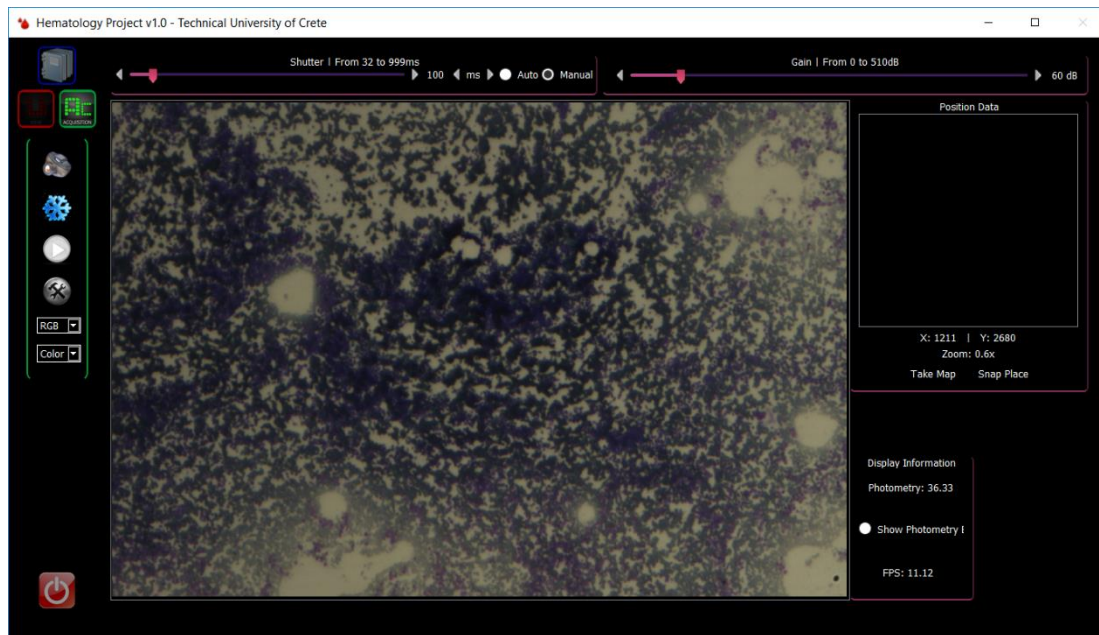


Figure 5.18: Low magnification while previewing using Acquisition Mode

The system is designed to function as following:

First, the user takes a picture of the area at very low magnification, using the “Take Map” button.

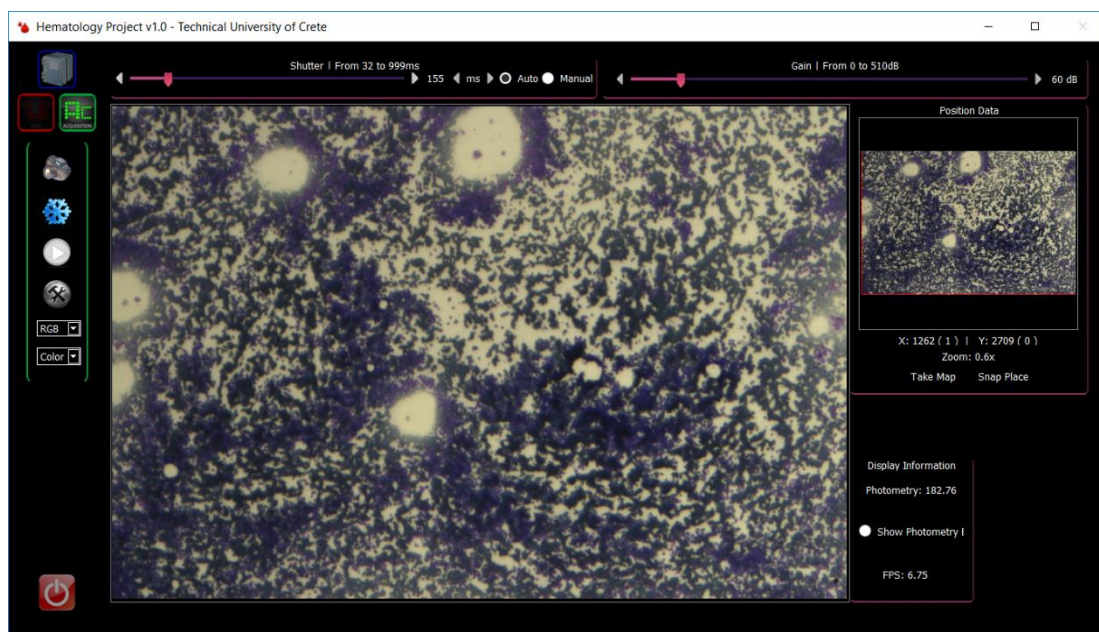


Figure 5.19: New map is taken and displayed

The image is the captured and displayed on the left. A red rectangle forms around that image, meaning that the user is in the same magnification value as the image was taken. Afterwards, the user can magnify the image and the rectangle will change accordingly, providing the user a sense of the area visited.



Figure 5.20: Higher magnification cause a rectangle inside the map to become smaller

The user can further magnify the image and explore the map, directly visiting the areas that seem interesting without worrying loosing track of the position or omitting places. Next to the X-axis and Y-axis values, a second number is now written which informs the user of the displacement against the original coordinates. This way, even if areas out of the map are visited, the user can locate back to the original.

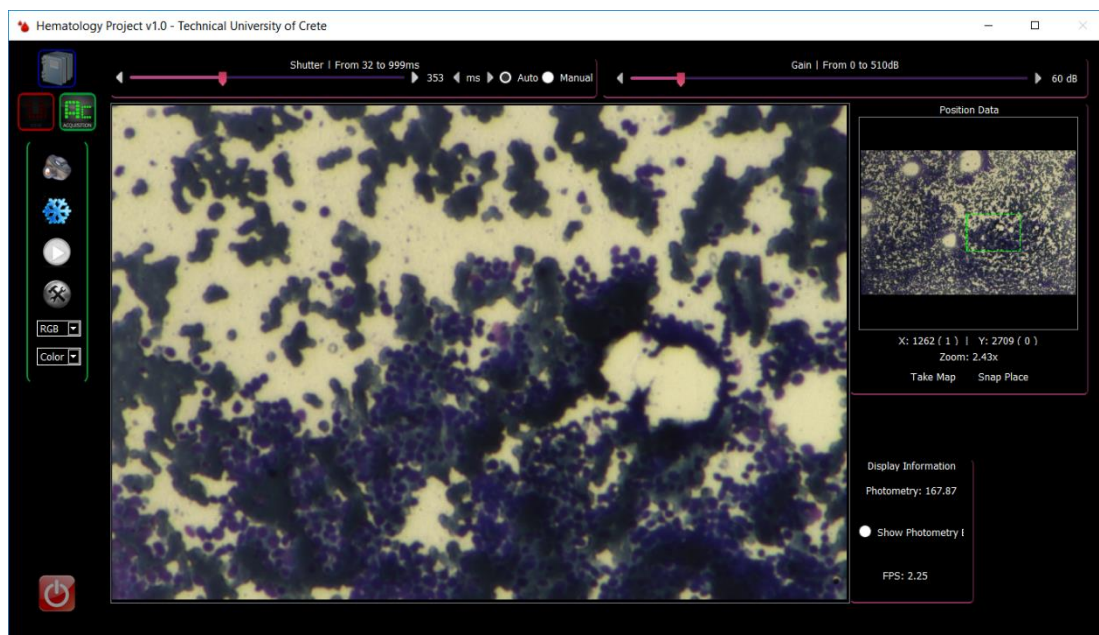


Figure 5.21: Even higher magnification and movement cause it to become smaller and move accordingly

The present subsystem will hopefully help the medical professionals to save a lot of time during the search of areas of interest. Around 8-14 number of maps, depending on the sample, are needed in order to be fully explored contrary to the current methods.

Conclusion & Future Work

A novel, integrated hyper-spectral microscopy system with application in the diagnostic improvement of leukemia was presented, synthesized by the talent and hard work of many capable people.

It is safe to assume that the goals set were achieved:

- Quantitative, objective measurements of high diagnostic value for further assisting the medical professional to evaluate an incidence.
- A stable, fast, accurate and consistent analysis of sample areas increasing both the throughput and accuracy of diagnosis.
- A practical, easy to use positioning and navigational system, making it easier and quicker for the user to explore the sample and locate the areas of interest.
- A stable, simple, straightforward yet powerful user interface encapsulating all the above in a well-defined manner.
- Maintain a relatively low cost of the overall system design.

The first goal was achieved by providing the user with the concentrations of each substance and plotting the distribution lines. The complementary and optimized algorithms analyze consistently and accurately the sample in unprecedented executions speed, further assisting and not delaying the diagnostic procedure, making it independent of various lighting issues.

A stable and practical user interface incorporates all the above and adds a positioning subsystem, which can be used for quick detection of areas of interest and navigation. Moreover, it is much less costly than the positioning systems currently available.

Nevertheless, this just marks the beginning of what will hopefully be a tool of great significance at the medical professionals' disposal. Although it is ready for application at its current stage, a lot of things have to be done or revised before it goes public and claim its capabilities. These are:

- Extensive clinical trials and validation of the algorithms, something that has already begun as those lines are typed. The results until now are very promising.
- Association of the distribution curves and concentrations with certain types and stages of leukemia and cell types. This would be breakthrough in the leukemia diagnosis and Eosin Y has already been linked with certain cells, thought too early to make a safe conclusion.
- Bug tracking of software.
- Further optimizations, for providing even faster execution times.
- Development of new tools to be incorporated in the software, such as per pixel distribution and analysis.
- Better accuracy of the positioning system.

Having said that, the present thesis has come to its end. Hopefully, the development of the system will continue steadily and reach the desired state soon.

References

- [1] "The Invention of the Microscope", David Bardell, BIOS Vol. 75, No. 2 (May, 2004), p. 78-84
- [2] "Janssen's Microscope", Michael W. Davidson, Florida State University
- [3] "Biotechnology 101", Brian R. Shmaefsky, p. 171, ISBN-13: 978-0313335280
- [4] "The unseen world: reflections on Leeuwenhoek (1677) 'Concerning little animals' ", Nick Lane, 2015, Phil. Trans. R. Soc. B
- [5] "Antony van Leeuwenhoek: Creation 'Magnified' Through His Magnificent Microscopes", Dr. Alan Gillen and Douglas Oliver, 2012
- [6] "Lentz Microscopy and Histology Collection", Thomas L. Lentz, 2015, Yale University
- [7] "Physics, Volume 2, 4th Edition", David Halliday, Robert Resnick, Kenneth Krane, ISBN: 978-960-7258-73-1
- [8] "Advanced Topics in Electronic Imaging, Lecture 7: Microscopy Basics", Professor Costas Balas
- [9] "Campbell Biology, 10th Edition", Jane B. Reece, Lisa A. Urry, Michael L. Cain, Steven A. Wasserman, Peter V. Minorsky, Robert B. Jackson, 2013, ISBN: 978-0-321-77565-8
- [10] "How the Immune System Works, 5th Edition", Lauren Sompayrac, PhD, 2012, ISBN: 978-1-118-99777-2
- [11] "Developments of Hyperspectral Microscopy for Improving the Diagnostic Accuracy in Leukemia Diagnosis", Dimitris Gkotsoulias, 2016
- [12] Journal of Clinical Oncology, Volume 22, Number 7
- [13] "Leukemia", U.S. National Cancer Institute
- [14] "Clinical presentation of childhood leukaemia: A systematic review and meta-analysis", Rachel T. Clarke, Ann Van den Bruel, Clare Bankhead, Christopher D. Mitchell, Bob Phillips, Matthew J. Thompson
- [15] "Laboratory Hematology", Ioannis Georgoulis, 2012, ISBN: 978-960-6894-49-7
- [16] "Development of a Computer Controlled Tunable Wavelength Light Source from Ultraviolet to Infrared", Christos Rossos, Bachelor Thesis, 2013
- [17] "Development of Coherent and Incoherent Light Sources with Computer Control of their Spectral Emission for Biomedical Applications", Christos Rossos, Master Thesis, 2016
- [18] "Spectral Deconvolution and Concentration Mapping in Complex Biochemical Stains", Fani Abatzi, 2014

Annex A: Data Analysis Pseudocode

- 1) Acquire image465, image505, image530, image600, image640, image685;
// Width = w, Height = h, data type is unsigned 8-bit

- 2) Abs_Image465 = beer_Labmert(image465); // data type changes to 32-bit float
Abs_Image505 = beer_Labmert(image505); // data type changes to 32-bit float
Abs_Image530 = beer_Labmert(image530); // data type changes to 32-bit float
Abs_Image600 = beer_Labmert(image600); // data type changes to 32-bit float
Abs_Image640 = beer_Labmert(image640); // data type changes to 32-bit float
Abs_Image685 = beer_Labmert(image685); // data type changes to 32-bit float

- 3) Ref_Image465 = reform(Abs_Image465, width = 1, height = w · h);
Ref_Image505 = reform(Abs_Image505, width = 1, height = w · h);
Ref_Image530 = reform(Abs_Image530, width = 1, height = w · h);
Ref_Image600 = reform(Abs_Image600, width = 1, height = w · h);
Ref_Image640 = reform(Abs_Image640, width = 1, height = w · h);
Ref_Image685 = reform(Abs_Image685, width = 1, height = w · h);

- 4) ConMatrix = new matrix(rows = w · h, columns = 7);
ConMatrix(:, 1) = Ref_Image465;
ConMatrix(:, 2) = Ref_Image505;
ConMatrix(:, 3) = Ref_Image530;
ConMatrix(:, 4) = Ref_Image600;
ConMatrix(:, 5) = Ref_Image640;
ConMatrix(:, 6) = Ref_Image685;

- 5) Ones_matrix = new matrix(rows = w · h, columns = 1, elements_value=1);
ConMatrix(:, 0) = Ones_matrix;

- 6) Prediction = ConMatrix * beta; //this results in a new (w · h) x 3 matrix

- 7) EosinY = ConMatrix(:, 0) · 1000;
AzureB = ConMatrix(:, 1) · 1000;
MethyleneBlue = ConMatrix(:, 2) · 1000;

- 8) EosinY = reform(EosinY, rows = h, columns = w);
AzureB = reform(AzureB, rows = h, columns = w);
MethyleneBlue = reform(MethyleneBlue, rows = h, columns = w);

- 9) Map_AzureB_Color = new image(width = w, height = h, format = RGB);
Map_EosinY_Color = new image(width = w, height = h, format = RGB);
Map_MethyleneBlue_Color = new image(width = w, height = h, format = RGB);

10) // Eosin Y Pseudo-color Color Map generation

for i=0; i<h; i=i+1

for j=0; j<w; j=j+1

if(EosinY(h, w) < eosin_threshold_1

Map_EosinY_color(w,h) = (0,0,0);

Else if(EosinY(h, w) < eosin_threshold_2

Map_EosinY_color(w,h) = (102,178,255);

Else if(EosinY(h, w) < eosin_threshold_3

Map_EosinY_color(w,h) = (0,255,0);

Else if(EosinY(h, w) < eosin_threshold_4

Map_EosinY_color(w,h) = (255,0,0);

Else if(EosinY(h, w) < eosin_threshold_5

Map_EosinY_color(w,h) = (255,255,50);

else

Map_EosinY_color(w,h) = (255,255,255);

end

end

11) // Azure B Pseudo-color Color Map generation

for i=0; i<h; i=i+1

for j=0; j<w; j=j+1

if(AzureB(h, w) < azure_threshold_1

Map_AzureB_color(w,h) = (0,0,0);

Else if(AzureB (h, w) < azure_threshold_2

Map_AzureB_color(w,h) = (102,178,255);

Else if(AzureB (h, w) < azure_threshold_3

Map_AzureB_color(w,h) = (0,255,0);

Else if(AzureB (h, w) < azure_threshold_4

Map_AzureB_color(w,h) = (255,0,0);

Else if(AzureB (h, w) < azure_threshold_5

Map_AzureB_color(w,h) = (255,255,50);

else

Map_AzureB_color(w,h) = (255,255,255);

end

end

12) // Methylene Blue Pseudo-color Color Map generation

for i=0; i<h; i=i+1

for j=0; j<w; j=j+1

```

    if( MethyleneBue(h, w) < MethyleneBue _threshold_1
        Map_ MethyleneBue _color(w,h) = (0,0,0);
    Else if( AzureB (h, w) < MethyleneBue _threshold_2
        Map_ MethyleneBue _color(w,h) = (102,178,255);
    Else if( MethyleneBue (h, w) < MethyleneBue _threshold_3
        Map_ MethyleneBue _color(w,h) = (0,255,0);
    Else if( MethyleneBue (h, w) < MethyleneBue _threshold_4
        Map_ MethyleneBue _color(w,h) = (255,0,0);
    Else if( MethyleneBue (h, w) < MethyleneBue _threshold_5
        Map_ MethyleneBue _color(w,h) = (255,255,50);
    else
        Map_ MethyleneBue _color(w,h) = (255,255,255);

    end
end

```

When making the monochrome maps though, instead of giving a specific color whether the value belongs to a specific range, the value is multiplied by 255, resulting in a “continuous” values. In this way, three monochrome maps and the final proportions map are produced. Eosin Y consists of the red channel of the final proportions map and the red channel of its monochrome map (the other are set to zero), Azure B the green channel and Methylene Blue the blue channel.

Annex B: WBC Isolation Pseudocode

- 1) Acquire colorImage;
- 2) channelRed = getRedChannel(colorImage); // Split image channels
channelGreen = getGreenChannel(colorImage);
channelBlue = getBlueChannel(colorImage);
- 3) A = channelRed + channelBlue; // Add corresponding elements
- 4) G = channelGreen · 2; // Multiply each element by 2
- 5) D = A/G; // Divide corresponding elements
- 6) MinValue = getMinValue(D); // Find and store minimum value of D
- 7) MaxValue = getMaxValue(D); // Find and store maximum value of D
- 8) if(MaxValue – MinValue < 2.2204e-16) then
RescaledImage = D;
else
RescaledImage = 255 · (D – MinValue)/ (maxVal – minVal);
end if
- 9) maxEntropyThresholding(RescaledImage); // Apply the Maximum Entropy Threshold

End of Phase 1

- 10) clone = RescaledImage; // Create a clone of RescaledImage
- 11) floodfill(clone, 255); // Fill connected components with value 255
- 12) invert(clone); // clone is a binary image and values are inverted (255→0, 0→255)
- 13) nucleiWBC= RescaledImage || clone; // Bitwise OR corresponding elements
- 14) n = getNumberOfBLOBS(nucleiWBC); // Get BLOBS

for(i = 0; i < n; i = i + 1)

 if(blobArea(i) < THRESHOLD) // If a BLOB is smaller than a THRESHOLD then
 removeBlob(i); // remove it by setting its pixels equal to zero

end for;

End of Phase 2

15) if(magnification \leq 20) then

 maskBloodCells = otsu(channelGreen); // Apply OTSU thresholding

else

 maskBloodCells = triangle(channelGreeb); // Apply Triangle thresholding

end if

16) invert(maskBloodCells); // Again, invert all elements of this binary image

17) n = getNumberOfBLOBS(maskBloodCells); // Get BLOBs

for(i = 0; i < n; i = i + 1)

 if(blobArea(i) < THRESHOLD) // If a BLOB is smaller than a THRESHOLD then
 removeBlob(i); // remove it by setting its pixels equal to zero

end for;

End of Phase 3

18) edgeBloodCells = findContours(maskBloodCells); // Find the contours of the image

End of Phase 4

19) se = getStructuringElement(ELLIPSE); // Get a standard Ellipse BLOB

20) create WBCMask; // Create an empty image of what is going to be the final mask

21) n = getNumberOfBLOBS(nucleiWBC); // Get BLOBs

for(i = 0; i < n; i = i + 1)

 a) currentNuclei = getBlob(i); // Get i BLOB

 b) do

 temp = currentNuclei && edgesBloodCell; // Bitwise AND

 sum = sumElements(temp);

 if(sum \leq THRESHOLD2) then

```
        dilate(currentNuclei, se); // Dilate the current BLOB using the Ellipse
    end if

    while(sum ≤ THRESHOLD2);

    c) WBCMMask = WBCMMask || currentNuclei; // Merge that BLOB to the image
end for;
```

End of Phase 5 (Final)
